FINAL REPORT

Venus Aerobot Surface Science Imaging System (VASSIS)

Worked performed under NASA Grants NAG5-4533 (ASU) and 157-10-10-04 (JPL)
of NRA 95-OSS-12

Principal Investigator: Dr. Ronald Greeley, Arizona State University

Submitted: 3 August 1999

To:
National Aeronautics and Space Administration
300 E Street SW
Washington DC 20546-0001

Attn: Dr. Bruce Betts

Venus Aerobot Surface Science Imaging System (VASSIS)

1.   Proposed work

The VASSIS task was to design and develop an imaging system and container for operation above the surface of Venus in preparation for a Discovery-class mission involving a Venus aerobot balloon. The technical goals of the effort were to: a) evaluate the possible nadir-viewed surface image quality as a function of wavelength and altitude in the Venus lower atmosphere, b) design a pressure vessel to contain the imager and supporting electronics that will meet the environmental requirements of the VASSIS mission, c) design and build a prototype imaging system including an Active-Pixel Sensor camera head and VASSIS-like optics that will meet the science requirements. The VASSIS science team developed a set of science requirements for the imaging system upon which the development work of this task was based. These requirements include:

- angular resolution of 1 mrad/pixel
- imaging array of at least 256 x 256 pixels
- imaging of Venus surface from various altitudes between 40 and <1 km with nested frames to provide context and link to Magellan data
- stereo coverage using frame overlap regions
- camera to be in focus for ranges from infinity to <10m
- image smear kept <1 pixel
- multispectral imaging capability at wavelengths of 0.55, 0.65, 0.77, 0.87, and 1.01 μm
- nadir pointing
- multi-frame buffer memory and data compression
- low-spatial-frequency constrast signal-to-noise ratio >40

2.   Feasibility of imaging the surface of Venus from altitude

Computer models were constructed and run of the atmospheric temperature and pressure and the spectral radiance of the Venus surface and atmosphere vs. aerobot altitude, wavelength, and solar zenith angle. It became apparent that imaging near 1-μm wavelength would be optimum. Imaging at other wavelengths as short as 0.75 μm appears feasible. An estimate of 50 msec was made for the practical limit on exposure time to keep image smear acceptably small in the presence of possible swaying motion of the instrument gondola beneath the aerobot balloon. Based on these modeling results, camera performance requirements were derived that would provide adequate signal-to-noise ratios (SNR) and spatial resolution for surface imaging at altitudes as high as 45 km.

Attachment 1 shows some model plots of the upward radiance of Venus (surface plus atmosphere) as a function of wavelength for various assumed surface albedos, observing altitudes, and solar zenith angles. The models and software used to produce these plots

are discussed in Reference 1. Attachment 2 shows how the apparent contrast at the surface of Venus at 1.01 μm is reduced as a function of altitude assuming the upward radiance models. Attachment 3 presents some of the results of our initial analysis of VASSIS camera surface contrast SNR; however, this analysis did not include an exposure time limitation due to possible gondola swaying. Attachment 4 presents updated results that do address possible exposure time limitations.

The results of these analyses generated a set of camera design goals to insure adequate image quality to meet the scientific goals of a Venus aerobot imaging mi sion. These include:

- maximizing camera sensitivity at 1 μm
- use of large detector pixels (20-25 μm) to increase signal
- electronic shuttering of the detector
- large detector full well (>200,000 e⁻)
- modest read noise (<150 e⁻ adequate; photon shot noise will typically dominate)
- fast (f/2 or faster) optics to allow short shutter times with good SNR
- minimal set back of camera behind enclosure window.

Image simulations were also generated to illustrate the effects of the diffuse illumination on the Venus surface and the obscuring effects of the intervening scattering atmosphere (Reference 2). Software models of the daylight sky were coupled with digital elevation maps of the Inyo craters of California and of Puu Oo volcano in Hawaii in creating a simulated Venus scene (Reference 3). Views were created from different simulated altitudes (see Attachment 5). In addition, stereo pairs were produced for visual evaluation. Surface-induced contrast remains visible and interpretable up to an altitude of at least 20 km (the highest altitude simulated due to the limited size of the elevation maps available). As altitude increases, the effects of surface elevation on scene contrast also increase while the effects of surface albedo decrease. Disentangling the contrast effects of these two sources is challenging and not necessarily intuitive for those used to interpreting surface images of planets and satellites without atmospheres. Stereo pairs should permit the effects of elevation and albedo on contrast to be separated to some extent.

3.   Instrument Containment Pressure Vessel

The instrument containment vessel required for a Venus aerobot mission that includes descents to near the surface will need to

- survive entry loads of up to 500 g
- survive pressure up to 100 bar
- maintain internal temperature of about 30°C for external temperatures ranging between 0°C and 460°C during a roughly 10-hr descent/ascent cycle
- provide a camera external nadir viewport that keeps heat leak acceptably small.

Several alternative concepts for a dual-wall instrument containment structure were evaluated using either multilayer insulation in a vacuum or a powder insulation backfilled with a heavy inert gas. The supports that suspend the inner wall within the outer wall were designed. Aerobot descent and ascent rates were computed along with the amount of heat transfer into the inner sphere for both insulation types. Heat transfer was shown to be primarily radiative across the insulation rather than leak through the instrument viewport or structural mounts. A thermal control system including a heat exchanger and heat pipe was designed that will freeze out a supply of phase-change material at high altitude while precluding rapid melting near the surface. A mass of about 4 kg of phase change material was shown to be needed to provide about two hours of operation within 1 km of the surface of Venus. A robust design for the seal between the pressure vessel walls and the viewport was developed that accommodates differing thermal coefficients of expansion in adjacent materials. An evaluation of the thermal gradients in the viewport material showed that their effects on optical performance will be acceptable. Initial mass estimates indicate a total container mass of about 25 kg and a total aerobot system mass of about 4 times this amount. The final results of the instrument containment vessel design work are documented in Attachments 6 and 7 and in Reference 4, which is included here as Attachment 8.

4.   Prototype Imaging System

Based on the science requirements and the mission constraints, a set of functional requirements for the VASSIS prototype camera and its support equipment were defined (see Attachment 9).

To minimize heating within the pressure vessel, minimum power dissipation by the camera is required. In addition, minimizing instrument mass is a high priority for the aerobot application. Therefore, a newly developed Active Pixel Sensor (APS) imaging detector was selected since it requires only about 200 mW of power to operate and does not require as much off-chip electronics to operate as other detectors. Due to cost constraints, VASSIS could not develop an APS detector optimized for the Venus aerobot application. Instead, we obtained for free a surplus 256 x 256 20-μm pixel photogate APS detector from the STRV-2 Project. This device was characterized and found to have quite narrow operating voltage windows.

A preliminary optics design was carried out yielding a 20-mm focal length, f/1.3 lens having an aperture diameter of only 15 mm. For the prototype camera, a similar optic already on hand was selected for implementation. The resulting field of view (FOV) of the camera was 15°, which required a fairly small viewport diameter. A 5-position filter changing mechanism was included in the camera design.

Although we were constrained in our choice of detector for our prototype camera, we did investigate the tradeoff between a photodiode vs. photogate APS pixel structure for future applications. The photodiode approach offers higher full well and better quantum

efficiency at the expense of a higher noise floor. Overall, the photodiode performance seems better suited to a Venus aerobot application.

Our prototype camera was designed and built using an APS camera design developed for the Rocky-7 rover application as a baseline. We wanted to be able to do on-chip electronic shuttering using sequencing of the applied clock voltages. For the short exposure times needed for Venus imaging and the modest detector readout rates possible, signal integration must be inhibited during image readout to obtain a true "snapshot" image without saturation. However, our APS device does not support this function. Therefore, we included a mechanical shutter in our camera design. This shutter was designed as a rotating wheel with two different width slits (3° and 60°) that can be made to pass in front of the detector. The exposure time is controlled by the choice of which slit to use and the angular rotation rate of the wheel. This design allows reliable exposure times as short as 1 msec or less as opposed to mechanical shutters with moving blades, which are only reliable down to about 5 msec. The shorter exposure times are needed at Venus where the incident Sunlight is high. Our rotating shutter is operated using a commercially available motor and controller commanded by the camera PC-based Ground Support Equipment (GSE). The limited scope of the VASSIS task did not allow us to prototype a flight-like motor controller; however, we see no reason why such a controller could not be designed and built within a reasonable mass allocation.

The prototype camera was fabricated, and mechanical mounting fixtures were made to assemble the camera head with the optics and shutter. Cost constraints precluded including the filter changing mechanism in this prototype; however, such a mechanism does not represent a new technology item and should be easily developed for a flight application. Attachment 10 shows several views of the VASSIS camera head alone, the camera head integrated with the optics and shutter wheel, and a front view of the optics and shutter wheel.

GSE camera operation and data capture, display, and storage software was written and tested.

The assembled camera was initially tested to verify its engineering performance. A more detailed description of the camera and its operation are given along with the results of the preliminary engineering tests in Attachment 11. These tests did not use the shutter wheel for exposure control; rather, image integration time was controlled using the APS clocks to start and end the exposure. Use of low light-source levels and exposure times of at least 400 msec made this mode of exposure control acceptable for these tests. No spectral filters were used. This preliminary testing demonstrated that the camera was operating properly. Some questionable response linearity data indicated that more careful further testing and calibration was needed.

Camera calibration using the GSE-controlled shutter wheel for exposure control was planned and carried out. Attachment 12 illustrates the test setup. Since the primary wavelength of interest for the VASSIS application is 1 μm, a 10-nm-wide spectral filter centered at that wavelength was placed in front of the optics for most of these tests. A

subset of the test images was taken using a 0.75-μm filter for comparison. Test images consisted of dark frames, flat field images at various signal levels, and focused images of various test targets at different signal levels.

The dark frames and flat fields were analyzed using the photon transfer technique to determine the electrons/DN conversion factor, read noise, and full well (Reference 5). Five different 30x30-pixel image areas were analyzed. A representative photon transfer curve is shown in Attachment 13. The asterisks plot the random noise level computed from the difference of two flat field frames, while the crosses plot the total raw image noise. The electrons/DN conversion factor was determined to be 20 electrons/DN. Full well occurs at about 2000 DN or 40,000 e⁻. Read noise was measured at 1.2 DN or 24 e⁻. The APS detector full well is about 2x lower than specified in the VASSIS camera functional requirements, and the read noise is about 2x higher.

These images were also used to measure the response linearity of the detector, which is plotted in Attachment 14. Linearity is quite good (within 5% or less) except at low signal levels. The response is less than would be expected from a perfectly linear device for signal levels below about 200 DN (4000 e⁻) above background. This effect is not currently understood and represents an important shortcoming in our APS detector performance.

Focused images were acquired of various test targets including a resolution chart, a pinhole, horizontal and vertical knife edges, and horizontal and vertical wide bars. These images were acquired at both 1.0- and 0.75-μm wavelengths. Samples of these images are shown in Attachment 15. Attachment 16 gives a contrast transfer plot based on the resolution target images. Performance is better at 0.75 μm than at 1 μm, least at mid-range spatial frequencies. This is most likely due to the optics being optimized for performance in the visible range. Or it could be a result of deeper penetration of light into the silicon detector at 1 μm causing some charge spreading within the device itself. The sharpness of the wide-bar and knife-edge brightness transitions is consistent with the results of the contrast transfer analysis. At 0.75 μm, the signal changes by about 85% of its maximum over the 3 pixels centered on the transition, while at 1 μm, these same 3 pixels only produce about 78% of the maximum transition.

The pinhole images were analyzed by constructing line spread plots of the signal above background summed along columns and rows and plotted in the orthogonal directions. Attachment 17 presents some typical examples. The line spread data are fit well by a Gaussian profile having a peak response of 0.4 of the total signal in the central pixel. No differences in profile shapes are observed as a function of signal level or wavelength (0.75 and 1.0 μm). The lack of wavelength dependence was expected since the geometric size of the pinhole image is about 1.8 pixels across. The only departure from symmetry in the line spread profiles was a slightly elevated wing (by a few percent of the total signal) on the left side of pinhole images located on the left half of the detector (Attachment 18). This asymmetry is most likely due to some misalignments and possibly some internal reflections in the test setup; however, the cause was not systematically investigated.

Overall, the performance of the VASSIS APS camera was satisfactory. It exhibited good imaging performance out to 1 μm with no objectionable artifacts observed. Its photometric performance was good except for a loss of linearity at low signal levels.

5.   Future Work and Possible Applications

The VASSIS camera and its conceptual pressure vessel container form a sound basis for a potential Venus surface imaging investigation involving an aerobot or drop probes. This concept was incorporated in our recent VEVA (Venus: Exploration of Volcanoes and Atmosphere) Discovery mission proposal.

Optimization of the APS detector for a Venus imaging application might involve the following enhancements over the capabilities of our inherited detector:

- larger array size (>640x640 pixels)
- on-chip ADC
- electronic snapshot shuttering
- improved near-IR quantum efficiency
- increased full well (possibly using a photodiode pixel structure)
- micro-lenses overlaid on the pixel array
- fiber-optic coupling to a curved focal plane or off-axis outside views.

Another instrument technology enhancement that is worth pursuing is tunable filters.

Continued development and environmental testing of protoype instrument containment pressure vessels suitable for carrying imaging or other instruments on a descent to the surface of Venus is also needed.

Further simulations of images of the Venus surface from altitude and development of methods for interpreting such images would provide essential experience in preparation for the first Venus surface imaging from altitude.

The VASSIS camera was developed primarily as an example of an imaging instrument for use in extreme environments requiring a protective container. As such, the camera system developed under this PIDDP task will now be used in an underwater probe seeking clues to the origin of ancient life forms. The camera is being incorporated into an Underwater Volcanic Vent Probe, which will be used during August and September 1999 to examine the insides of seamount volcanic vent cracks in the South Pacific as part of a program partially funded by the NASA Code S Exobiology Program. The Probe will be attached to the manned submersible *Nautile* for placement under human control into vents emitting water at extremely high temperatures (150 - 350°C) at depths between 600 and 4000 m. The camera will image vent walls, which will be illuminated by red and green laser light for direct reflected-light imaging, and will be detecting UV flourescent signatures from minerals and organic material that have been stimulated by a new-technology UV laser in the Probe. The camera will provide spatial information on the
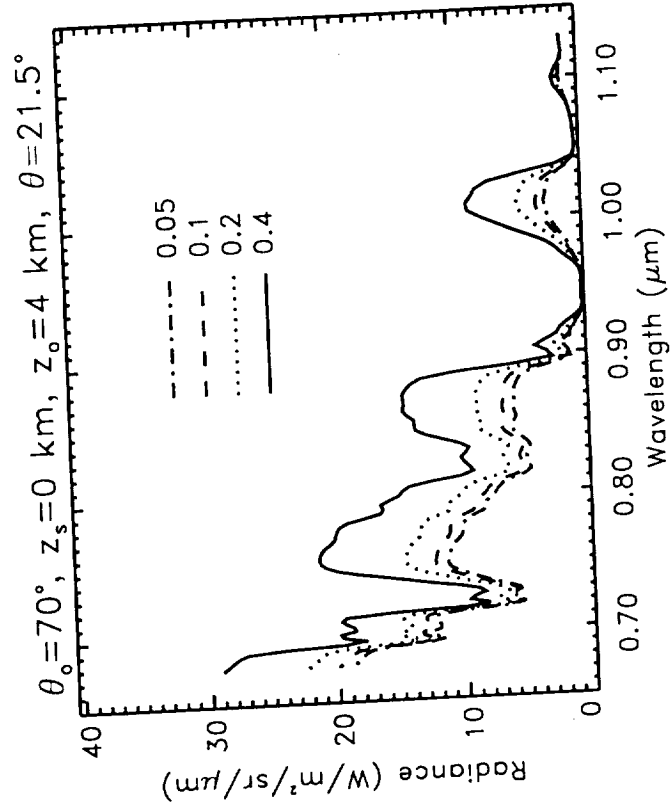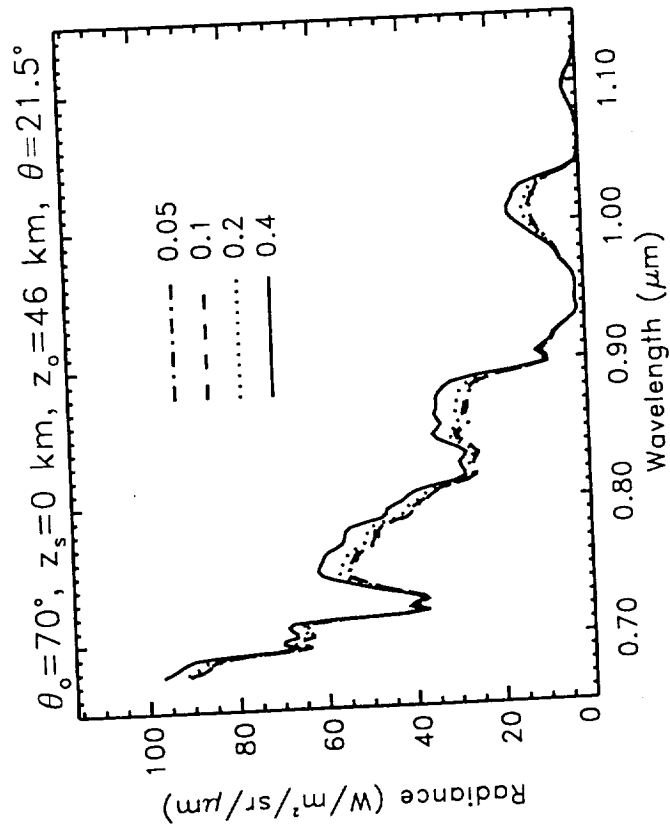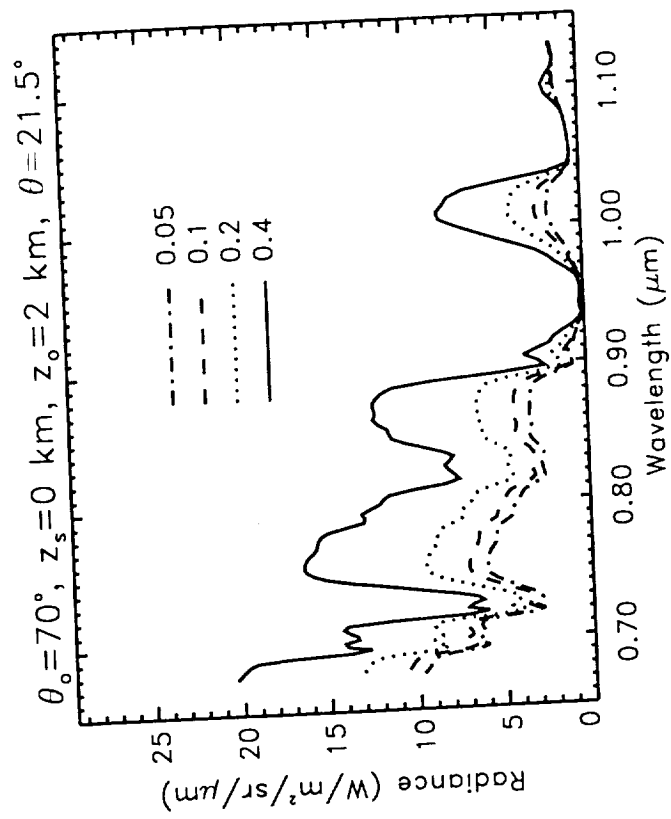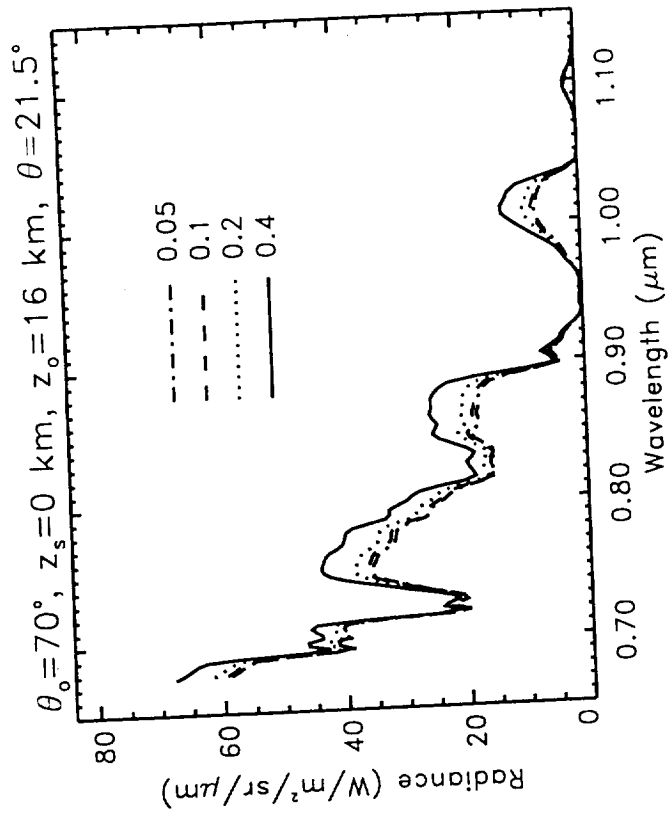
potential presence of thermophilic bacteria. So the VASSIS camera is already finding a useful scientific application in a situation not too different from its originally envisioned application in a Venus probe.
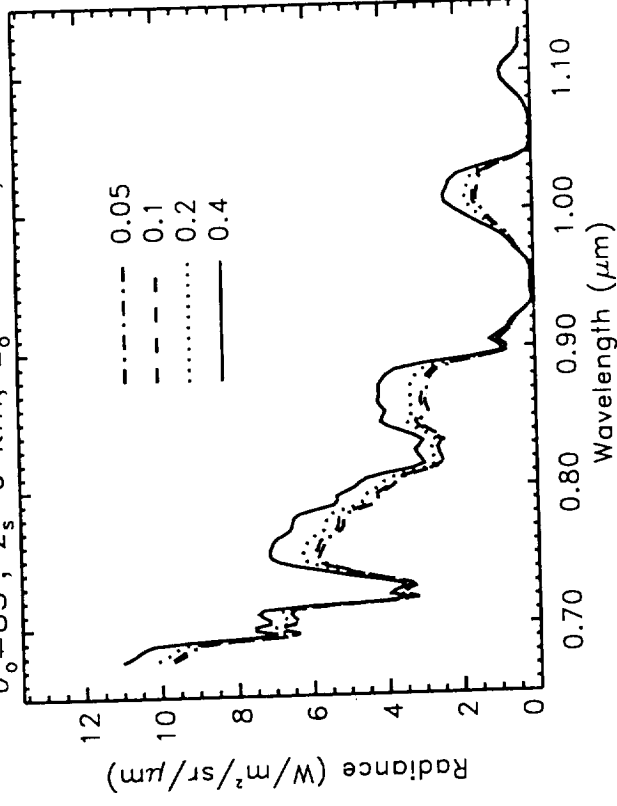
6. References

1. Meadows, V.S. and D. Crisp. "Ground-based near-infrared observations of the Venus nightside: The thermal structure and water abundance near the surface," *JGR*, 101, E2, 4595-4622, February 25, 1996.

2. Campbell, B. and M.K. Shepard. "Effect of Venus surface illumination on photographic image texture," *GRL*, 24, 6, 731-734, March 15, 1997.

3. Campbell, B, R. Greeley, E.R. Stofan, R. Gaskell, M.K. Shepard, and K. Klaasen. "Imaging the surface of Venus: feasibility of drop-probe photography," LPSC XXIX, 1998.

4. Heun, M.K., J.A. Jones, and J.L. Hall. "Gondola design for Venus deep atmosphere Aerobot operations," Paper AIAA 98-0897, 36th AIAA Aerospace Sciences Meeting & Exhibit, Reno, NV, January 12-15, 1998.

5. Janesick, J., K. Klaasen, and T. Elliott. "CCD charge collection efficiency and the photon transfer technique," SPIE Solid State Imaging Arrays Proceedings, vol. 750, August 1985.
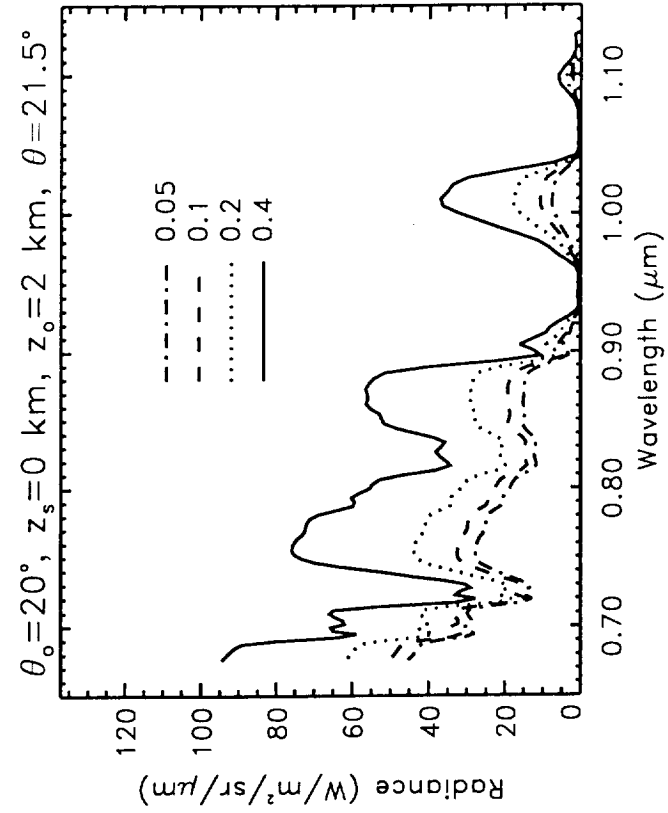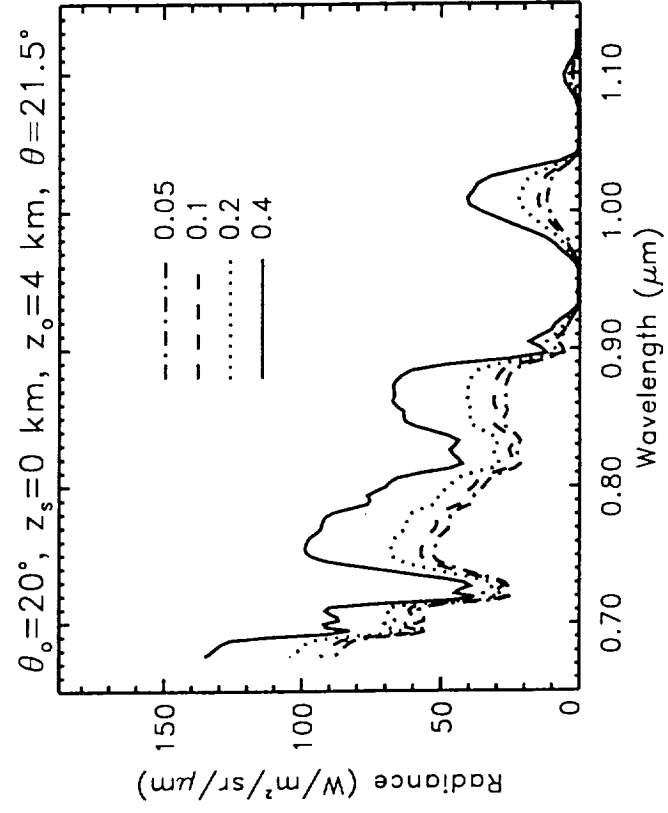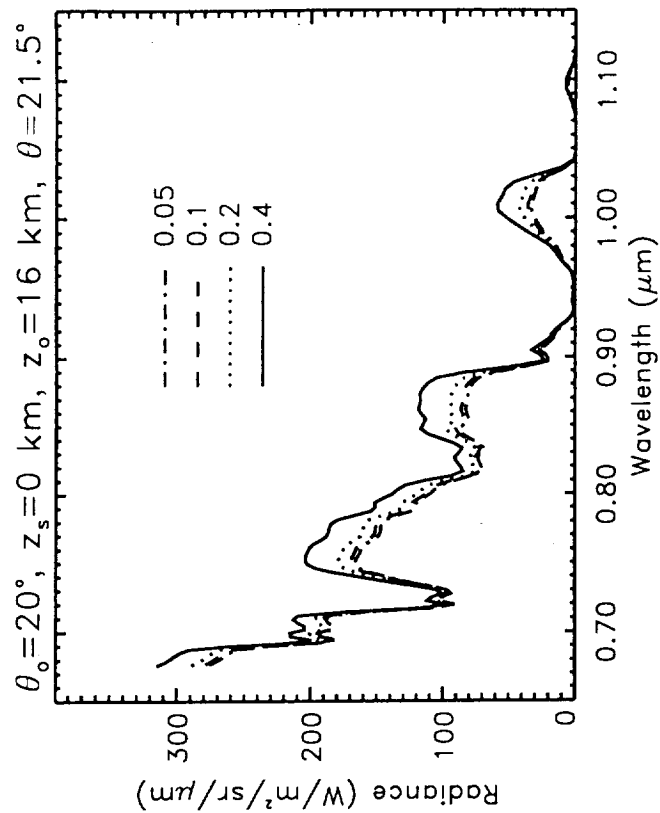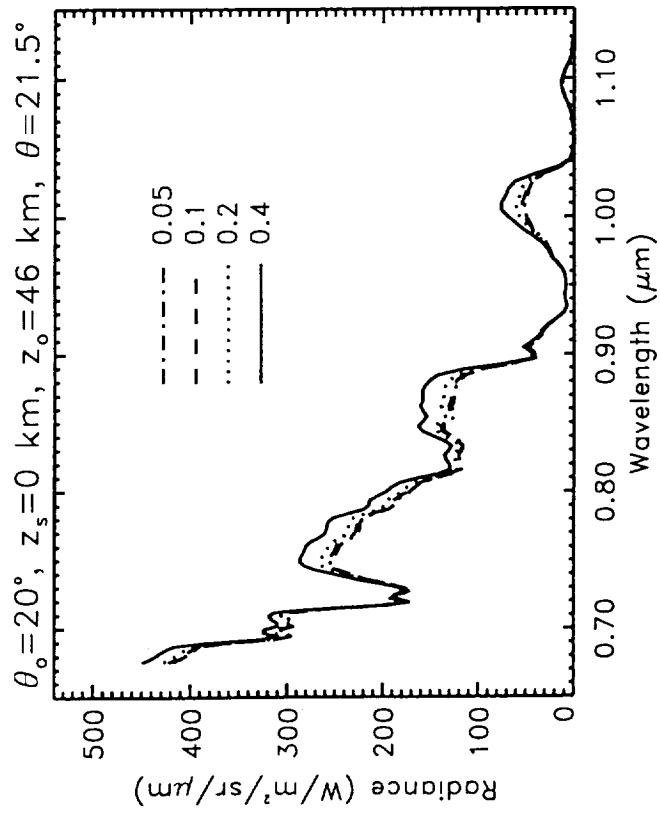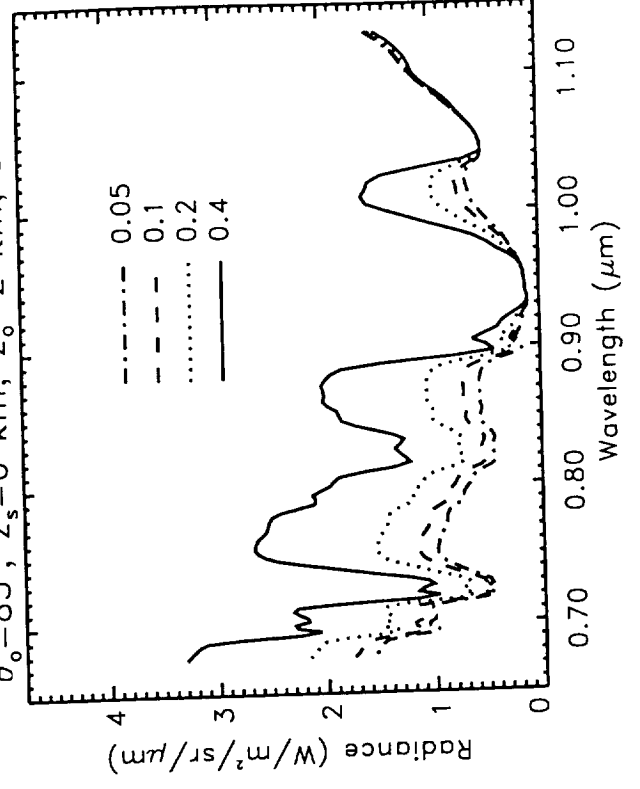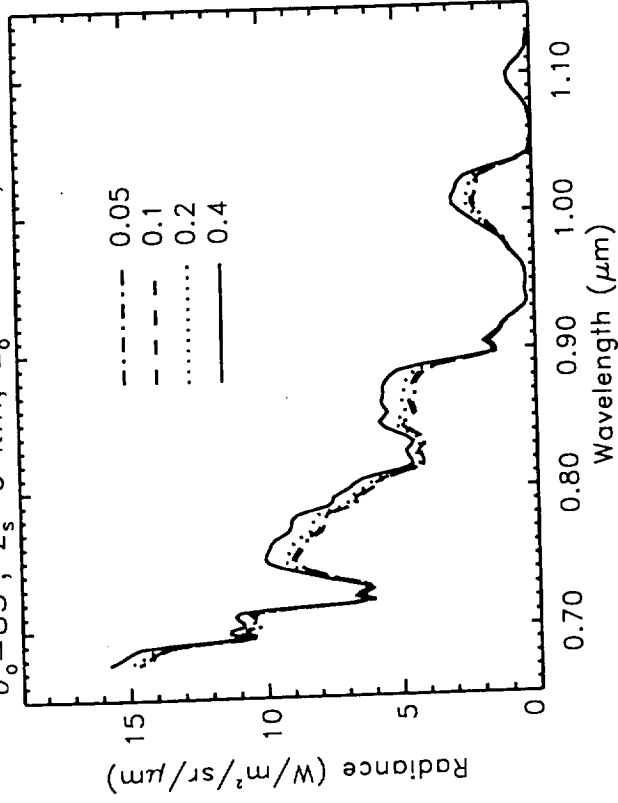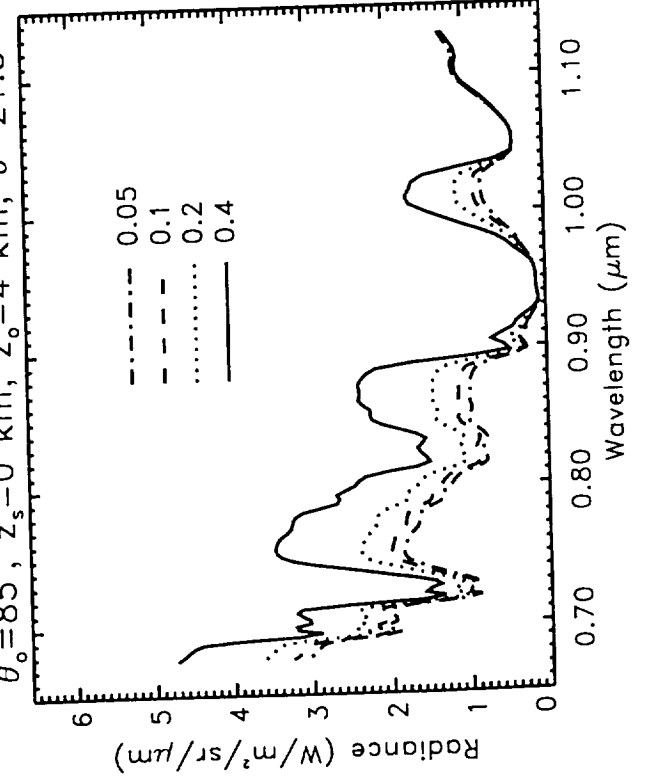
Venus Contrast Reduction w/ Altitude
1.01 um, 20-deg solar zenith

Contrast in image/contrast of surface
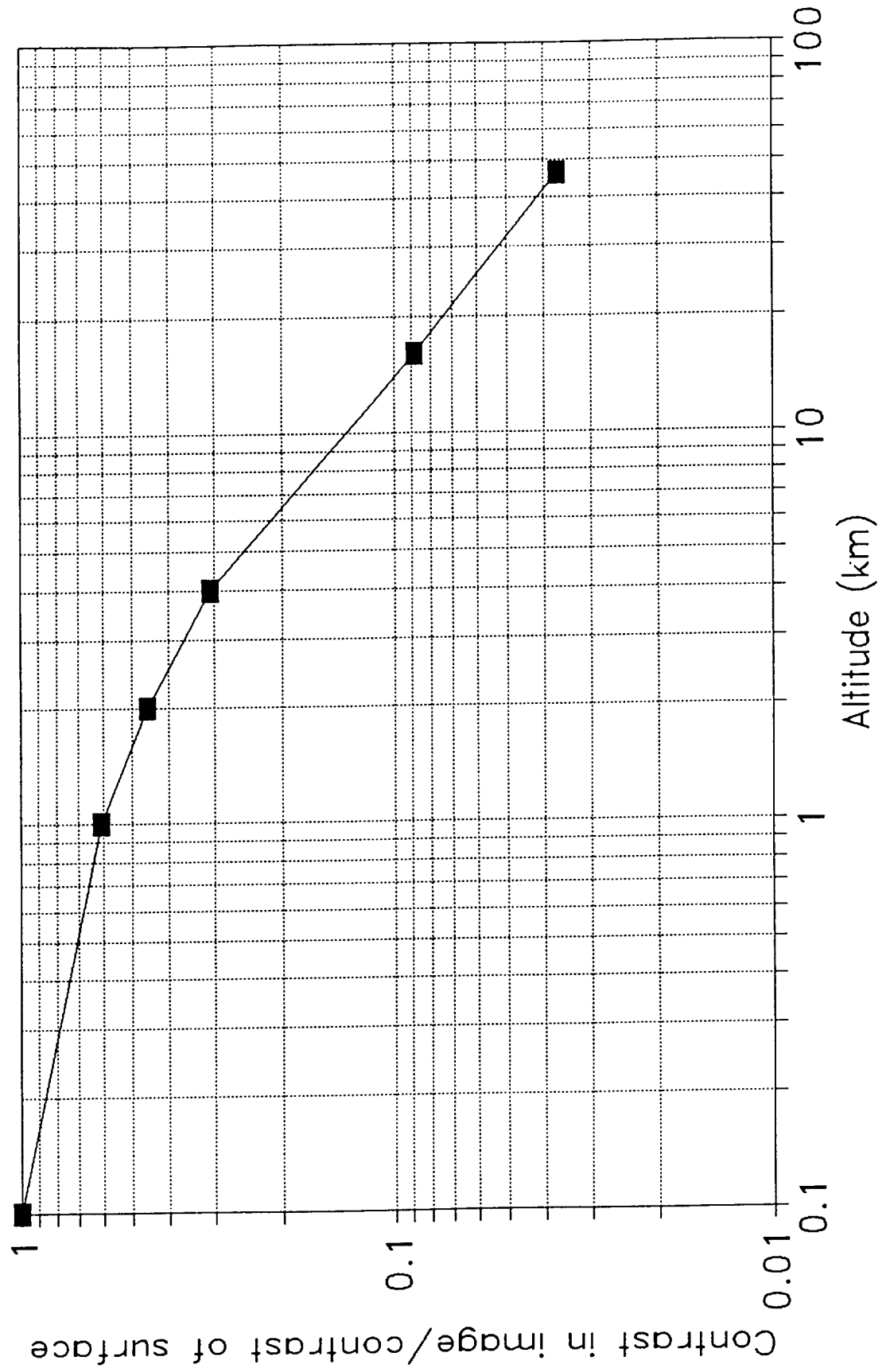
Altitude (km)

VASSIS Camera SNR Analysis

as a Function of

Wavelength, Altitude, and Sun Angle

7/2/96

K. Klaasen

Assumptions/observations

The results presented here are based on an analysis of the upward radiance from the Venus surface and atmosphere as calculated by Dave Crisp using his modeling software. The following assumptions were made:

The detector full well will support a mean signal level of
up to 250,000 e
The optics f/# = 1.9
Unless otherwise indicated, a maximum exposure time of 50
msec is used to keep smear to <1 pixel
Detector read noise is 200 electrons
The detector quantum efficiencies for the selected filters
are -

1.01 um	0.025
0.87	0.125
0.77	0.200
0.65	0.180

Albedo contrasts are at least 33%
The contrast levels measured are over areas of several
pixels (i.e., MTF = 1.0)
Pixels are 20 um square
Filter bandpasses are 0.04 um
Low-frequency contrast at SNR<10 is not useful; SNR>40
should be of good quality (=> high-frequency SNR of
>10)

Conclusions/observations

At high Sun angles, imaging improves as the wavelength increases (Figure 1). As long as the scene contains albedos as large as 0.4, good quality imaging can be done at all wavelengths at and above 0.77 um from altitudes of at least 46 km. For lower albedo scenes, imaging at 0.77 um is only possible below about 13 km for maximum albedos of 0.2 (or below about 3 km if the maximum albedo is 0.1 or less). At 0.87 um, maximum albedos of 0.2 can be imaged at altitudes as high as 25 km, while albedos of 0.1 can only be imaged well below about 5 km. At 1.1 um, albedos as low as 0.2 can be imaged from at least 46 km altitude. But with the albedo reduced to 0.1, the maximum altitude drops to about 10 km.

As the solar zenith angle increases, imaging performance drops for detecting albedo-induced contrasts at 1.01 um (Figures 2 - 4), and the contrast SNR becomes nearly independent of observing altitude (it depends only on the albedo and contrast levels in the scene). For low-albedo scenes, in fact, quality imaging becomes impossible for solar zenith angles of 70 deg or more at 1.01 um. At 85 deg zenith angle, only scenes with contrasts of at least 75% with maximum albedos of at least 0.4 can be imaged well at 1.01 um. This reduction in performance is due primarily to insufficient light at this wavelength (where the detector QE is getting very low) given our assumed maximum ex-

posure level of 50 msec. At wavelengths of 0.85 and 0.77 um, the higher light levels and higher detector QE values result in performance near the terminator that actually surpasses that at 1.01 um (Figure 3). For low albedo scenes, imaging at 0.77 and 0.87 um is best at about 70 deg solar zenith angle (Figures 5 and 6).

For imaging on the dark side, the 50-msec exposure time limit will never yield adequate elevation-induced contrast SNR even for a 2-km elevation difference. So high-spatial-resolution imaging at night is not possible. But elevation imaging probably does not need the highest possible resolution. For example, even a 45-deg slope will ascend 2 km only over a distance of 2 km. From an altitude of 40 km, a 2-km horizontal distance spans 50 pixels. So allowing some pixel smear for darkside imaging may be permissible. We can get adequate SNR for a 2-km elevation difference when imaging at 1.01 um with an exposure time of about 0.4 sec, or a maximum smear level of 8 pixels. At 0.87 um, the exposure needed is about 2 sec with a maximum smear level of about 40 pixels. Clearly, use of the 1.01-um filter is best for darkside imaging. Its performance varies little with observing altitude (Figures 10 and 11). However, elevation differences of 2 km are probably not very likely over the FOV coverage of the VASSIS camera (10 km from 40 km altitude).
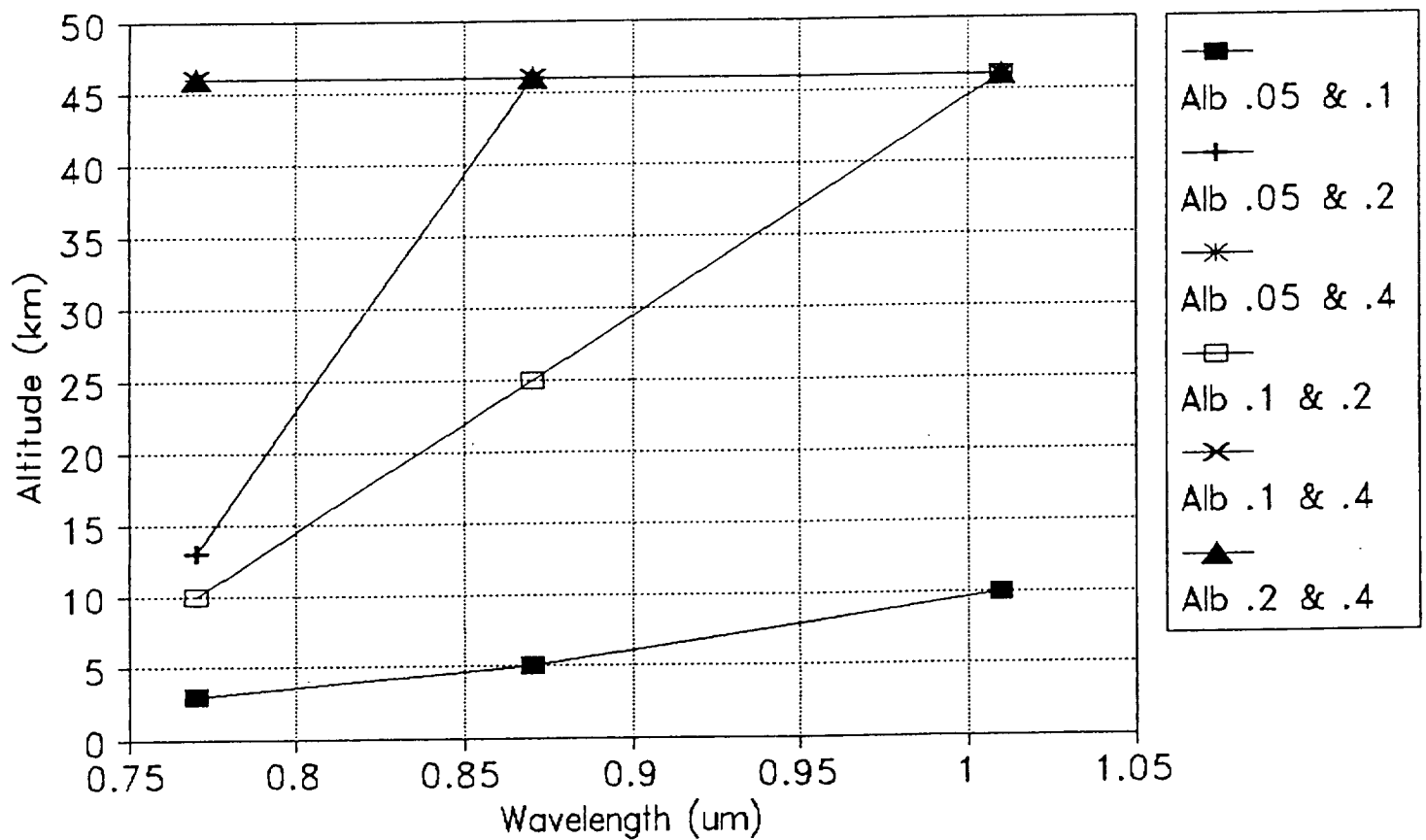
Some degree of elevation induced contrast will be detectable also in dayside imaging under certain circumstances. In fact, the elevation contrast induced by a 2-km elevation difference is within a factor of 3 of that induced by surface albedo differences in most cases examined. Differences larger than a factor of 3 occur at high Sun angles, where albedo contrasts dominate for albedos greater than 0.2 at 1.01 um while elevation contrasts dominate for an albedo of 0.05 at 0.87 um. At low Sun angles, albedo and elevation contrasts are generally comparable with elevation tending to produce larger contrasts for low albedo cases and the shorter wavelengths while albedo contrasts become larger as the albedos and wavelengths increase. The contrast ratios do not not vary greatly with observing altitude. Again, it seems unlikely that elevation differences of 2 km will occur often within a VASSIS image. So as a practical matter, elevation contrasts in dayside images are unlikely to be comparable with albedo-induced contrasts. Perhaps radiance data should be generated for elevation differences more appropriate to the scale of the planned VASSIS images.

Additional Data Needed

Radiance data are still missing for the zero elevation dayside cases at wavelengths of 0.55 and 0.65 um as well as for both the 2-km elevation dayside and 0- and 2-km elevation cases on the nightside at 0.55, 0.65, and 0.77 um.

Albedo Induced Contrast Detectability
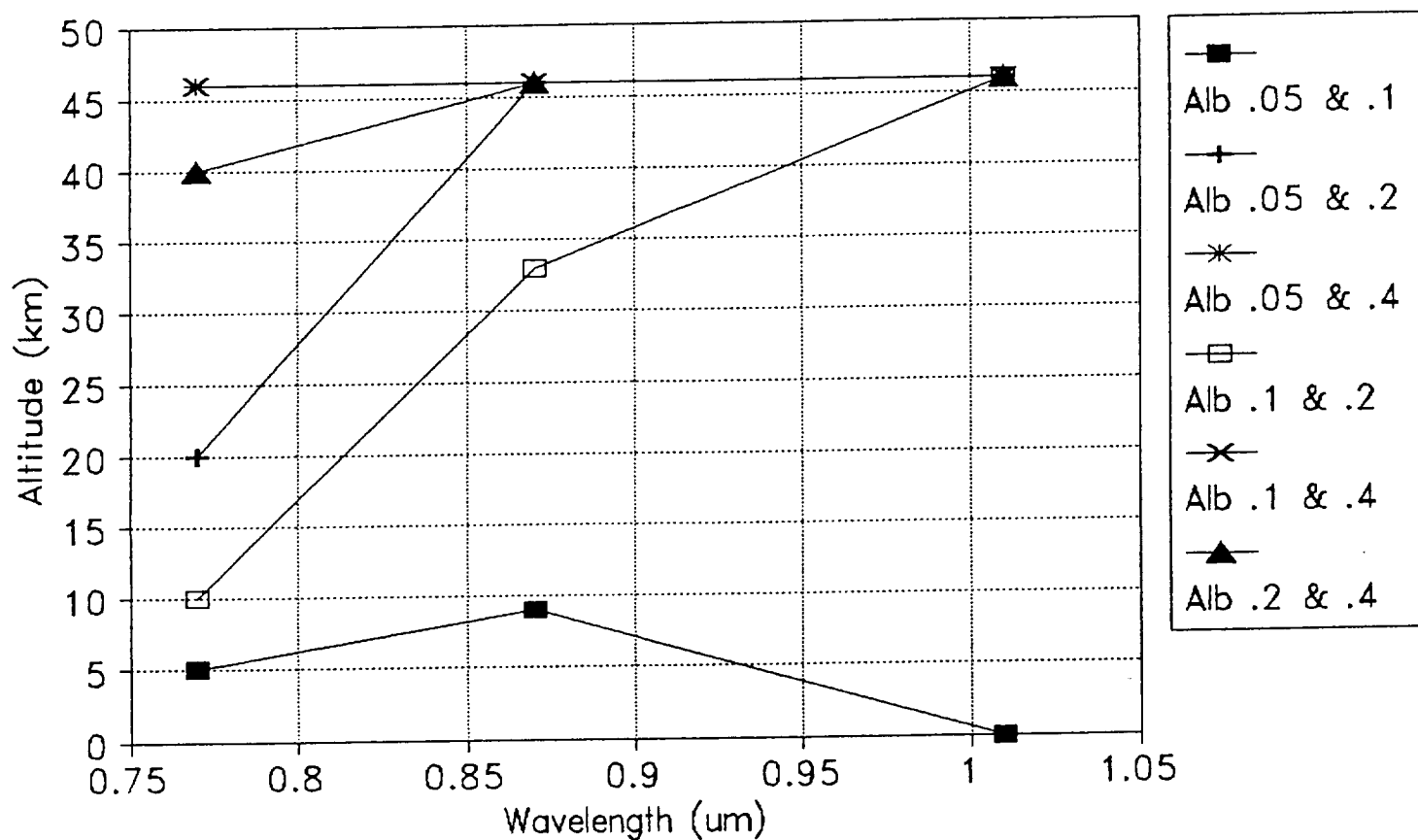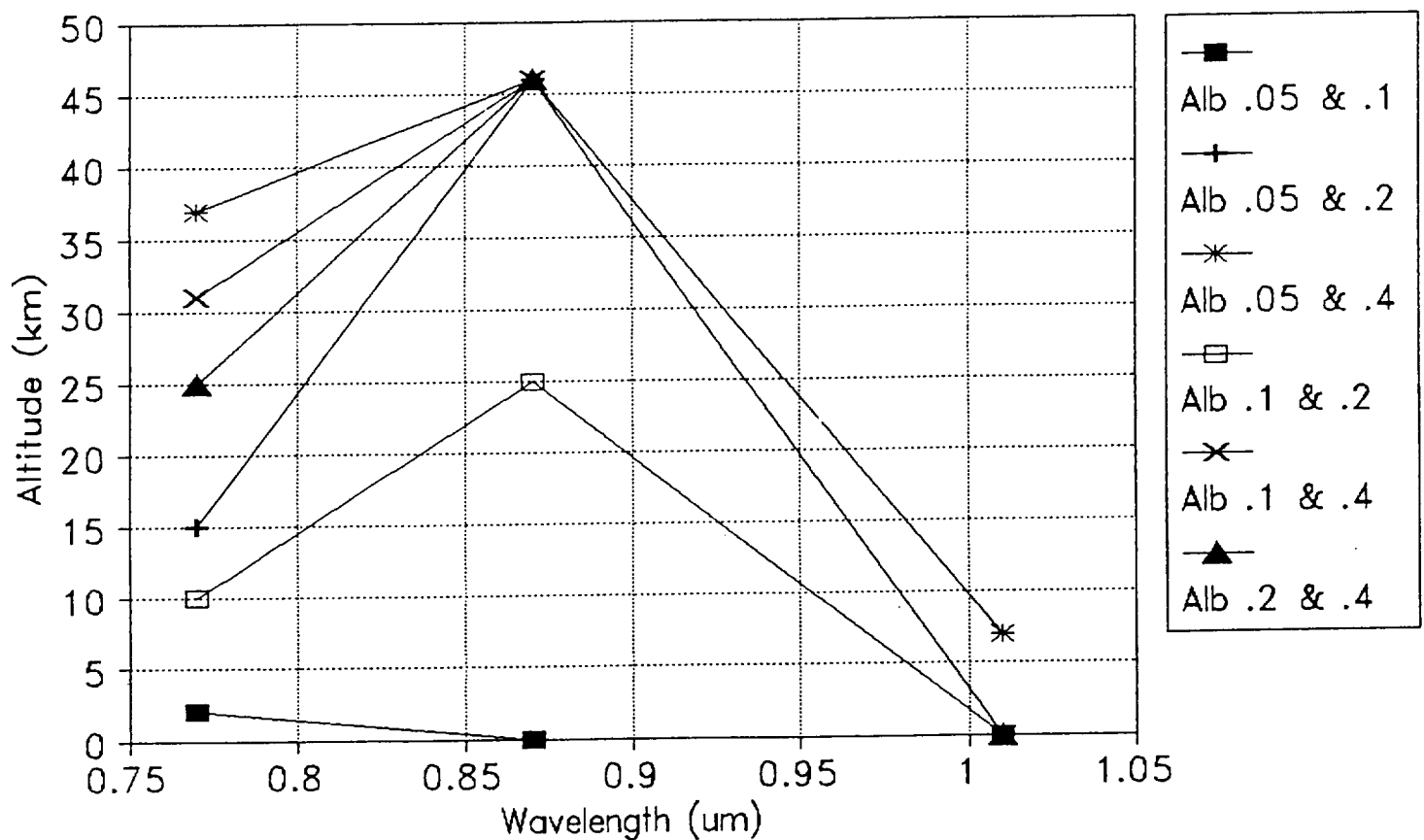## Solar Zenith = 20, Contrast SNR >40

Legend:
- ■ — Alb .05 & .1
- + — Alb .05 & .2
- ✱ — Alb .05 & .4
- □ — Alb .1 & .2
- ✕ — Alb .1 & .4
- ▲ — Alb .2 & .4

X-axis: Wavelength (um)
Y-axis: Altitude (km)

I

Albedo Induced Contrast Detectability .
Solar Zenith = 70, Contrast SNR >40

Legend:
- ■ Alb .05 & .1
- + Alb .05 & .2
- ✳ Alb .05 & .4
- ⊟ Alb .1 & .2
- ✕ Alb .1 & .4
- ▲ Alb .2 & .4

X-axis: Wavelength (um)
Y-axis: Altitude (km)

Albedo Induced Contrast Detectability
Solar Zenith = 85, Contrast SNR >40

Albedo Induced Contrast Detectability
Wavelength = 1.01 um, Contrast SNR >40

4
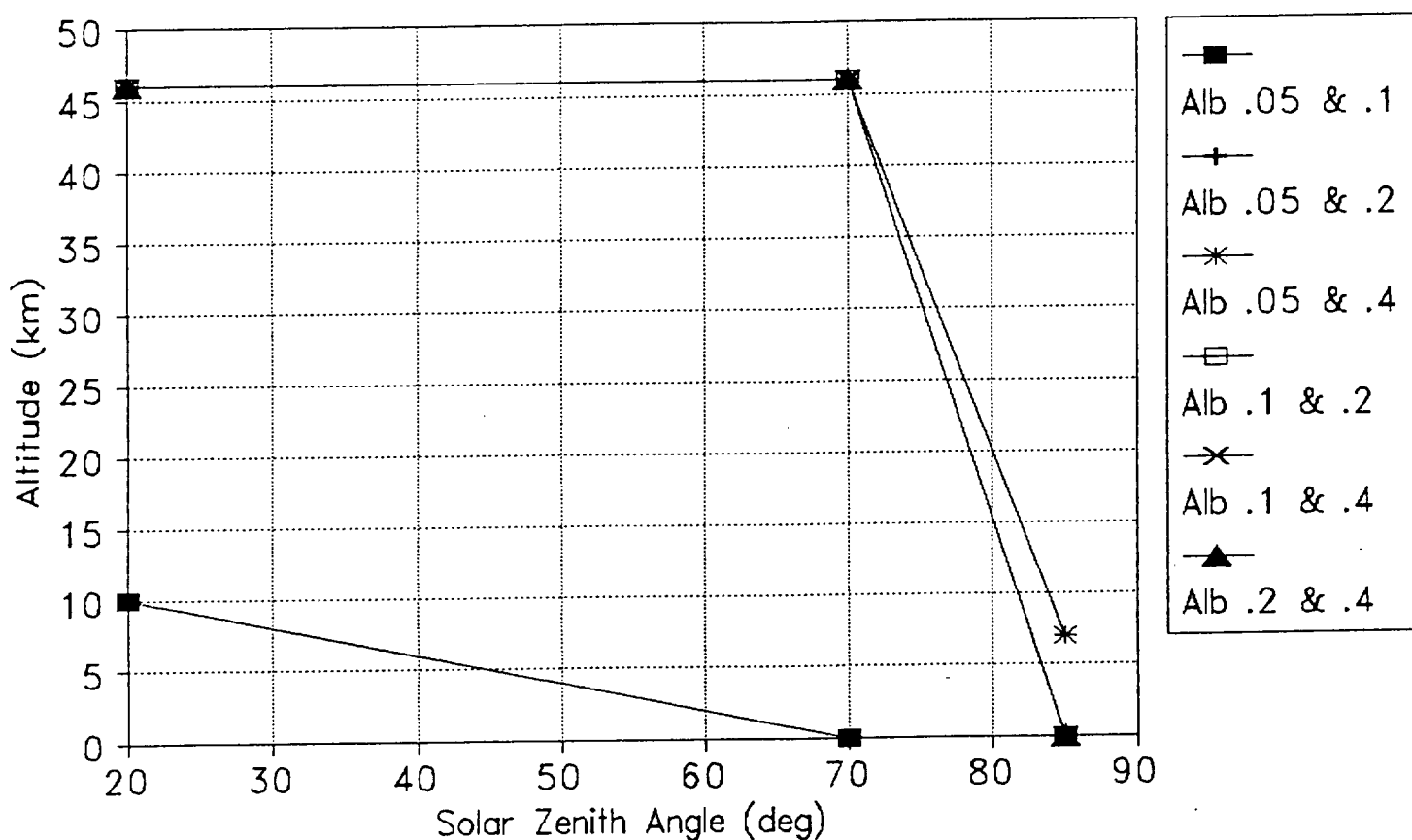
Albedo Induced Contrast Detectability
Wavelength = 0.87 um, Contrast SNR >40

5
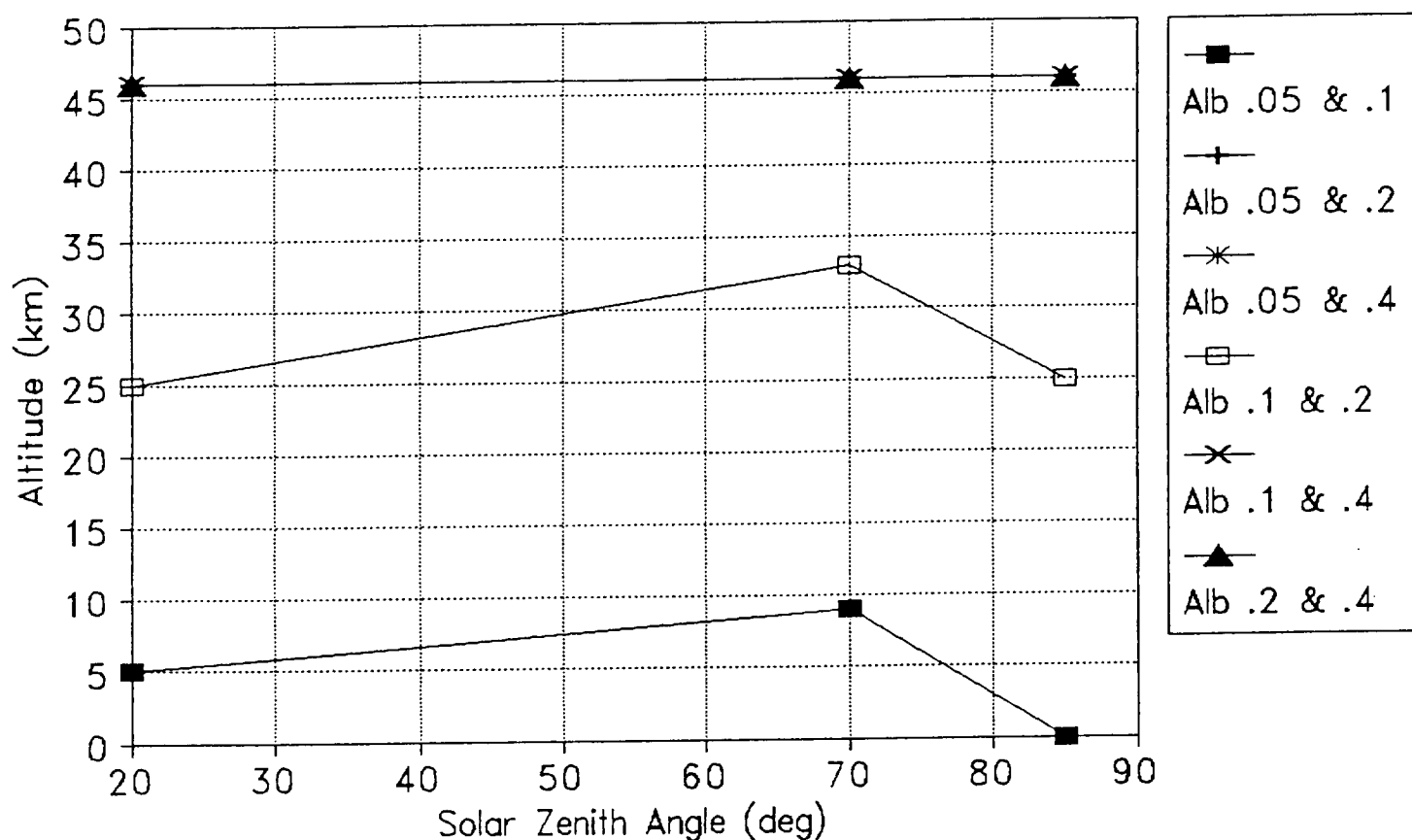
Albedo Induced Contrast Detectability
Wavelength = 0.77 um, Contrast SNR >40
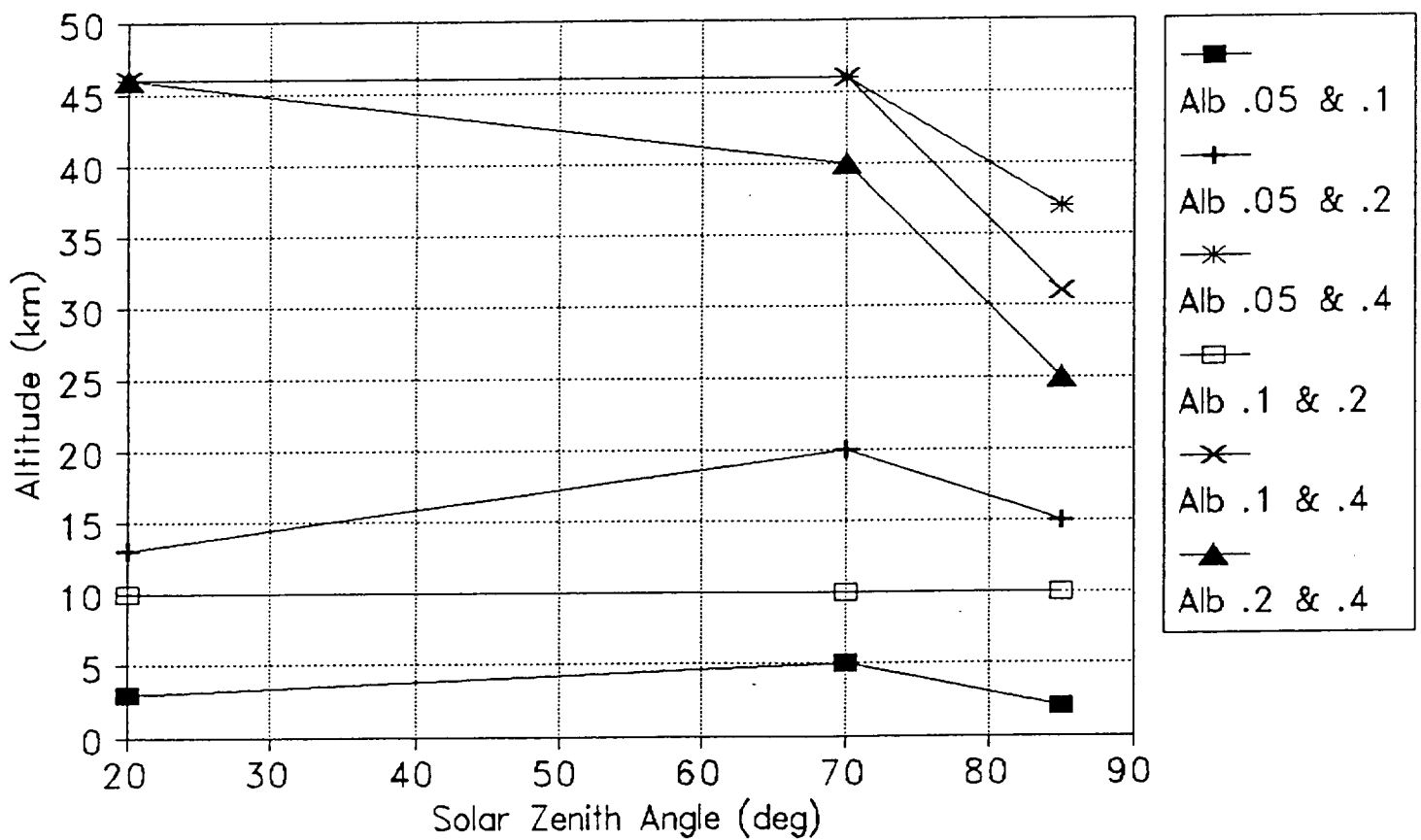
ALBEDO CONTRAST SNR
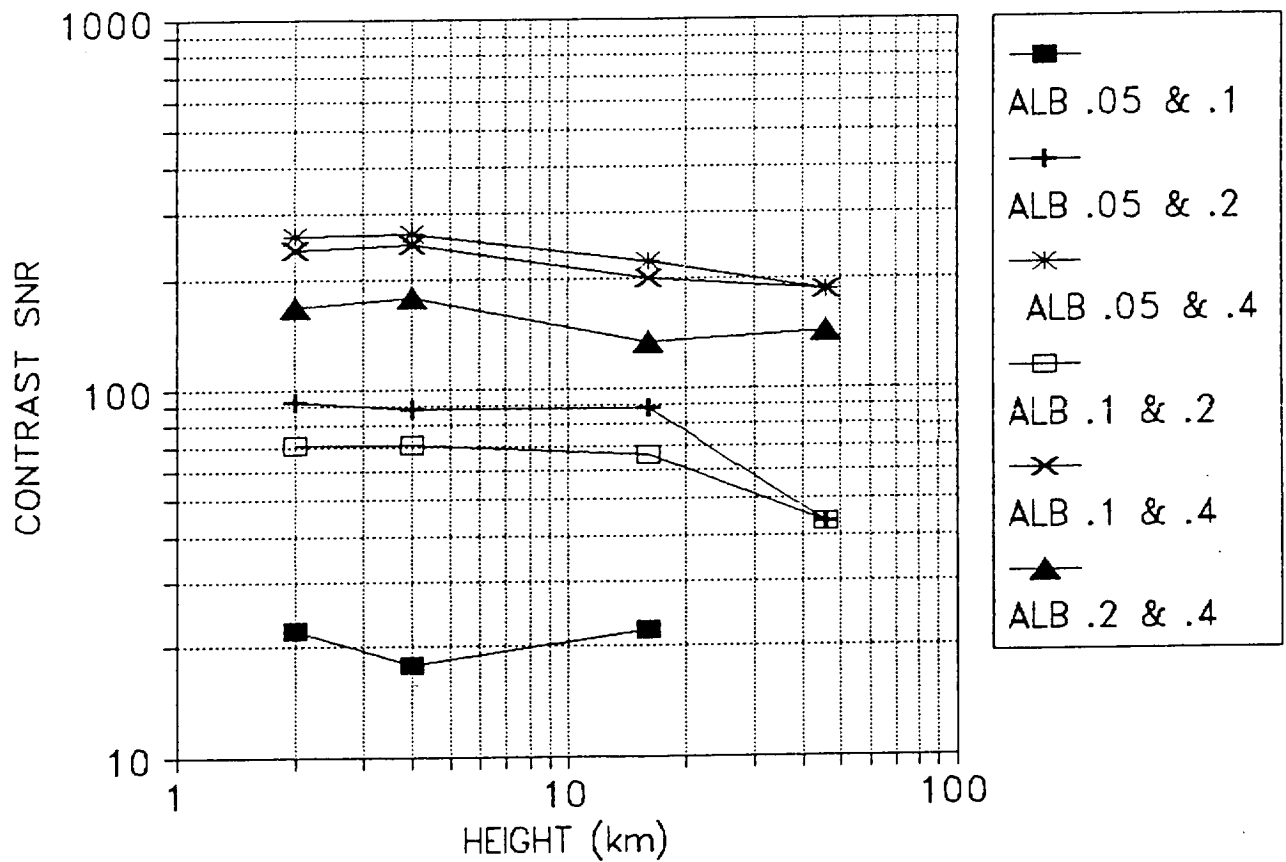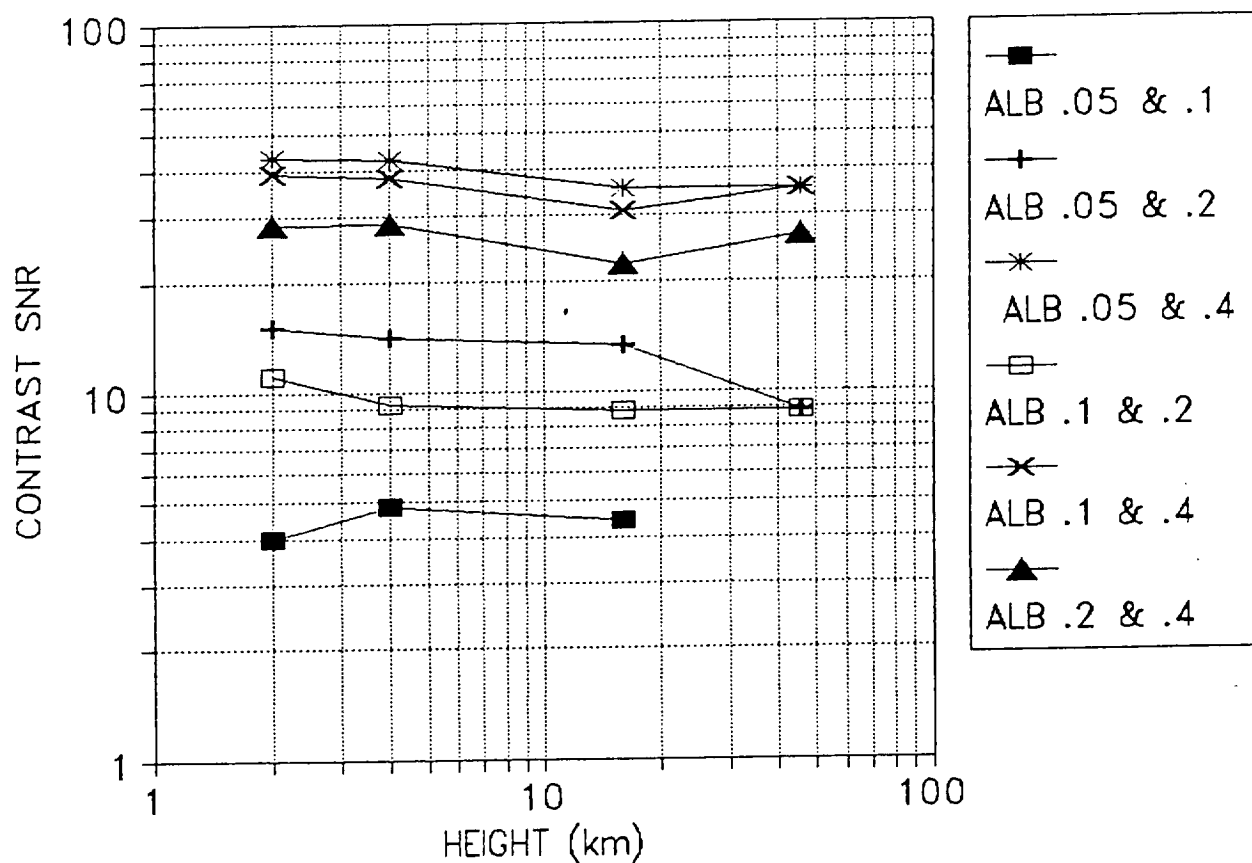## 1.01 um, 20 deg solar zenith, 0 elev
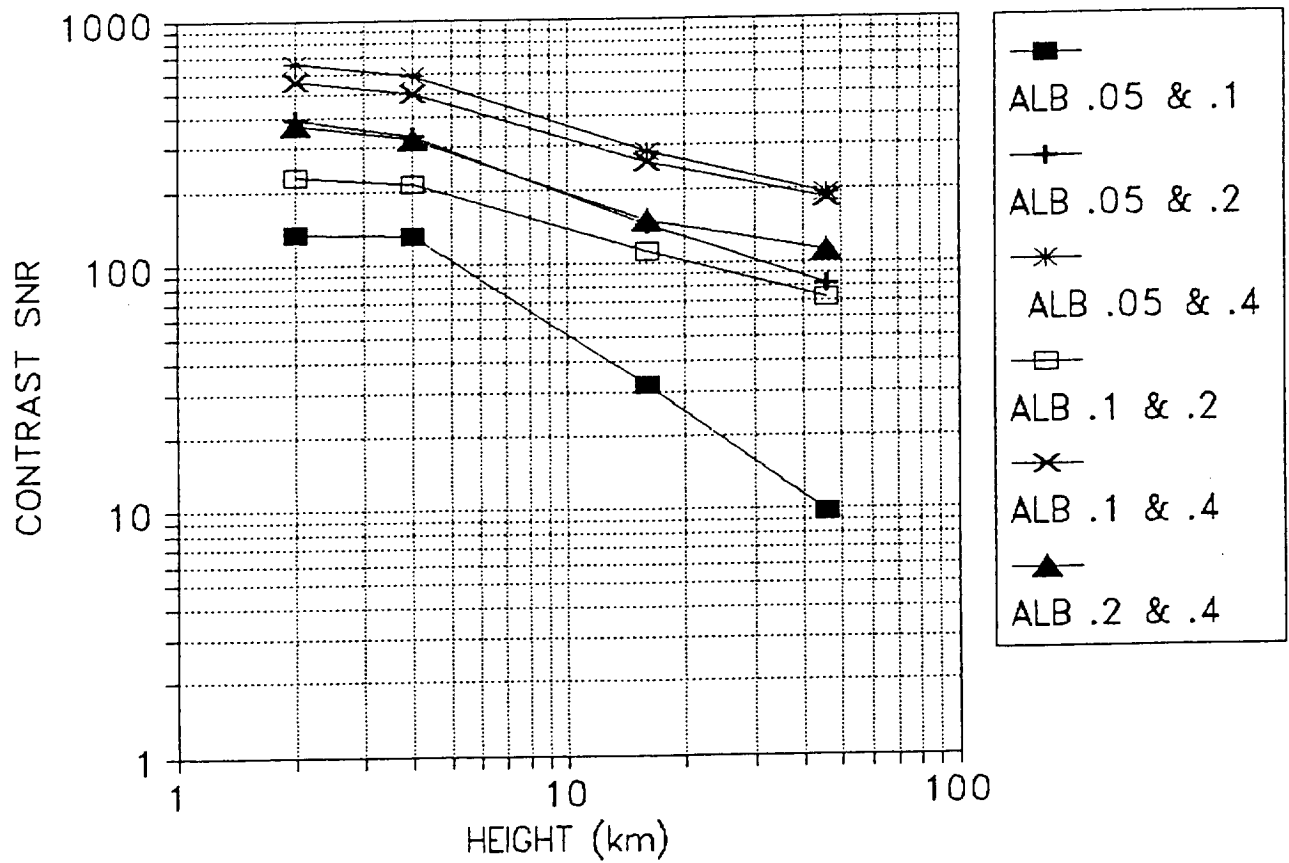
Legend:
- ALB .05 & .1
- ALB .05 & .2
- ALB .05 & .4
- ALB .1 & .2
- ALB .1 & .4
- ALB .2 & .4

Y-axis: CONTRAST SNR

X-axis: HEIGHT (km)

ALBEDO CONTRAST SNR
1.01 um, 70 deg solar zenith, 0 elev

Legend:
- ALB .05 & .1
- ALB .05 & .2
- ALB .05 & .4
- ALB .1 & .2
- ALB .1 & .4
- ALB .2 & .4

Y-axis: CONTRAST SNR (10 to 1000)
X-axis: HEIGHT (km) (1 to 100)

8

ALBEDO CONTRAST SNR

1.01 um, 85 deg solar zenith, 0 elev

Legend:
- ALB .05 & .1
- ALB .05 & .2
- ALB .05 & .4
- ALB .1 & .2
- ALB .1 & .4
- ALB .2 & .4

X-axis: HEIGHT (km)

Y-axis: CONTRAST SNR
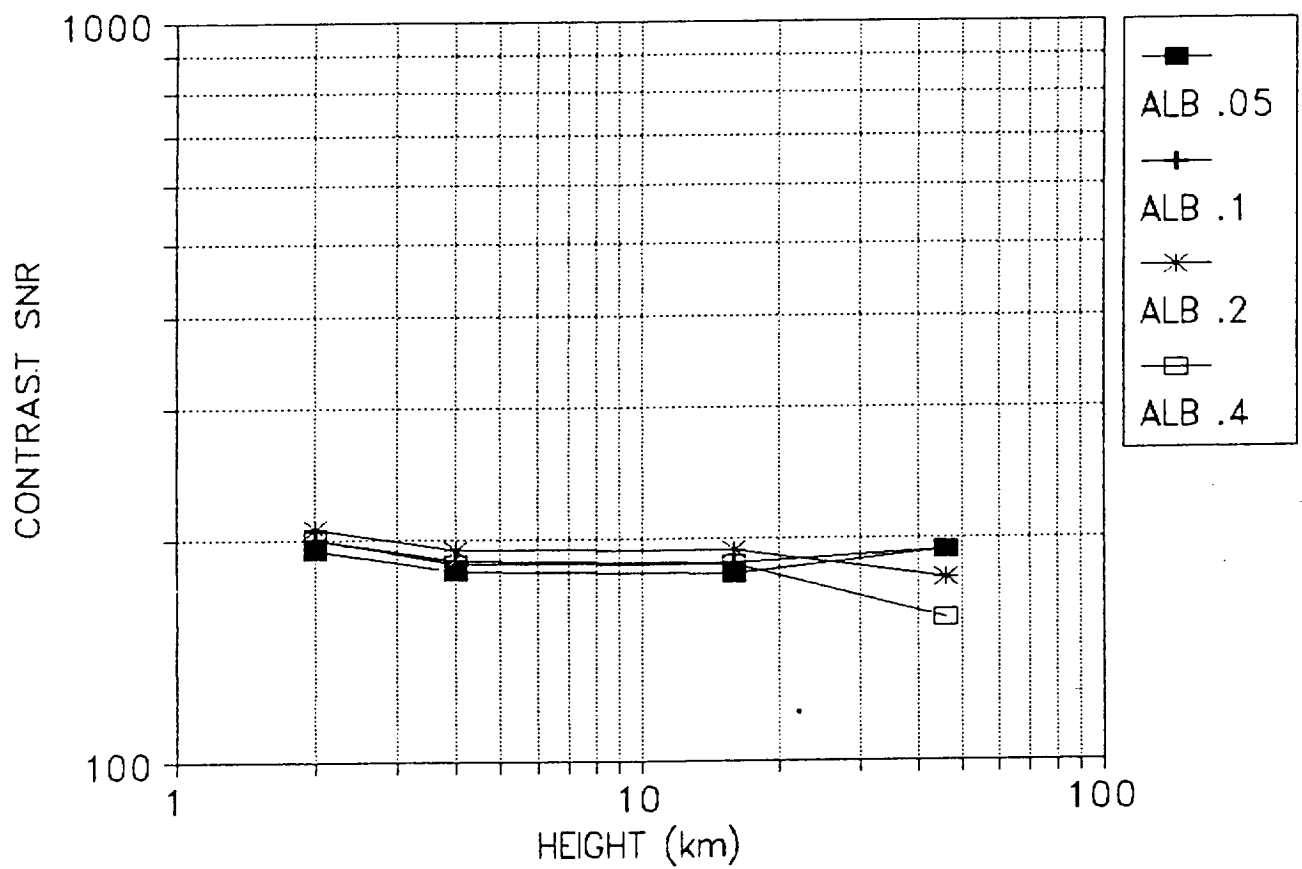
2-KM ELEVATION CONTRAST SNR
1.01 um, DARK, 50-msec EXPOSURE LIMIT

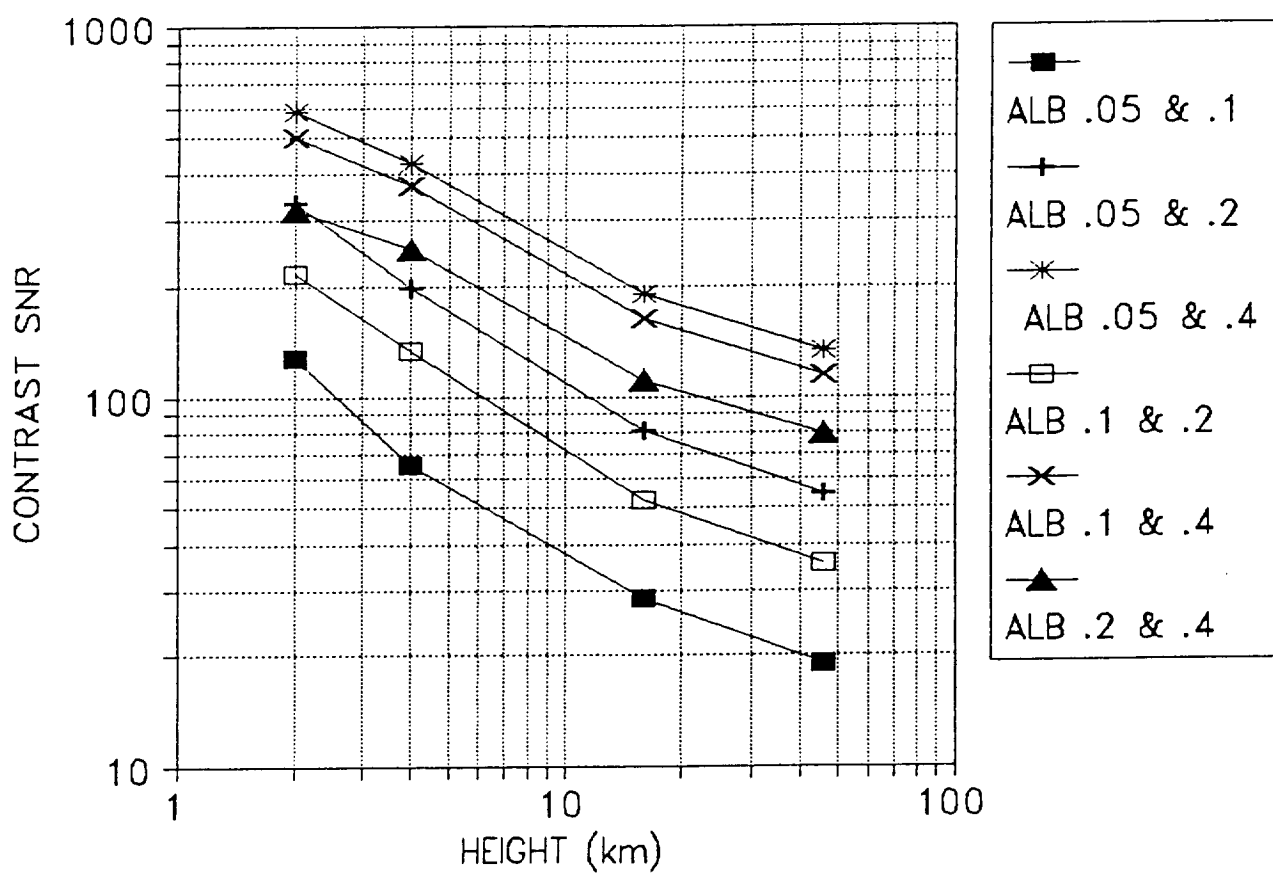# 2-KM ELEVATION CONTRAST SNR
1.01 um, DARK, FW EXPOSURE (~2 SEC)

Legend:
- ■ ALB .05
- + ALB .1
- * ALB .2
- □ ALB .4

Y-axis: CONTRAST SNR (100 to 1000)
X-axis: HEIGHT (km) (1 to 100)

ALBEDO CONTRAST SNR
0.87 um, 20 deg solar zenith, 0 elev

Legend:
- ALB .05 & .1
- ALB .05 & .2
- ALB .05 & .4
- ALB .1 & .2
- ALB .1 & .4
- ALB .2 & .4

Axis labels: CONTRAST SNR (y-axis), HEIGHT (km) (x-axis)

15

ALBEDO CONTRAST SNR

0.87 um, 70 deg solar zenith, 0 elev

Legend:
- ■ ALB .05 & .1
- + ALB .05 & .2
- ＊ ALB .05 & .4
- ☐ ALB .1 & .2
- ✕ ALB .1 & .4
- ▲ ALB .2 & .4

Y-axis: CONTRAST SNR (10 to 1000)
X-axis: HEIGHT (km) (1 to 100)

16
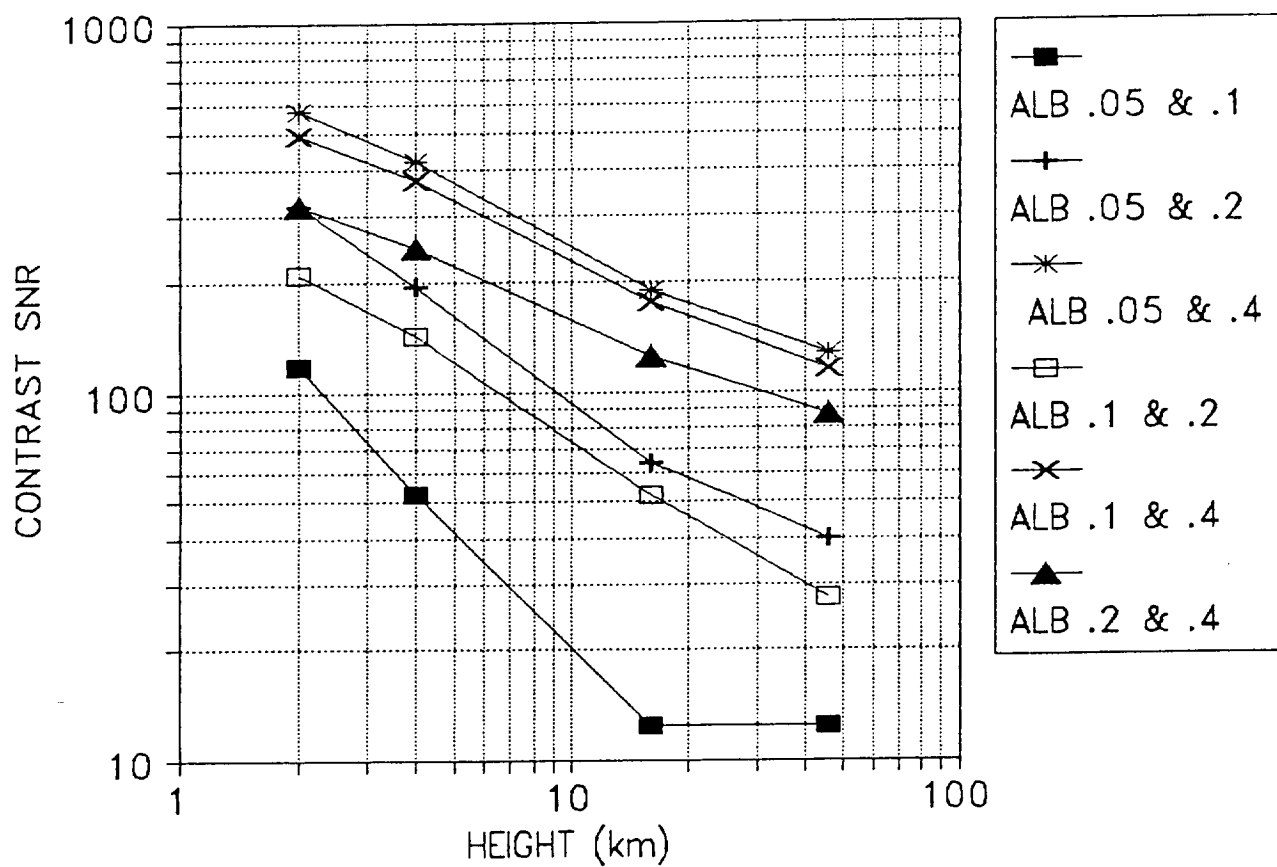
Author: Kenneth P Klaasen at JPL-38DIVISION
Date: 12/13/97 9:27 PM
Priority: Normal
TO: J Balaram at Gateway, Robert Gershman at Zenith, Ronald Greeley at Internet,
     Jeffery L Hall at Gateway, Jack A Jones at jpl-354mail,
     Viktor V Kerzhanovich at Jpl-Div34, Kenneth P Klaasen,
     Elliott Cutting at Gateway
Subject: Venus Imaging Exposure Times

A camera with f/2 optics and an APS or CCD detector with 20-um square
pixels should generate signal at a rate of about

2.5 x 10^5 electrons-sr-m^2-um/(w-sec)

in response to a scene of radiance R w/(m^2 um sr) at a 1-um
wavelength over a bandpass of 0.04 um.

If mounted on a platform that swings at a rate of 1 deg/sec and if the
angular size of a pixel is 1 mrad (to yield 1 m/pixel at an altitude
of 1 km), the exposure time should be kept to less than 50 msec to
keep image smear to 1 pixel or less.

Scene radiances at 1 um below 5 km altitude range from 0.5 to 40 w/(m^2
um sr) depending on the solar zenith angle, the average surface albedo,
and the altitude. To reach a contrast signal-to-noise (SNR) ratio of
40 for a scene with contrast = 0.3, a mean signal level of at least
5000 e- is required. With a 50-msec exposure limit, the scene radiance
would need to be at least 0.4 w/(m^2 um sr). So a 50-msec exposure
limit does not by itself preclude successful Venus surface imaging.
However, this signal level is still far below what I had assumed could
be generated for my previous contrast SNR vs. altitude plots, which had
assumed signal levels of 250,000 e-. This high signal level can be
achieved at 50 msec only for scene radiances in excess of 20 w/(m^2 um
sr). Placing a limit on exposure time to keep smear acceptably small
therefore causes the contrast SNR calculation to depend on a number of
additional parameters that affect the mean signal level, such as
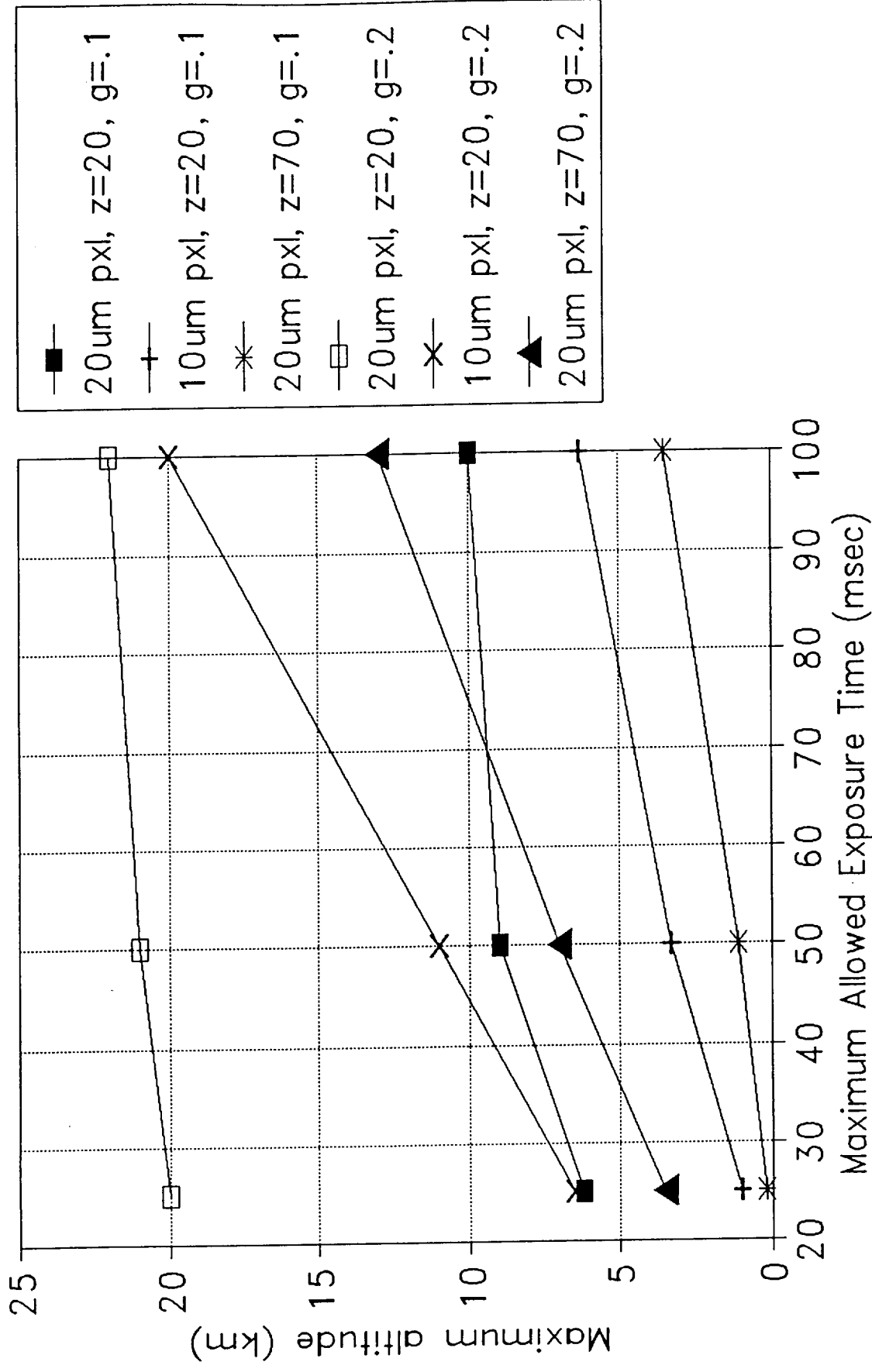surface albedo, optics f/#, and detector pixel size.

I have redone the contrast SNR vs. altitude plots at 1 um assuming
various maximum exposure times while varying the assumed Venus surface
albedo and contrast values and camera parameters such as f/# and/or
pixel size. For a 50-msec maximum exposure time, surface albedo of
0.1, and contrast of 0.3, adequate contrast SNR (40) can be achieved
at altitudes up to about 9 km for 20-um pixels at f/2 and a 20-deg
solar zenith angle. Increasing the solar zenith angle to 70 deg
reduces the maximum possible altitude to about 1 km. If the average
surface albedo is really 0.2 or if the optics are made f/1, the
maximum altitudes increase to 21 and 7 km, respectively. So
acceptable imaging with a 50-msec limit appears to require fairly low
solar zenith angles and either 20-um pixels at f/2 or 10-um pixels at
f/1 given a reasonable set of assumptions about the albedo and
contrast of the Venus surface.

The previously recommended gondola window size of 2-cm diameter was
based on a detector with 10-um pixels rather than the 20-um pixels
assumed here. That window sizing also allowed for resolutions of 0.5
m/pixel from an altitude of 1 km (vs. 1 m/pixel here) and assumed a
1024x1024 detector array. Realizing a resolution of 0.5 m from 1 km
would limit exposures to 25 msec unless the gondola swing rate is less
than 1 deg/sec. So we should probably not try for better than 1
m/pixel from 1 km. Accepting a resolution of 1 m/pixel from 1 km
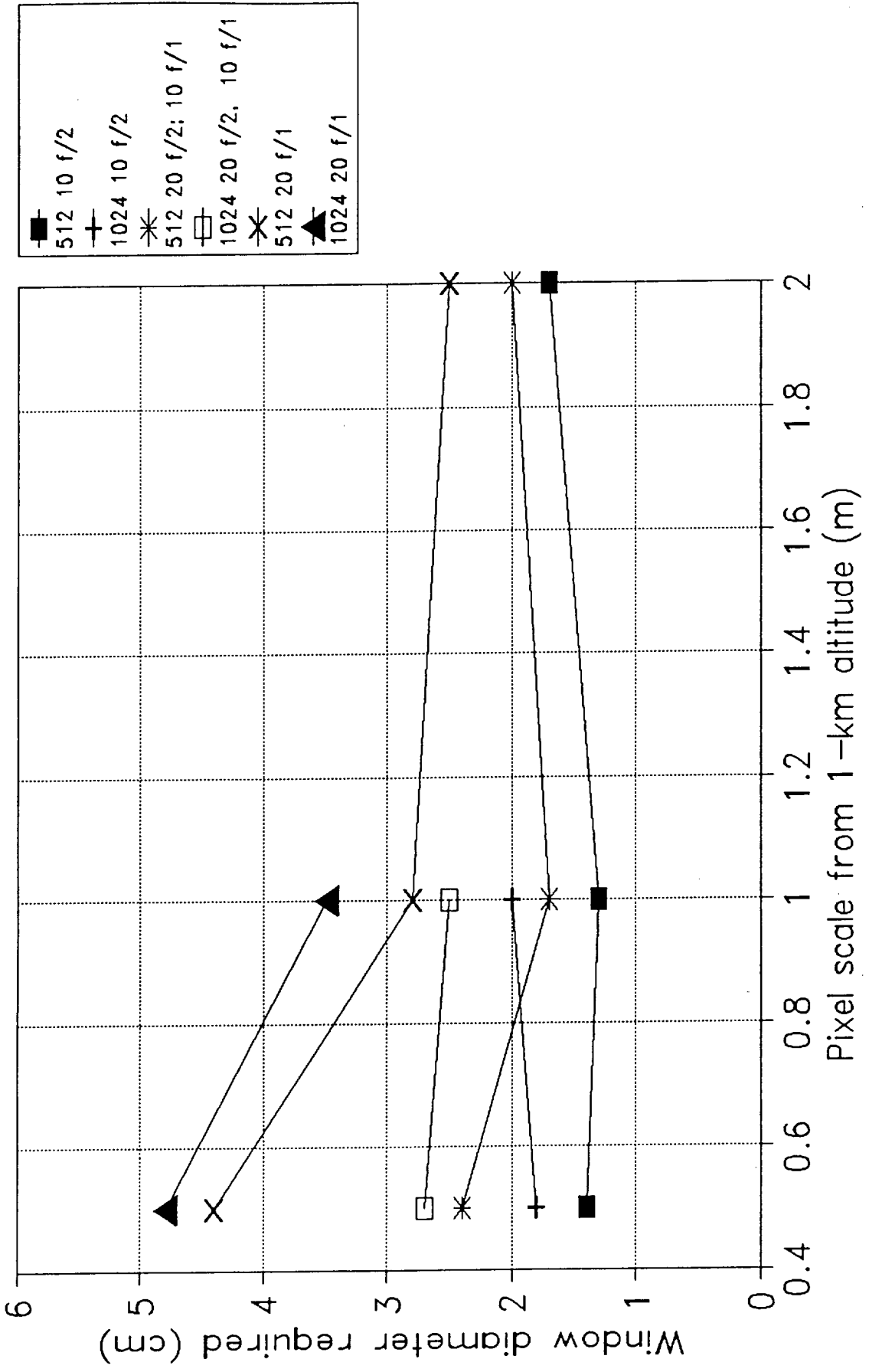altitude requires the window diameter to be 2.5 cm for a 1024 array

assuming we can reduce the setback distance between the optics entrance aperture and the exterior of the gondola window to 1 cm (vs. the 2 cm I had assumed in the previous study). Limiting the window to the previously recommended value of 2 cm restricts the detector array to 512x512.

Increases to the altitude and/or solar zenith angle at which adequate contrast SNR can be achieved would be possible if the gondola stability were better than assumed thus allowing longer exposures, the surface albedo or contrast were higher than assumed, or faster optics with 20-um pixels (with a window diameter of 3 to 3.5 cm) could be used. Performance at shorter wavelengths than 1 um still needs to be evaluated.

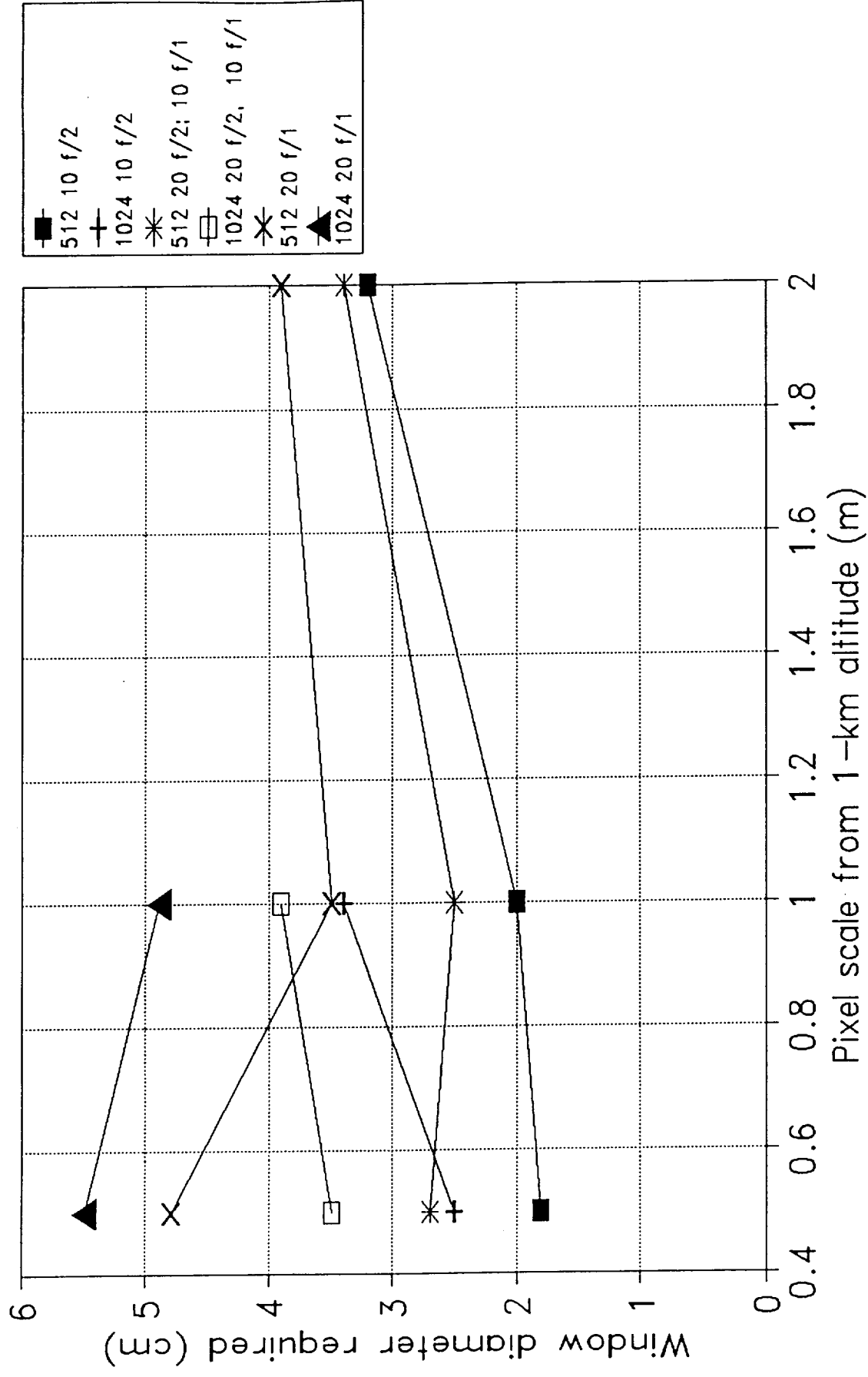Maximum Altitude for Quality Imaging
1.01 um, f/2, SNR=40, c=0.3

Legend:
- 20um pxl, z=20, g=.1
- 10um pxl, z=20, g=.1
- 20um pxl, z=70, g=.1
- 20um pxl, z=20, g=.2
- 10um pxl, z=20, g=.2
- 20um pxl, z=70, g=.2

Maximum Allowed Exposure Time (msec)

Maximum altitude (km)

Gondola Window Diameter
1-cm optics-to-window setback

Legend:
- 512 10 f/2
- 1024 10 f/2
- 512 20 f/2; 10 f/1
- 1024 20 f/2, 10 f/1
- 512 20 f/1
- 1024 20 f/1

Pixel scale from 1-km altitude (m)

Window diameter required (cm)

Gondola Window Diameter
2-cm optics-to-window setback
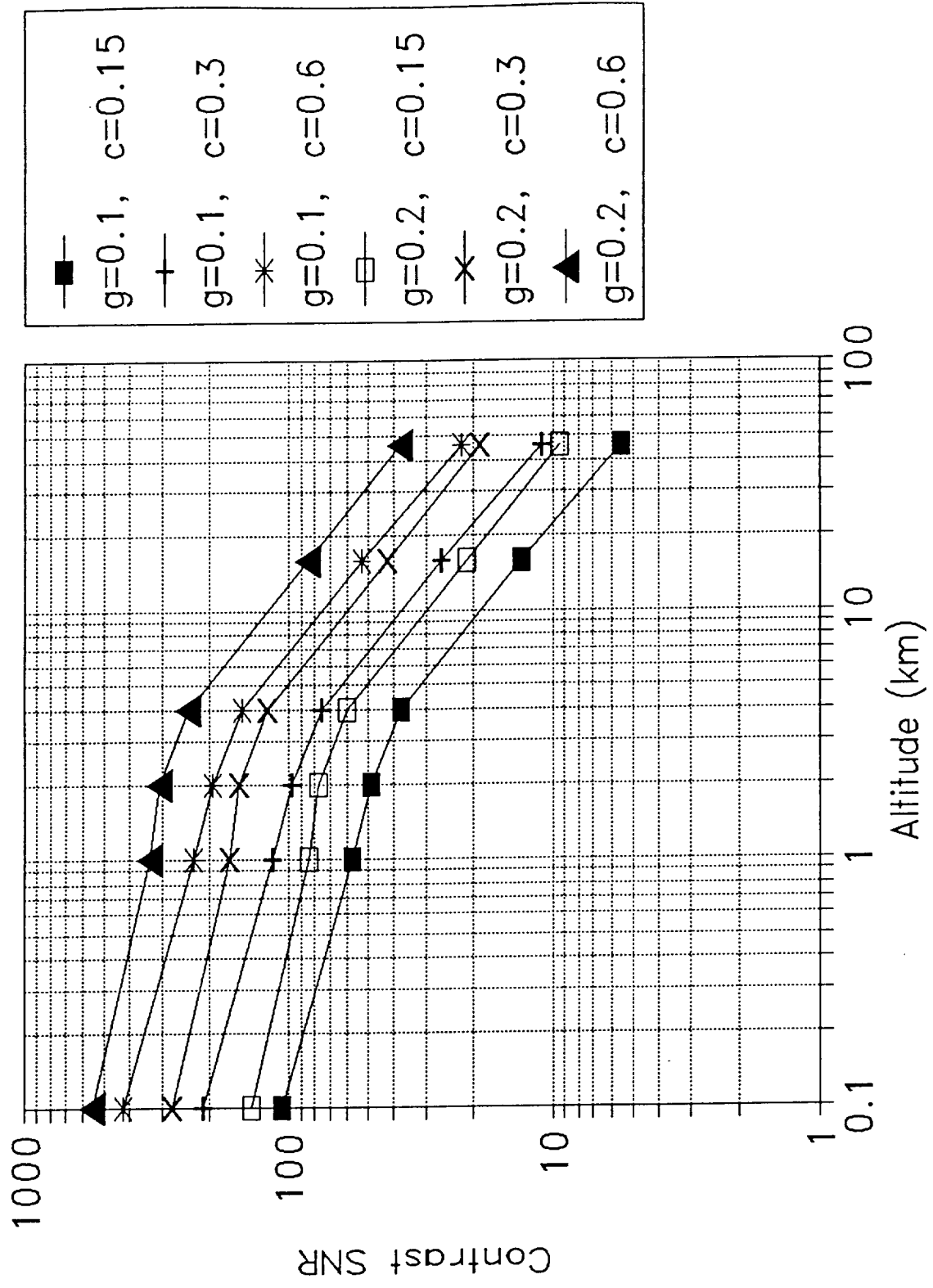
Legend:
- ■ 512 10 f/2
- + 1024 10 f/2
- ✳ 512 20 f/2; 10 f/1
- □ 1024 20 f/2, 10 f/1
- ✕ 512 20 f/1
- ◀ 1024 20 f/1

X-axis: Pixel scale from 1-km altitude (m)

Y-axis: Window diameter required (cm)

Venus Albedo Contrast SNR

1.01 um, z=20, f/2, 20-um pxl, 50 msec

■	g=0.1, c=0.15
+	g=0.1, c=0.3
*	g=0.1, c=0.6
□	g=0.2, c=0.15
✕	g=0.2, c=0.3
◀	g=0.2, c=0.6

Venus Albedo Contrast SNR
1.01 um, z=70, f/2, 20-um pxl, 50 msec

■	g=0.1,	c=0.15
+	g=0.1,	c=0.3
✱	g=0.1,	c=0.6
□	g=0.2,	c=0.15
✕	g=0.2,	c=0.3
◀	g=0.2,	c=0.6

Contrast SNR

Altitude (km)

e

Venus Albedo Contrast SNR
1.01 um, z=85, f/2, 20-um pxl, 50 msec

Legend:
- g=0.1, c=0.15
- g=0.1, c=0.3
- g=0.1, c=0.6
- g=0.2, c=0.15
- g=0.2, c=0.3
- g=0.2, c=0.6

X-axis: Altitude (km)
Y-axis: Contrast SNR

4

Venus Albedo Contrast SNR

1.01 um, z=20, f/2, 20-um pxl, 25 msec

■	g=0.1, c=0.15
+	g=0.1, c=0.3
✳	g=0.1, c=0.6
☐	g=0.2, c=0.15
✕	g=0.2, c=0.3
◄	g=0.2, c=0.6

Altitude (km)

Contrast SNR

a

Venus Albedo Contrast SNR
1.01 um, z=20, f/2, 20-um pxl, 100 msec

Legend:
- ■ g=0.1, c=0.15
- + g=0.1, c=0.3
- ✳ g=0.1, c=0.6
- □ g=0.2, c=0.15
- ✕ g=0.2, c=0.3
- ◀ g=0.2, c=0.6

X-axis: Altitude (km)
Y-axis: Contrast SNR

Venus Albedo Contrast SNR
1.01 um, z=20, f/2, 10-um pxl, 50 msec

■	g=0.1, c=0.15
+	g=0.1, c=0.3
✳	g=0.1, c=0.6
☐	g=0.2, c=0.15
✕	g=0.2, c=0.3
◄	g=0.2, c=0.6

Contrast SNR

Altitude (km)

m
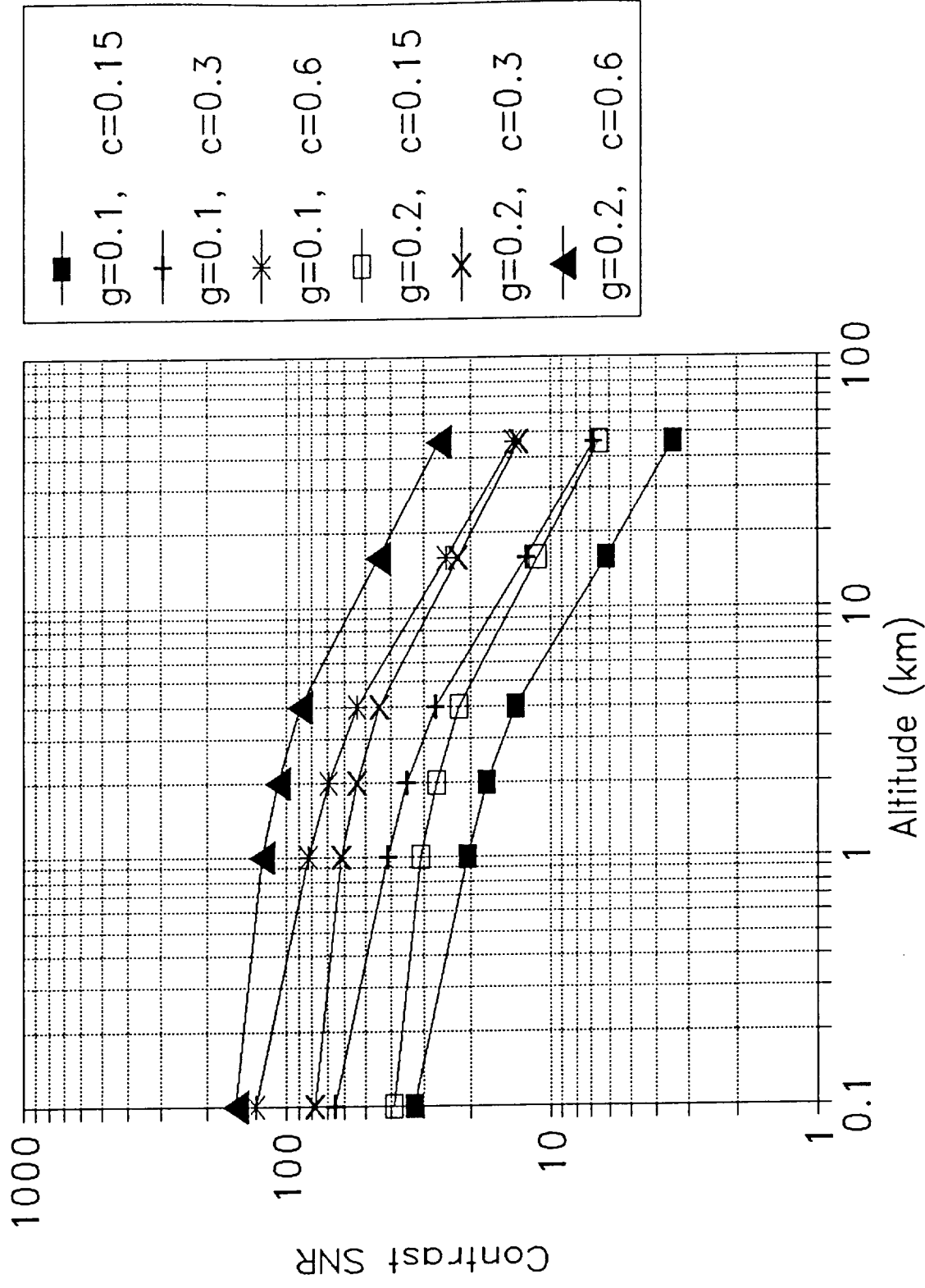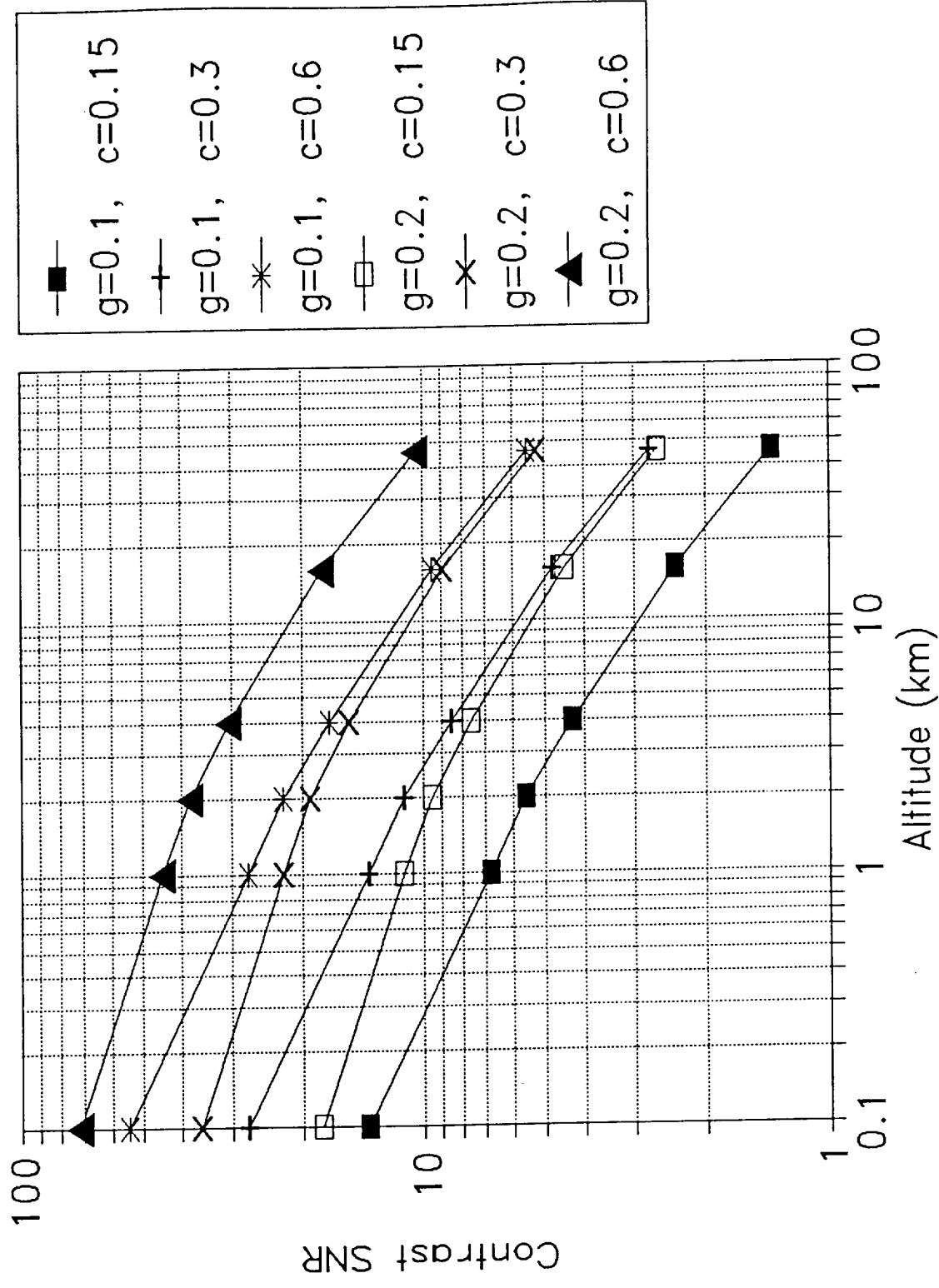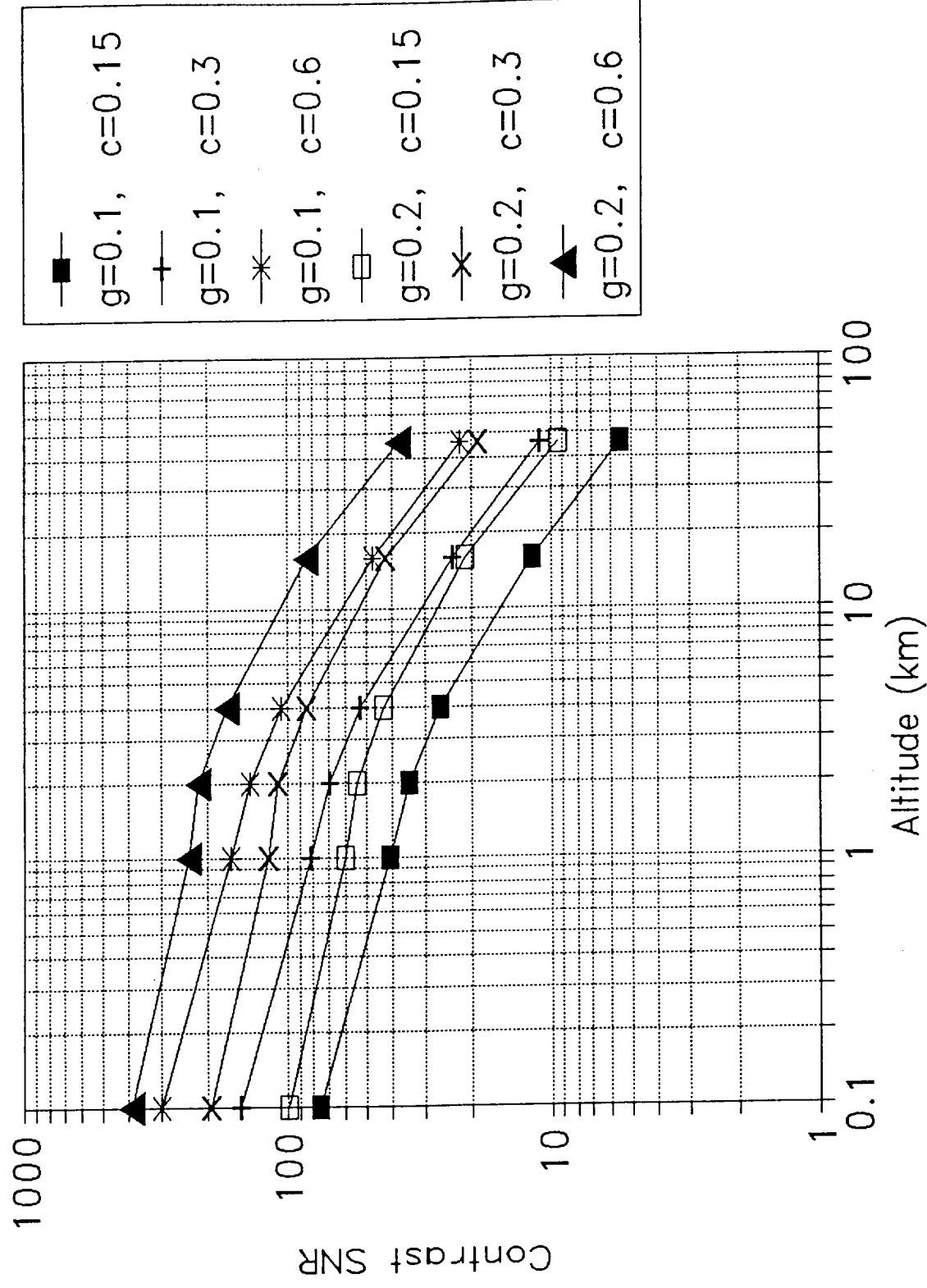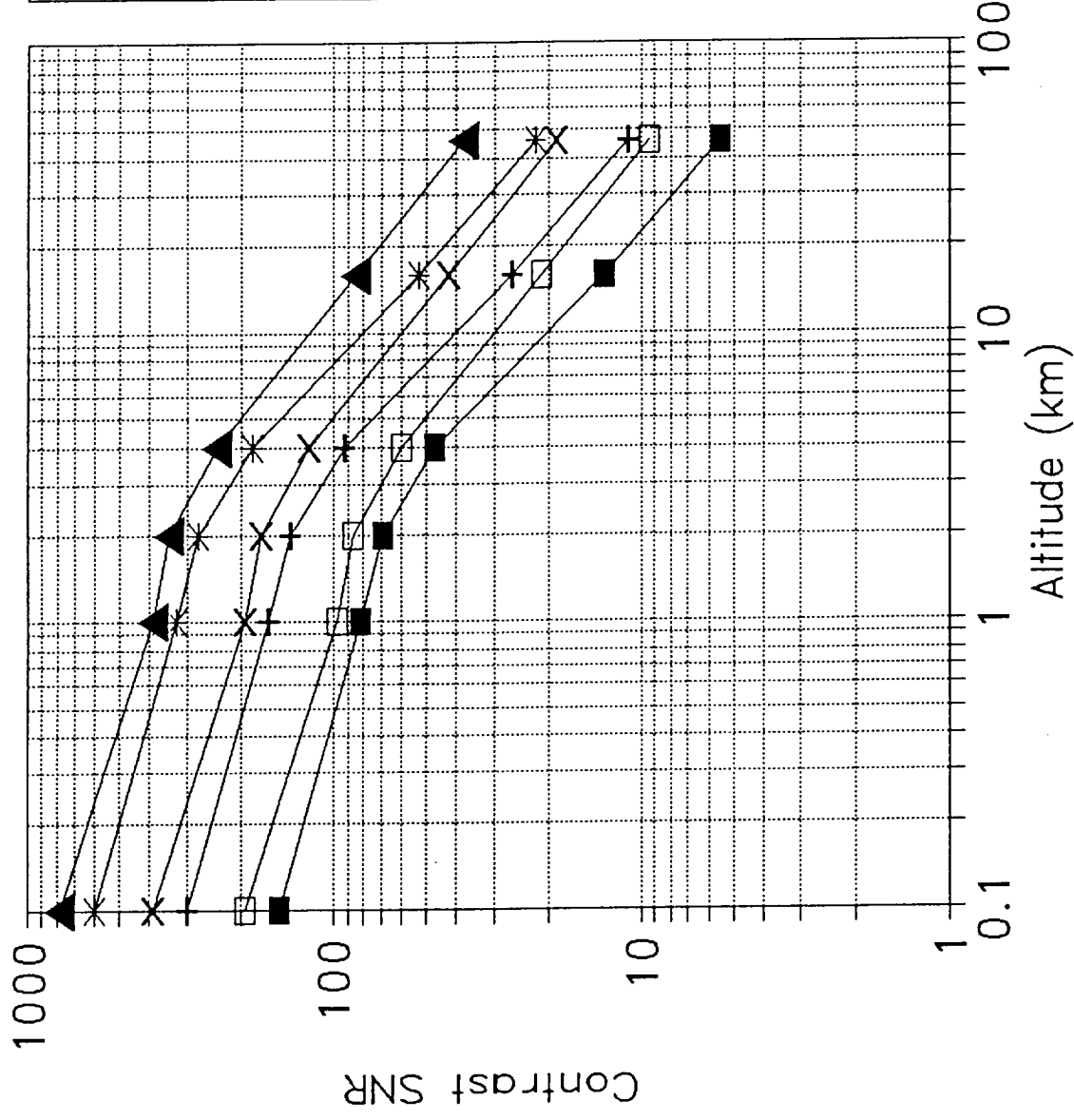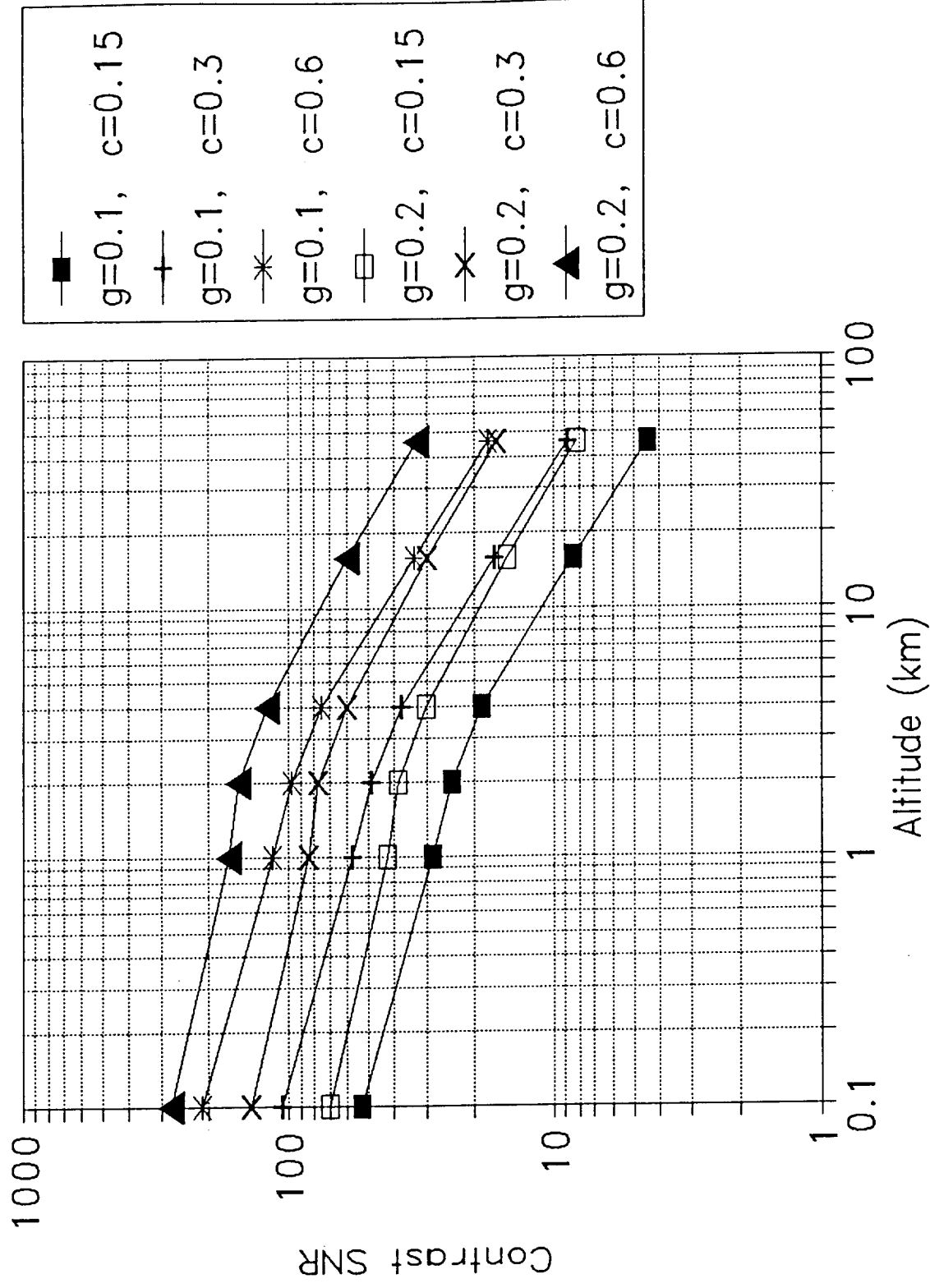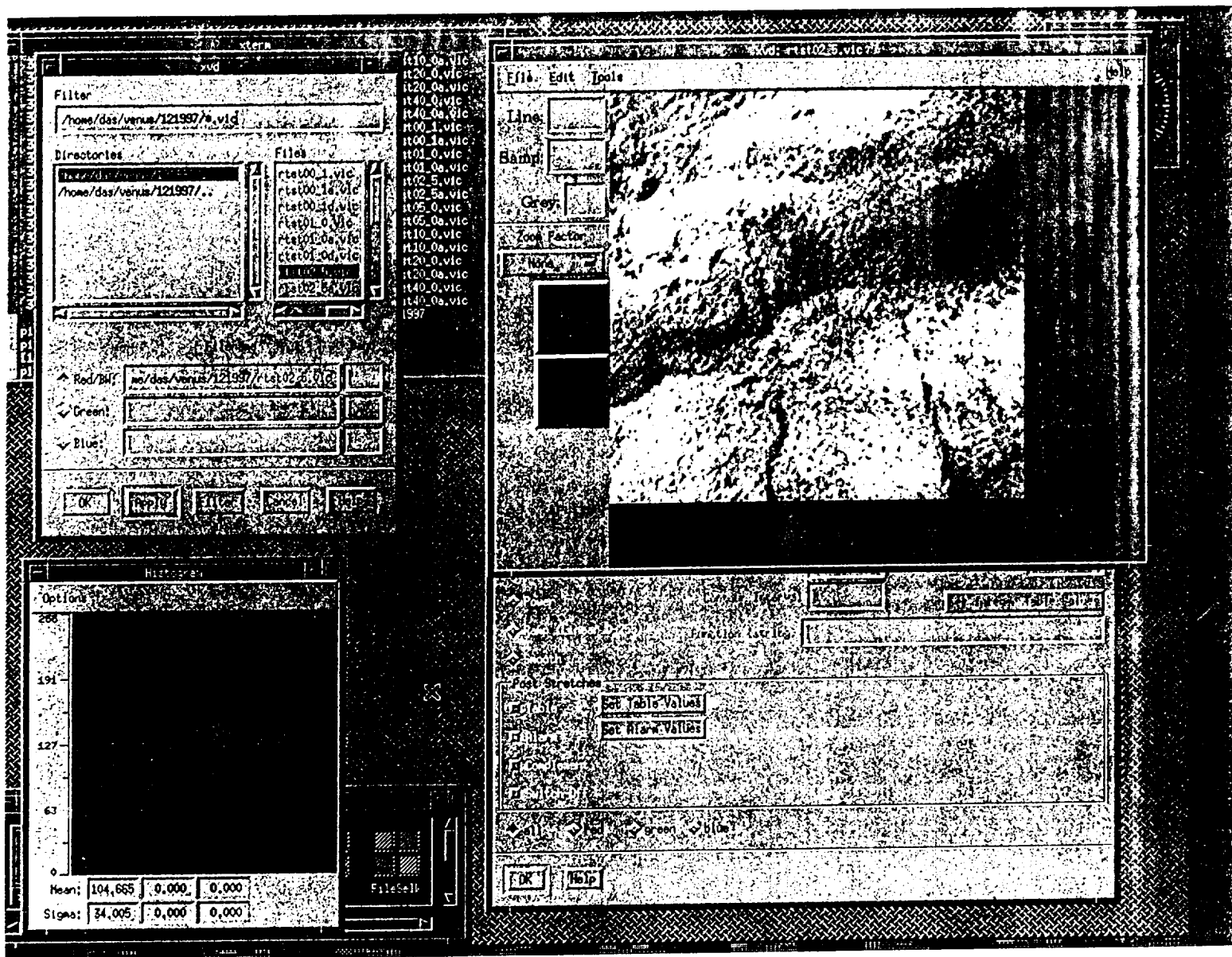
Inyo elevation   2.5 km altitude view
Direct illumination
No atmosphere or albedo variations
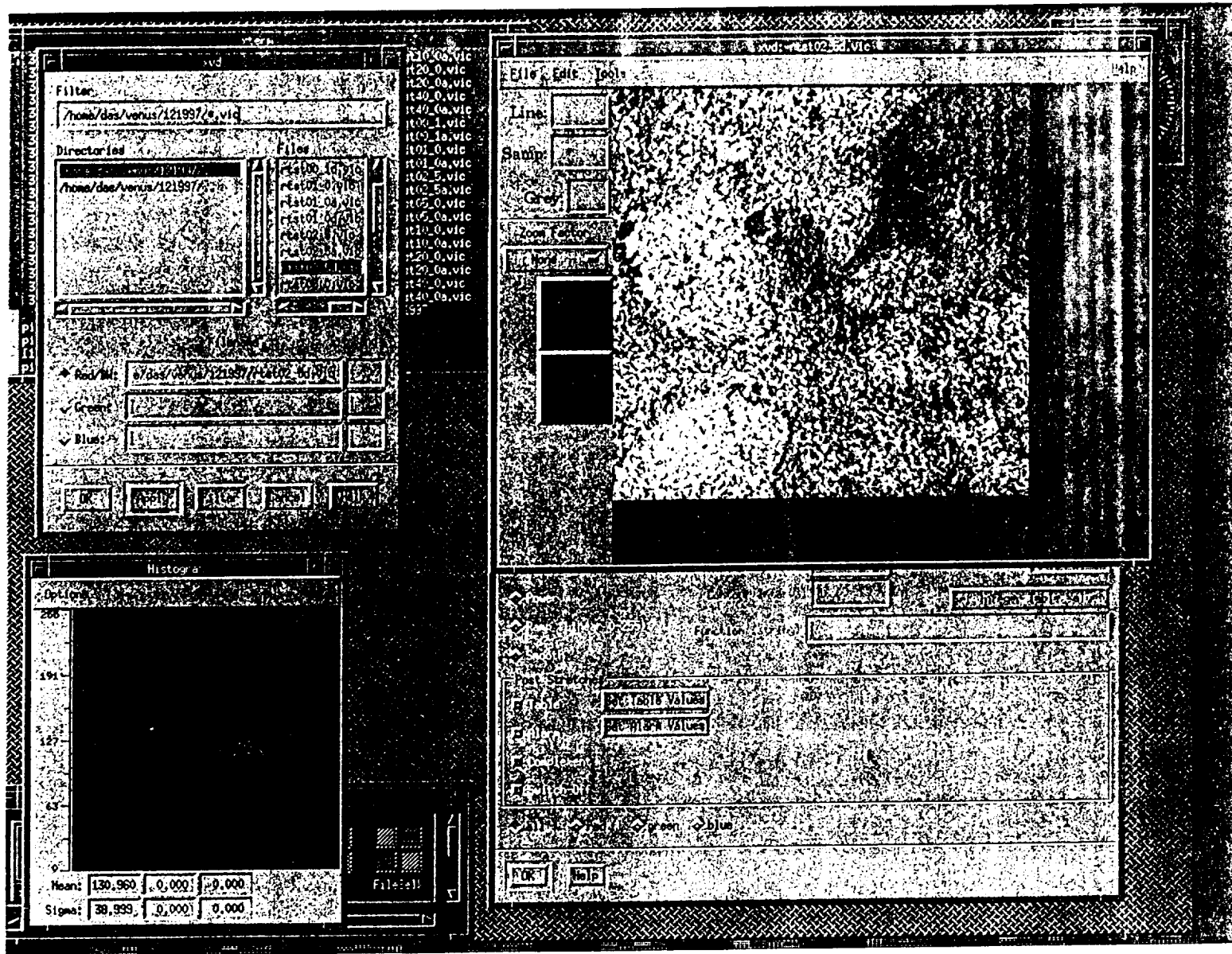
Imyo albedo   2.5-km attitude view

0.04 - 0.16

contrast = 0.55
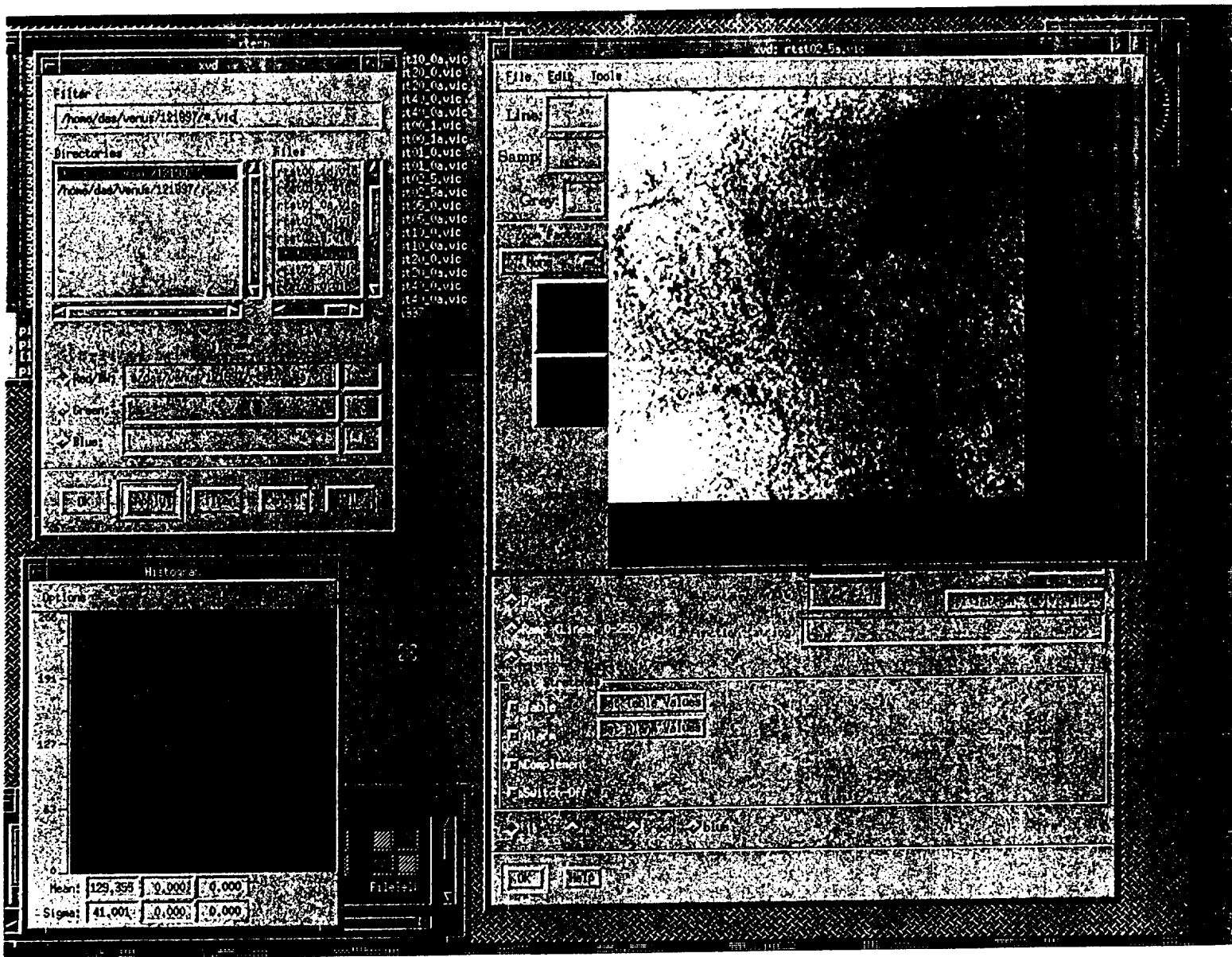
Imago elevation + albedo contrast   2.5-km altitude
Diffuse illumination viewed   view
      thru atmosphere
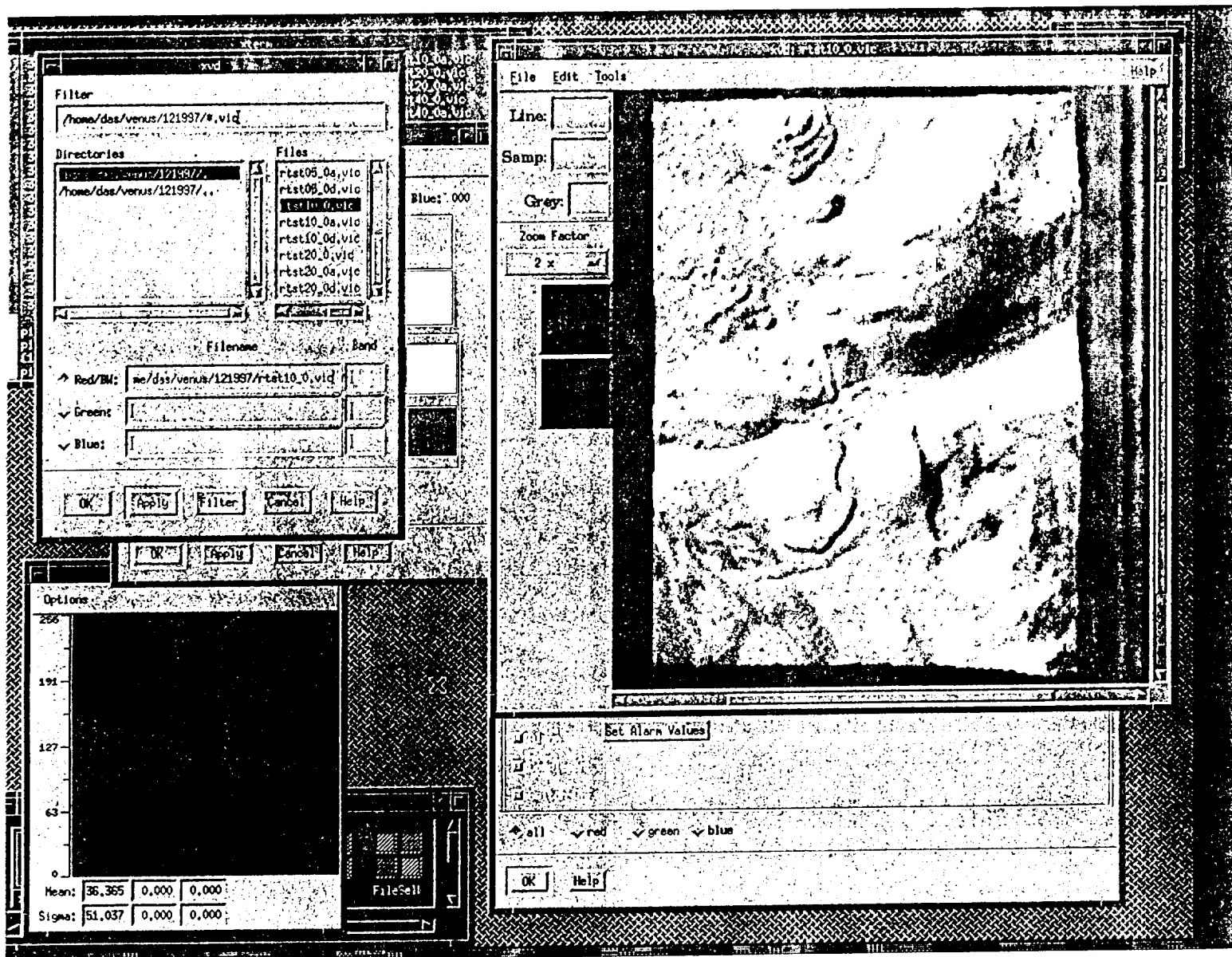
Inyo elevation   10-km altitude view (2x
Direct illumination
No atmosphere or albedo variations
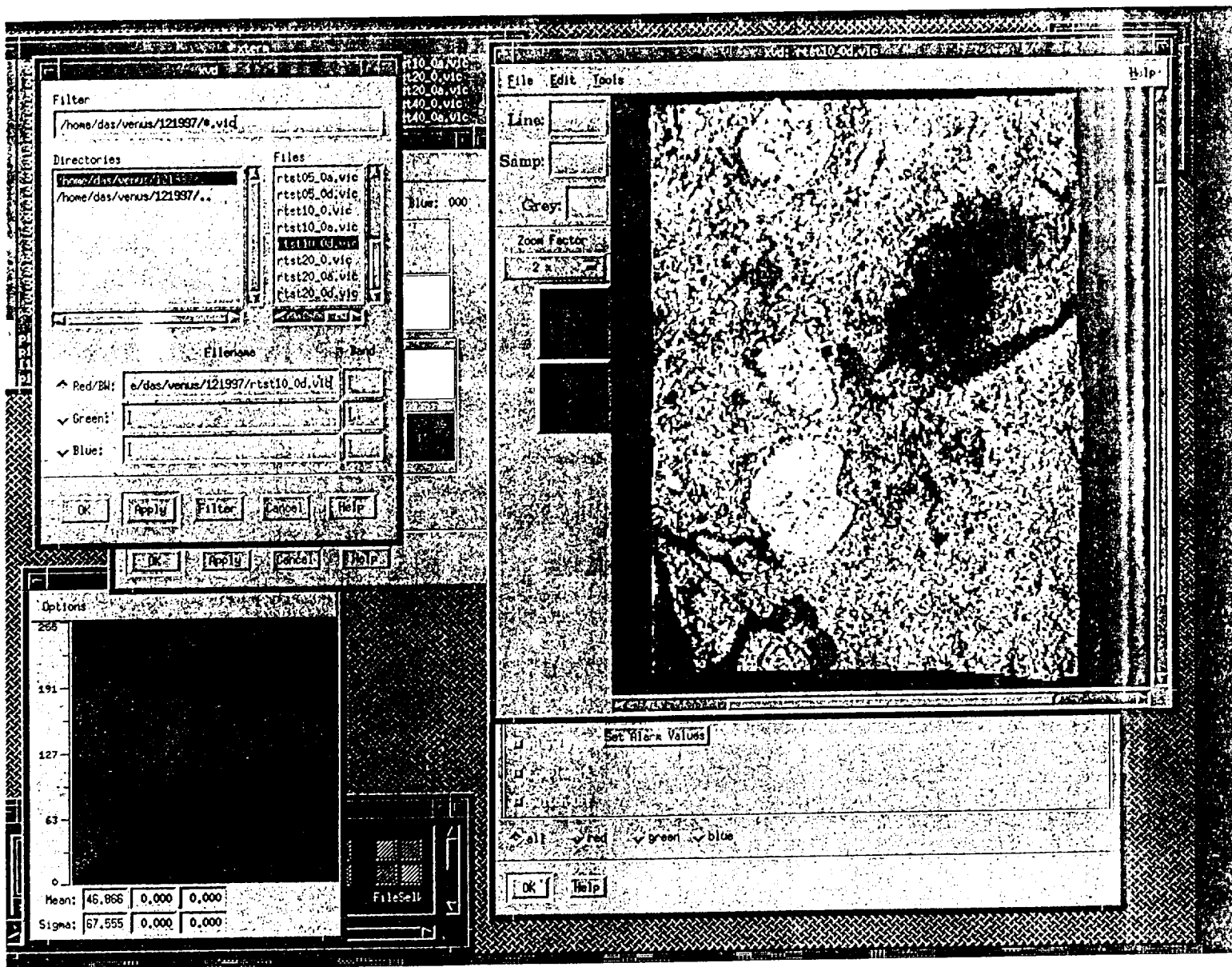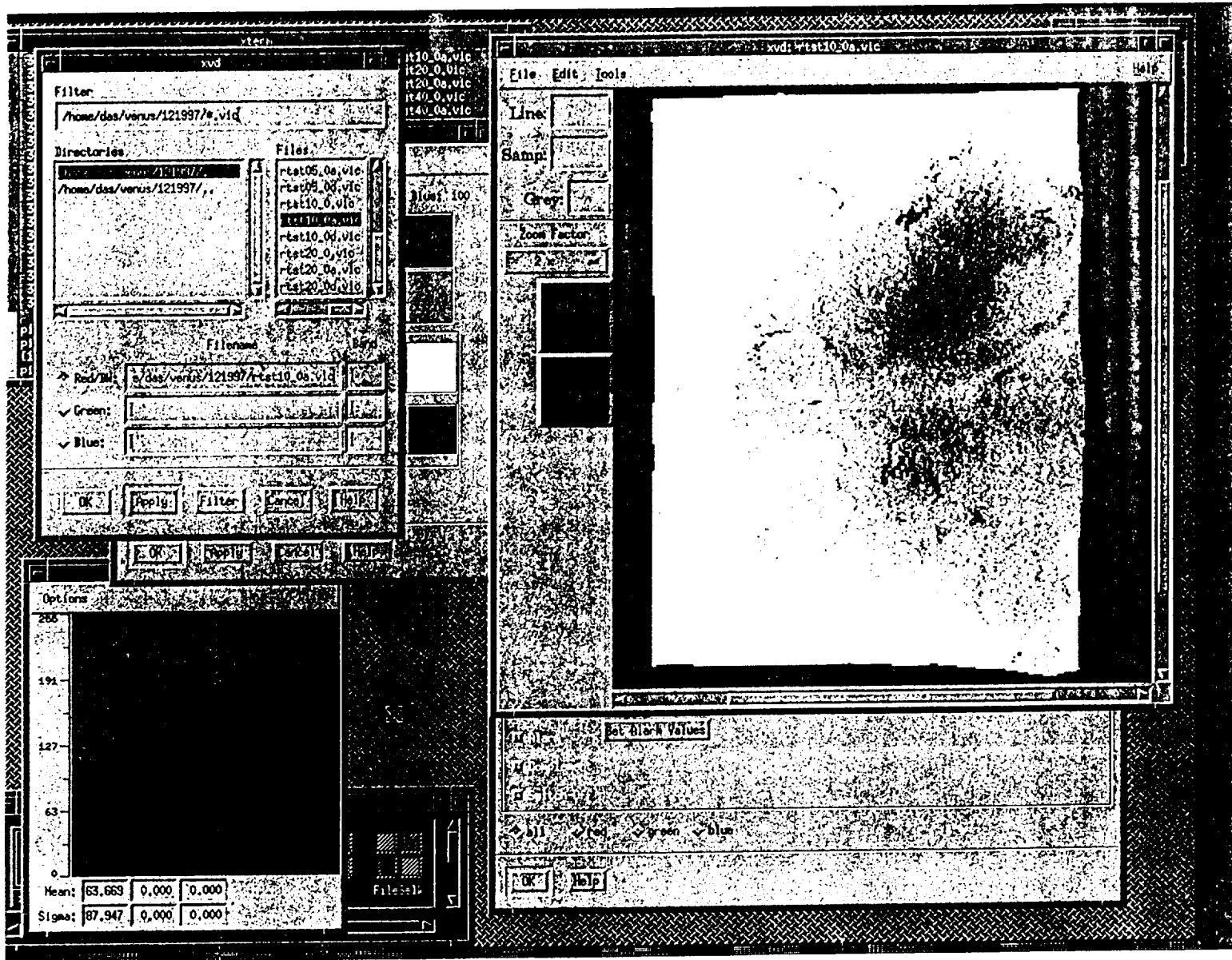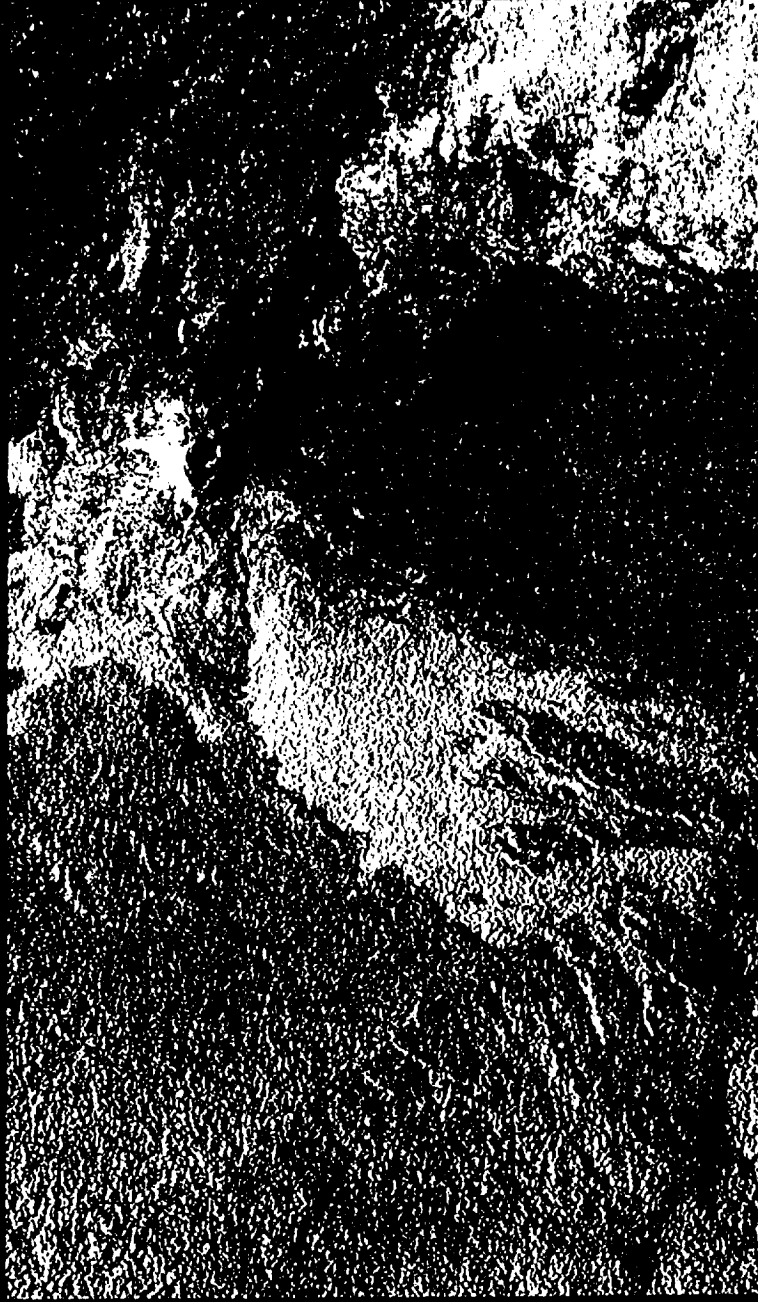
Inyo albedo 10-km altitude view (2x)

0.06 → 0.15

contrast 0.41

Imago elevation + albedo contrast   10-km altitude
Diffuse illumination viewed   view (2x)
thru atmosphere.

Puu Oo, Hawaii
Directional Illumination, Zenith Angle = 60 deg
Sun from top of image

Puu Oo, Hawaii
Isotropic Illumination

JET PROPULSION LABORATORY

INTEROFFICE MEMORANDUM
352G:96:146:MS

November 6, 1996

TO: Ken Klaasen

FROM: Moktar Salama

SUBJECT: The VASSIS Gondola Structural Design

The attached gives a summary of the VASSIS gondola structural design concept and an analytical assessment of its viability for use in Venus Aerobot Surface Science Imaging System.

MS:mvc

cc: J. Cutts
       G. Forsberg
       J. Garba
       M. Heun
       S. Langenbeck
       J. Jones
       B. Kent
       T. Nock
       D. Senske
       A. Vaughan
       E. Villegas
       A. Yavrouian

I. VASSIS Gondola Design Concept:

After considering several options, environmental design conditions, and constraints, the mechanical design for the gondola structure evolved into the layouts detailed in the attached drawings .

A spherical shape is ideal for a pressure vessel. The VASSIS gondola consists of a 15 inch diam, 0.10 inch thick Ti alloy outer spherical shell enclosing a 12 inch diameter inner spherical shell. As a housing for the science instruments such as the camera, the inner spherical shell is made of 0.05 inch thick Ti alloy and is secured in place by a set of tension band supports which suspend the inner spherical shell from the outer one (see drawing # 10169316). The tension bands can be cable-like members made of braided Polybenzoxazole (BPO) fiber material discussed in Ref. (1), or they can be Ti alloy rods having a circular cross section. The attached drawings show conceptual details of how the bands are used as a suspension system to join the inner and outer spherical shells. The number and size of the bands is a design parameter discussed in a later paragraph.

In addition to the tension band suspension system, the one inch vacuum space between the two spherical shells is intended to contain the multi-layer thermal insulation material (MLI), diode heat pipe, phase change material (PCM), and the camera viewport. Both of the inner and outer spherical shells are constructed from two half-spherical shells, with ring reinforcements at the interface between the two halves of each of the inner and outer spherical shells. One of the important considerations for the gondola design was that the sequence of assembly of the entire gondola system be amenable to easy assembly and disassembly, with minimum re-work. The assembly sequence for the proposed design is summarized in the sketch in Fig. (1).

The optical bench and camera layout are discussed elsewhere, but their design drawing are attached here for relevant details as drawing # 10170667 and 10172016.

II. Environmental Design Conditions:

The gondola system must be designed to withstand launch, atmospheric entry, and in-flight environments at Venus. Of these environments, the most severe conditions are predicted to be about 500 g deceleration during Venus atmospheric entry, and 100 bars pressure at 460 C near Venus surface. Clearly, the 500 g deceleration loading occurs independent from the other conditions, but the 100 bars pressure and the 460 C occur simultaneously. The instruments contained in the inner shell housing are to be maintained at normal room operating temperature. The table below summarizes the various components of the gondola system and the degree to which its design is dependent upon the environmental conditions.

Table (1)
DESIGN DRIVERS FOR COMPONENTS OF THE GONDOLA SYSTEM

| | Environmental Conditions | | | | |
	500 g	100 bars	460 C	Thermal Path	Corrosives
Outer Shell	P	P	P		P
Inner Shell	P	S			
Suspension Bands	P	S	P	P	
Sience Instruments	P				
Viewport &Lens	P	P	P	P	P

P: primary consideration
S: secondary consideration

III. Mass Estimate:

In order to verify the initial design discussed above, an estimate of the corresponding total mass is calculated to be about 14.5 kg, excluding the camera, optical bench and other instruments. The break down of this mass is as follows:

- Outer spherical shell   :   5.4 kg
- Inner spherical shell   :   1.9 kg
- Tension band supports :   0.5 kg
- Fittings and seals   :   0.5 kg
- Thermal control system :   5.7 kg (see the thermal design for details)
- Miscellaneous   :   0.5 kg

IV. Analysis Model and Results:

After initial sizing based on approximate hand calculations, a finite element model was created to assess the capabilities of the load carrying components of the gondola. This includes the outer and inner spherical shells, the tension bands which connect them, and the local details of the camera viewport and lens area. The model is shown in Figs. 2a, b, c, and d. The following four loading cases were considered. In all cases, three pairs of bands (each is pre-taut to 150 lb) were used to suspend both halves of the inner shell from the outer one. The pre-load is induced to avoid compressive loading and the possibility of slacking of the bands.

1. Thermal excursions of 460 C on external spherical shell superimposed on 1450 psi pressure. The reference temperature inside the inner spherical shell is about 20 C , which was kept constant. The distribution of temperature in the area surrounding the fused silica camera lens and the Ti conical viewport joining the outer-to-inner spherical shells was based on a separate thermal analysis model shown in Fig 3a, b (curtsey of Matt Heun).

2. A 500 g deceleration vector coincident with the camera lens axis of symmetry (Z-axis). That is, the camera is looking down along the normal to Venus surface.

3. A 500 g deceleration vector tilted 15 degrees in the XZ-plane from the Z-axis.

4. A 500 g deceleration vector tilted 15 degrees in the YZ-plane from the Z-axis.

The results are sampled in Figs 4a, ..., j. The maximum stresses (in psi) due to each of the above four cases in various components of the gondola system are summarized in Table (2) below. In addition, the maximum relative radial displacement (in inches) between the inner and outer shell in the vicinity of the lens and viewport is listed. All stresses are below the critical stresses for the titanium alloy spherical shells, fused silica lens, and BPO (or titanium) tension bands. The exception is the outer sphere stresses under pressure and 460 C temperature.. According to Guss Forsberg, at 460 C, Ti looses about 60% of its room temperature yield strength of about 145000 psi. The remaining 58000 psi is too close to the predicted 55115 psi. A thicker Ti outer sphere (i.e. increase thickness from 0.1 in to 0.125) can provide enough design margins. But the outer sphere mass is increased from 5.4 kg to 6.32 kg. Optionally, at the expense of nearly doubling the mass of the outer sphere (to about 10. kg), the nickel alloy known as Inconel 718 could be a better choice for the outer sphere material.

The maximum relative displacement in the last column of Table (2) is between the inner and outer spherical shells in the vicinity of the viewport - lens. The maximum displacement of 0.114 inch represents "gapping", which can be designed for by allowing sufficient overlap at the junction between the conical viewport and the inner spherical shell.
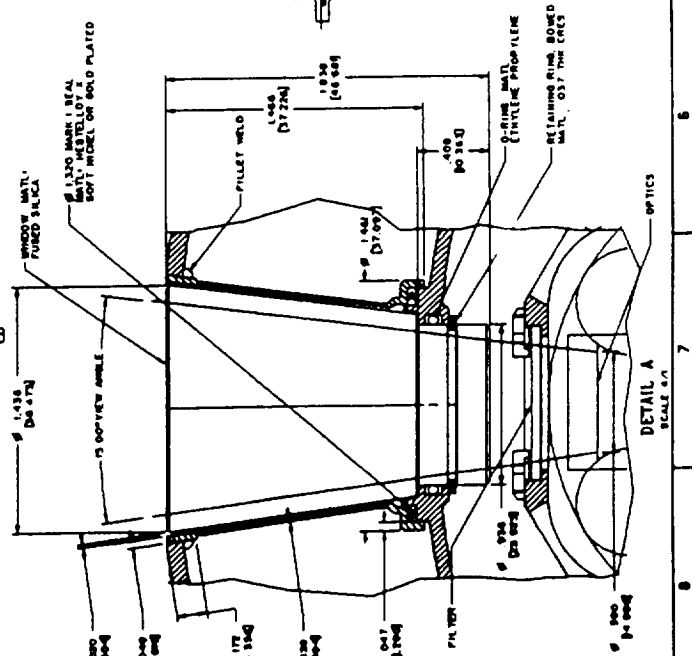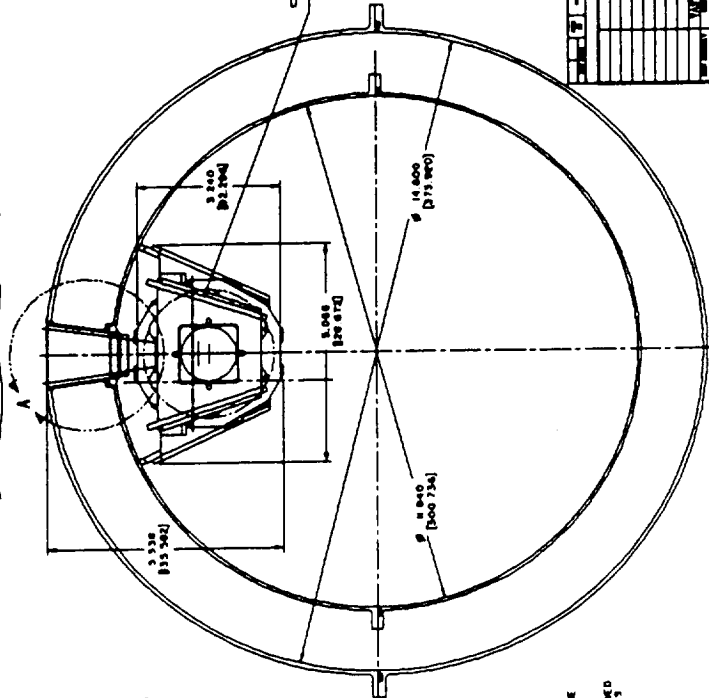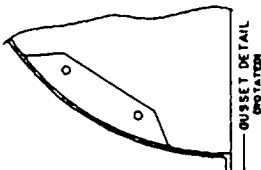
V. SUMMARY

With minor modifications to the preliminary design of the Venus Gondola concept proposed herein, it appears that the proposed concept is structurally viable for entry into Venus atmosphere.
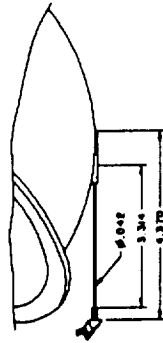
VI. Reference:

1. A. Yavrouian, et al, "High temperature Material for Venus Balloon Envelopes", AIAA, 1995.

Table (2)
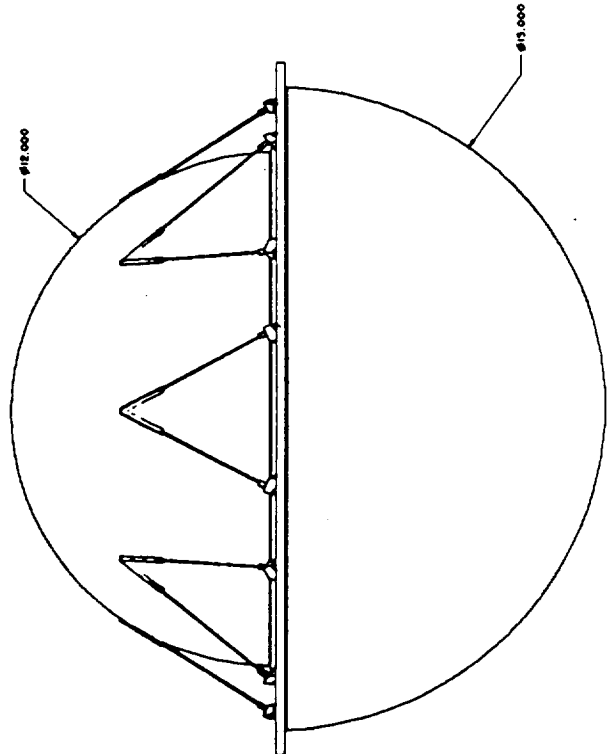Maximum Stresses and Deformation in Gondola

		Maximum Stresses (psi)				Max Disp
	Outer shell	Inner shell	Outer ring	Lens	Band	(inch)
1. Pressure & Thermal	55115	58995	26416	25364	9400	0.026
2 500 g along Z	22982	65800	61557	577	18500	0.048
3 500 g. 15 deg Tilt in X	35114	103800	119050	2211	38478	0.114
4 500 g. 15 deg Tilt in Y	31264	96505	102152	2238	32964	0.114

GUSSET DETAIL
(ROTATION)

WINDOW

OPTICS

SHUTTER

MOTOR

MOTOR

CCD

FILTER CAROUSEL

WINDOW MATL
FUSED SILICA

FILLET WELD

O-RING MATL
ETHYLENE PROPYLENE

RETAINING RING, BOWED
MATL. O37 THK CRES

OPTICS

FILTER

DETAIL A

SUPPORT DETAIL

1/4 SCALE PRINT
DATED 10/10/96

Ø15.000

Ø12.000

SHUTTER

OPTICS

FILTER

WINDOW

ABS ELECTRONICS

MOTOR

ASSEMBLY

Connect Thermal Science Connect Thermal Close
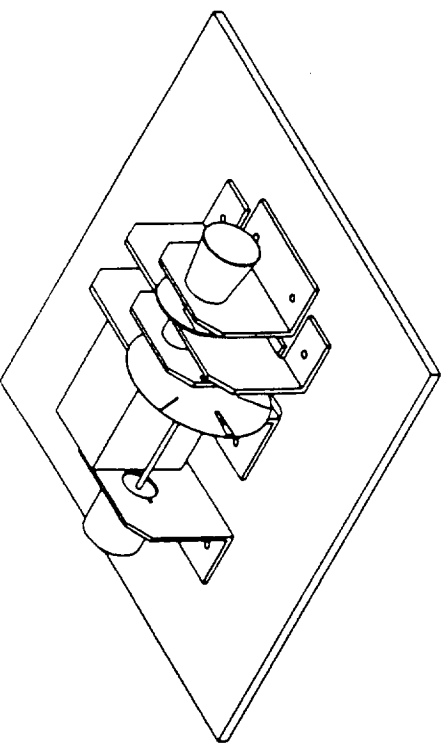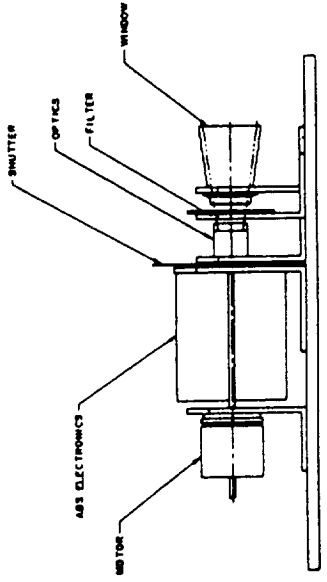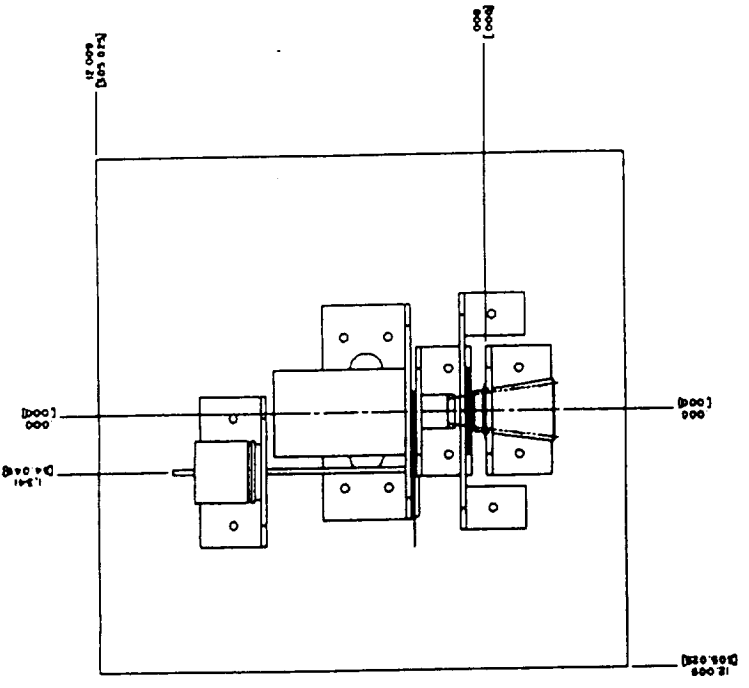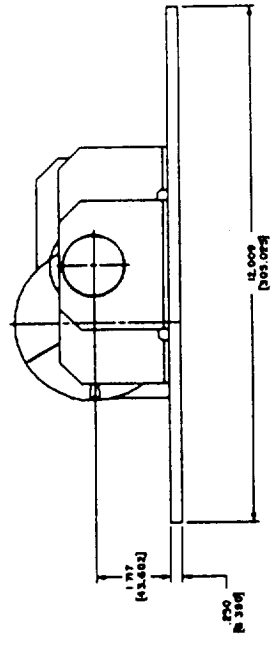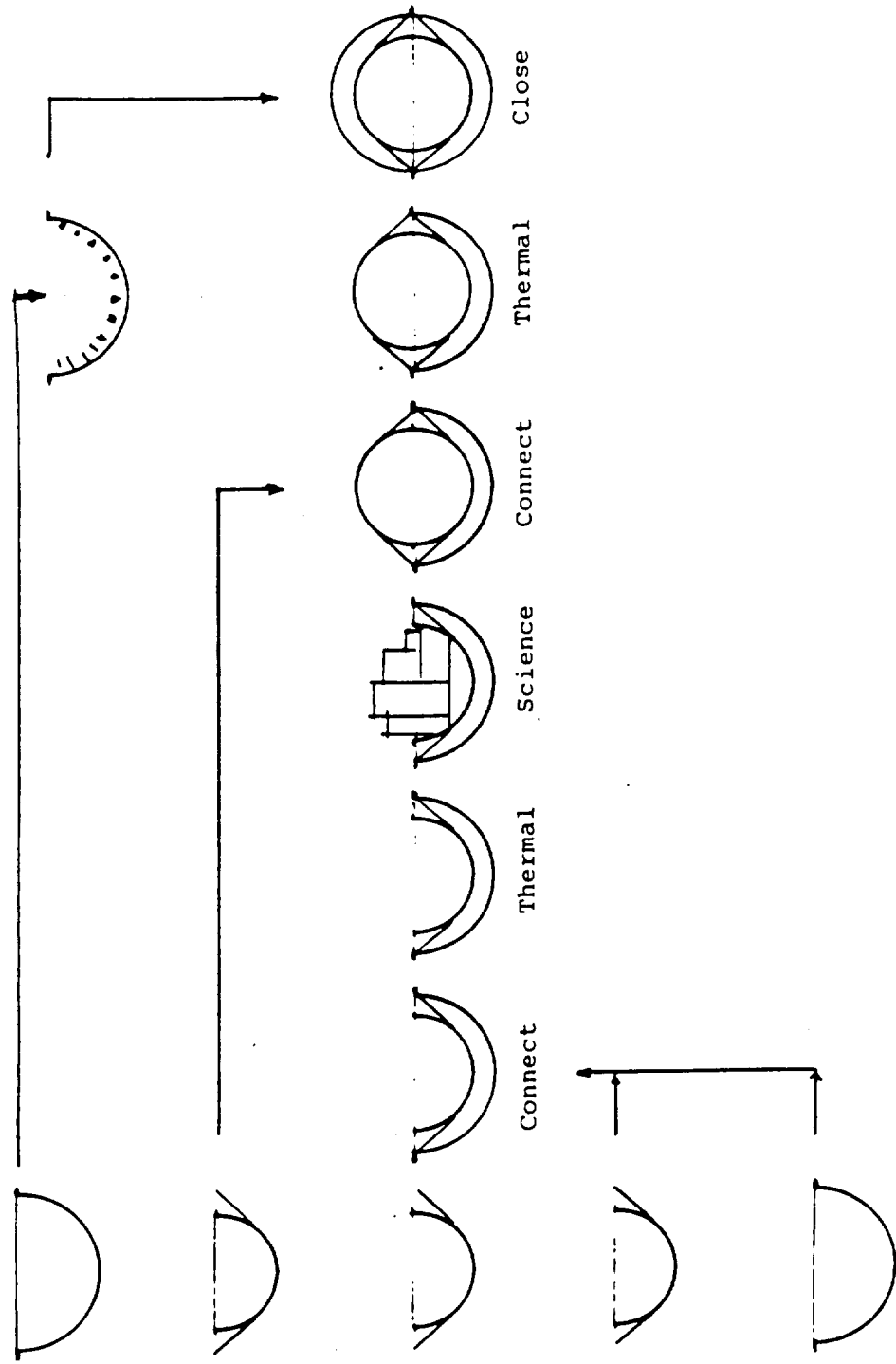
Fig. (1)
Assembly Sequence

VASSIS, UNDEFORMED NASTRAN MODEL

Fig. 2a

X

Z   Y

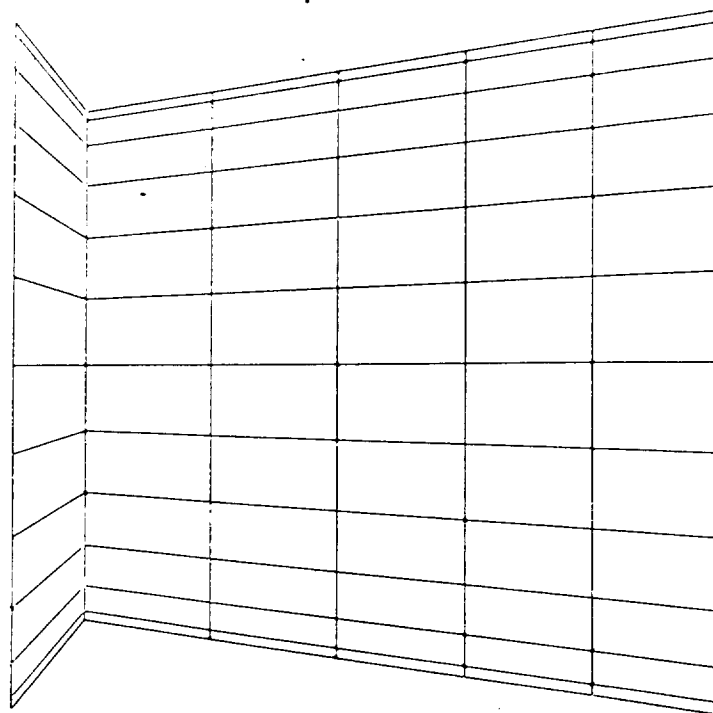VASSIS, UNDEFORMED NASTRAN MODEL

Fig. 26.

Y
Z
X
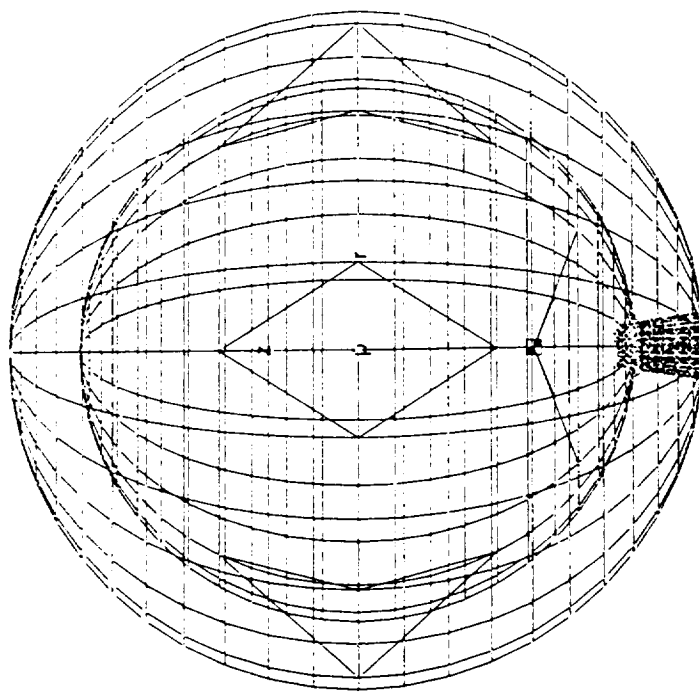
V1
L2
C2
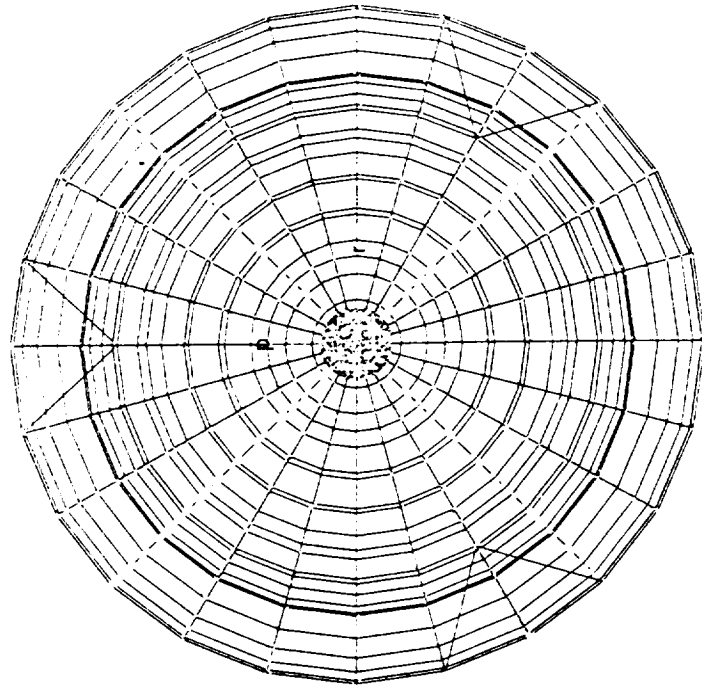
VASSIS, UNDEFORMED NASTRAN MODEL
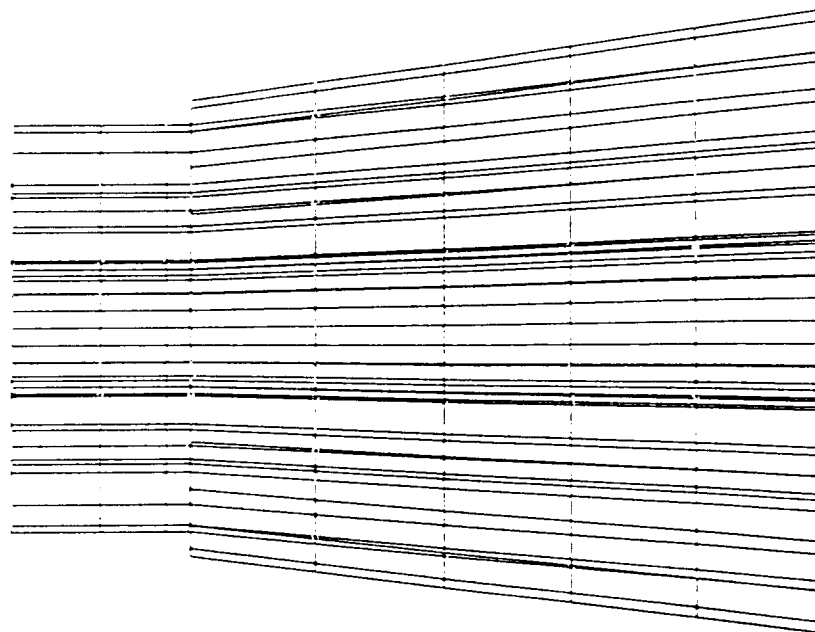
V1
L2
C2
G27

Z

Y

X

Fig. 2C

VASSIS, UNDEFORMED NASTRAN MODEL

V1
L2
C2
G12

Z
Y
X

Fig. 2d
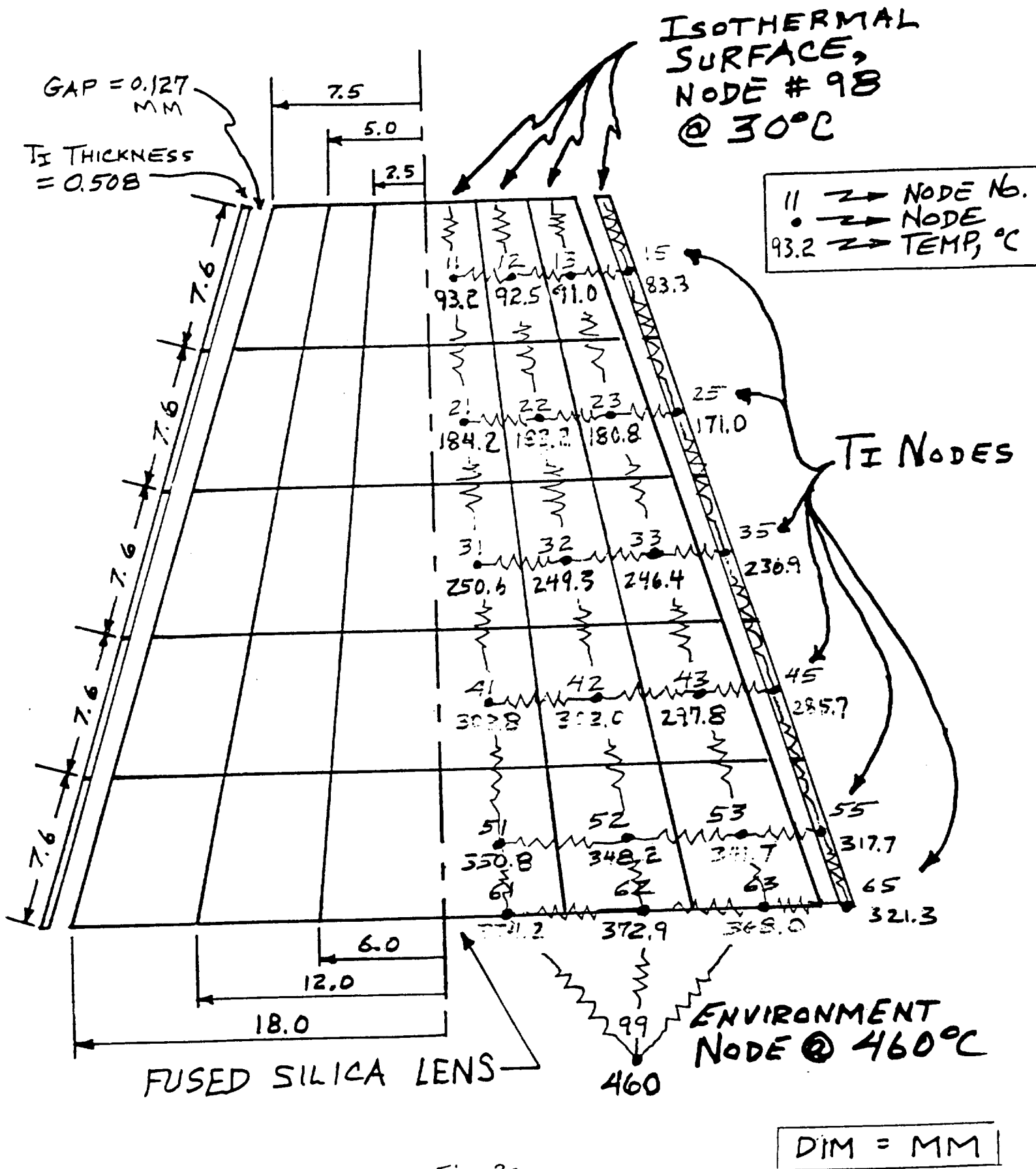
Fig. 3a
12 - WATTS HEAT LEAK

THERMAL ANALYSIS OF VENUS
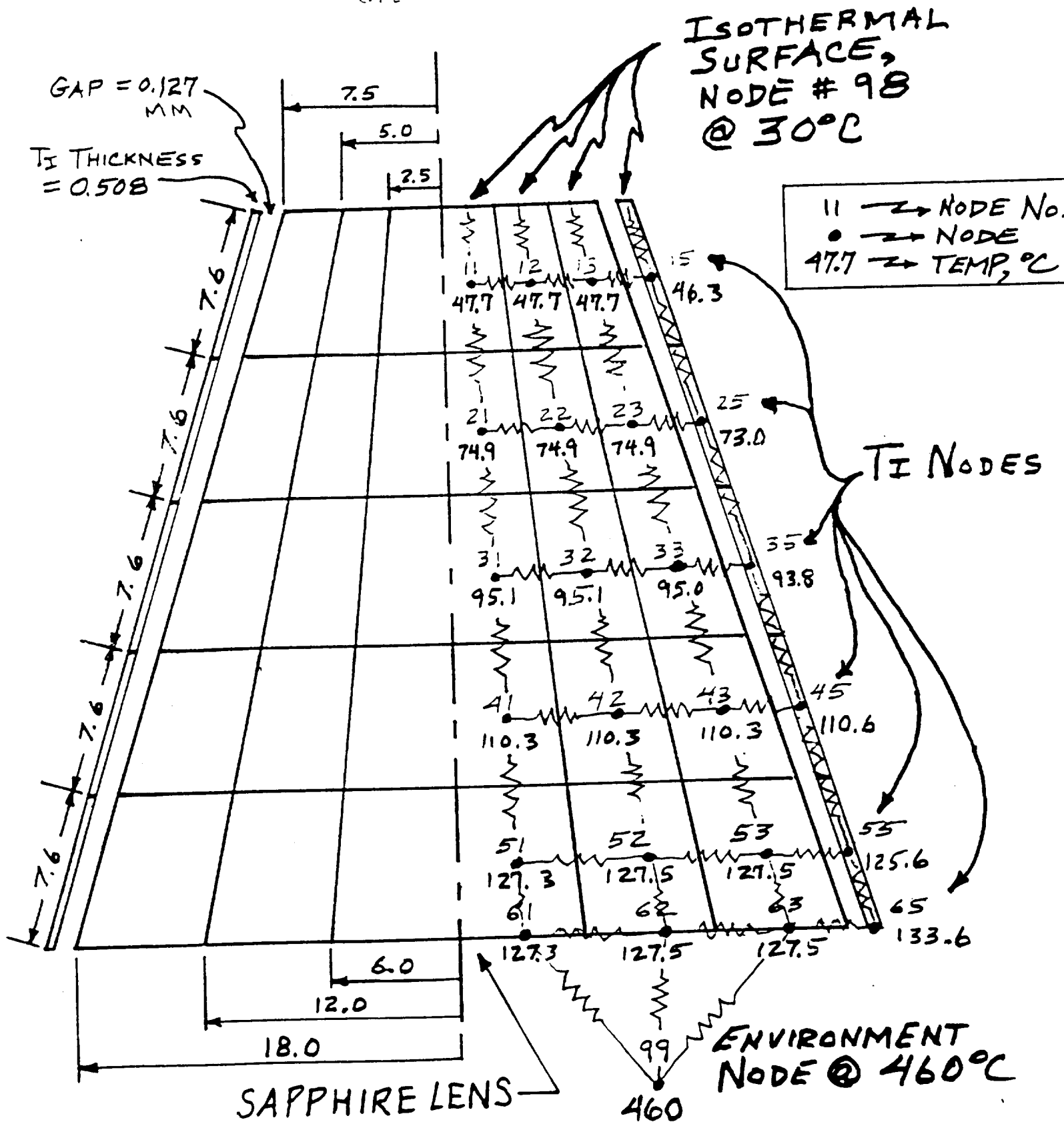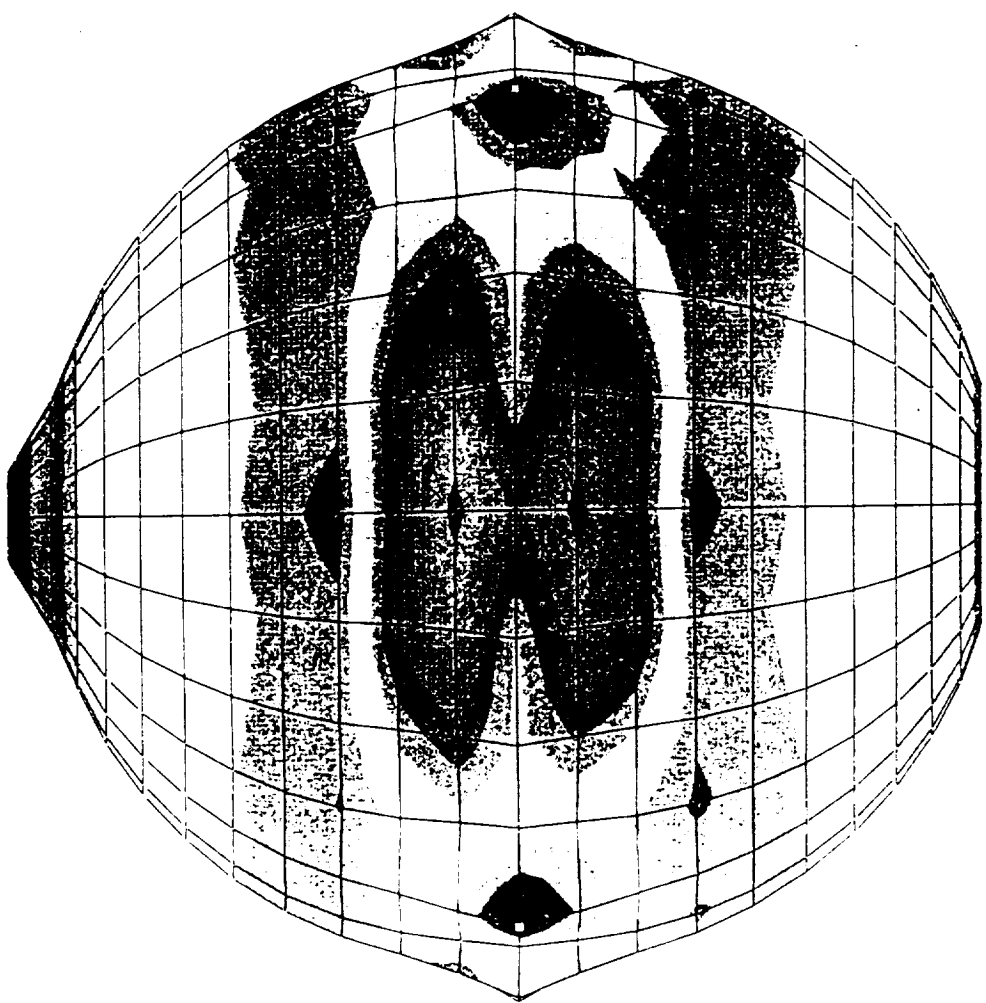AEROBOT GONDOLA CAMERA LENS

Fig. 36.
45 W. HEAT LEAK

THERMAL ANALYSIS OF VENUS
AEROBOT GONDOLA CAMERA LENS

THERMAL + 1450 PSI, VT10

V1
L2
C2
G1

Output Set: vt10, T+P, lens joint & o
Deformed(0.0257): Total Translation
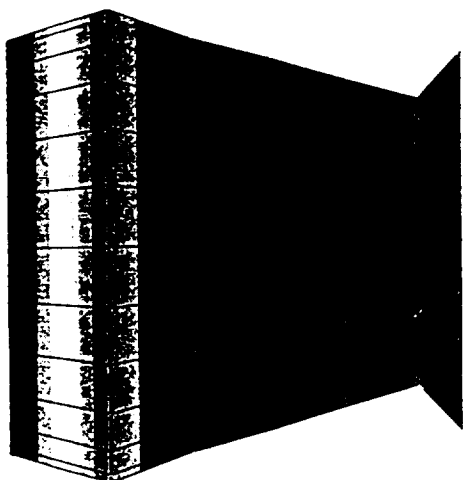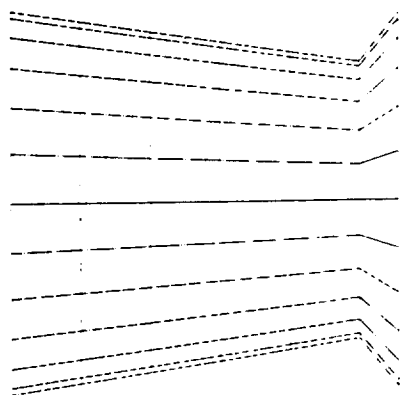Contour: Plate Bot VonMises Stress

Z

Y   X

Fig. 4A

55115.
54728.
54342.
53956.
53570.
53183.
52797.
52411.
52025.
51639.
51252.
50866.
50480.
50094.
49707.
49321.
48935.

M1
L2
C2
G13

Output Set: vt10, T+P, lens joint & o
Deformed(0.0257): Total Translation
Contour: Plate Bot VonMises Stress

Z

Y   X

Fig. 4b

21889.
20544.
19199.
17854.
16509.
15165.
13820.
12475.
11130.
9786.
8441.
7096.
5751.
4407.
3062.
1717.
372.3

THERMAL + 1450 PSI, VT10

V1
L2
C2
G12

19427.	
18293.	
17160.	
16026.	
14892.	
13759.	
12625.	
11491.	
10357.	
9224.	
8090.	
6956.	
5823.	
4689.	
3555.	
2422.	
1288.	

Z

Y   X
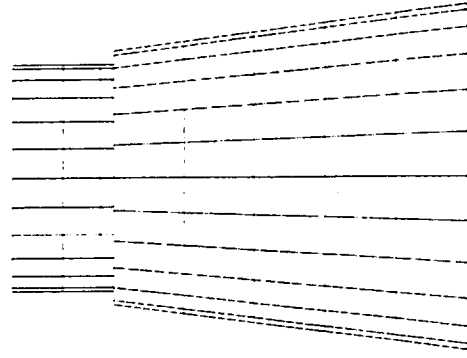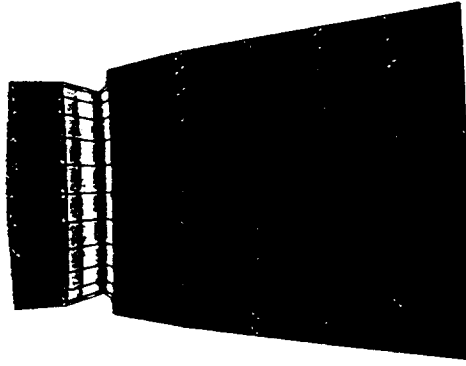
Output Set: v110, T+P, lens joint & o
Deformed(0.0257): Total Translation
Contour: Solid VonMises Stress

Fig. 4C

500 g z, vg1

V1
L1
C2

Z

Y   X

Output Set: UAI/NASTRAN Case 1
Deformed(0.0479): Total Translation

Fig. 4d
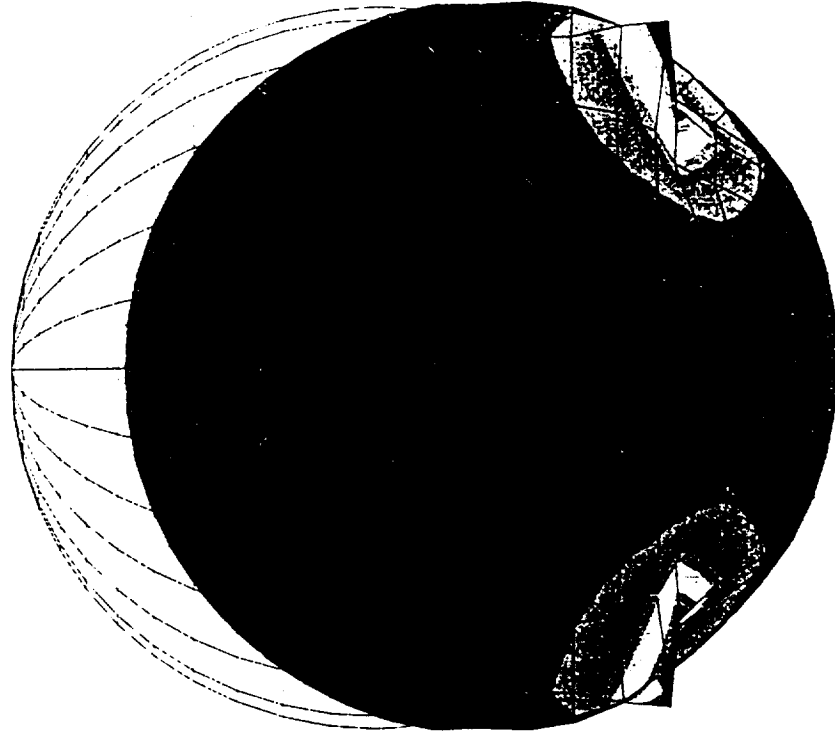
500 g z , vg1

	58709.
	55064.
	51418.
	47773.
	44128.
	40482.
	36837.
	33192.
	29546.
	25901
	22256.
	18610.
	14965.
	11320.
	7674.
	4029.
	383.6

V1
L1
C2
G25

Z

Y   X

Output Set: UAI/NASTRAN Case 1
Deformed(0.0479): Total Translation
Contour: Plate Top VonMises Stress

Fig. 4e

500 g z, vgl
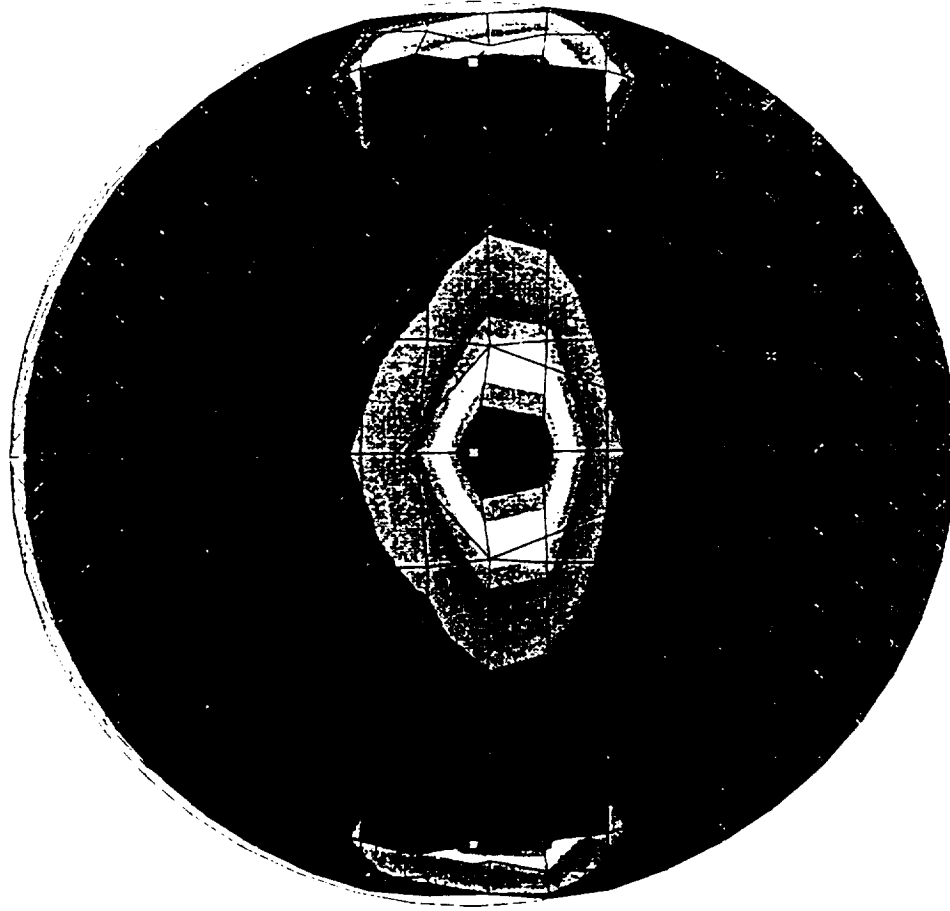
22992.
21573.
20154.
18734.
17315.
15896.
14477
140..
11638
10210
8799
7380
5961
4541
3122.
1703.
283.6

V1
L1
C2
G1

Z

Y   X

Output Set: UAI/NASTRAN Case 1
Deformed(0.0479): Total Translation
Contour: Plate Top VonMises Stress

Fig. 4f

500 g z tilt 15 deg in x, vglxl

Fig. 49

V1
L1
C2

Z

Y   X

Output Set: UAI/NASTRAN Case 1
Deformed(0.114): Total Translation

500 g z tilt 15 deg in x, vg1x1

Fig. 4b

Z

Y

X

Output Set: UAI/NASTRAN Case 1
Deformed(0.114): Total Translation
Contour: Plate Bot VonMises Stress

V1
L1
C2
G1

35114
32937
30750
...
...
...
...
...
...
...
4906
...
2451
2737

500 g z tilt 15 deg in x, vg1x1

V1
L1
C2
G25
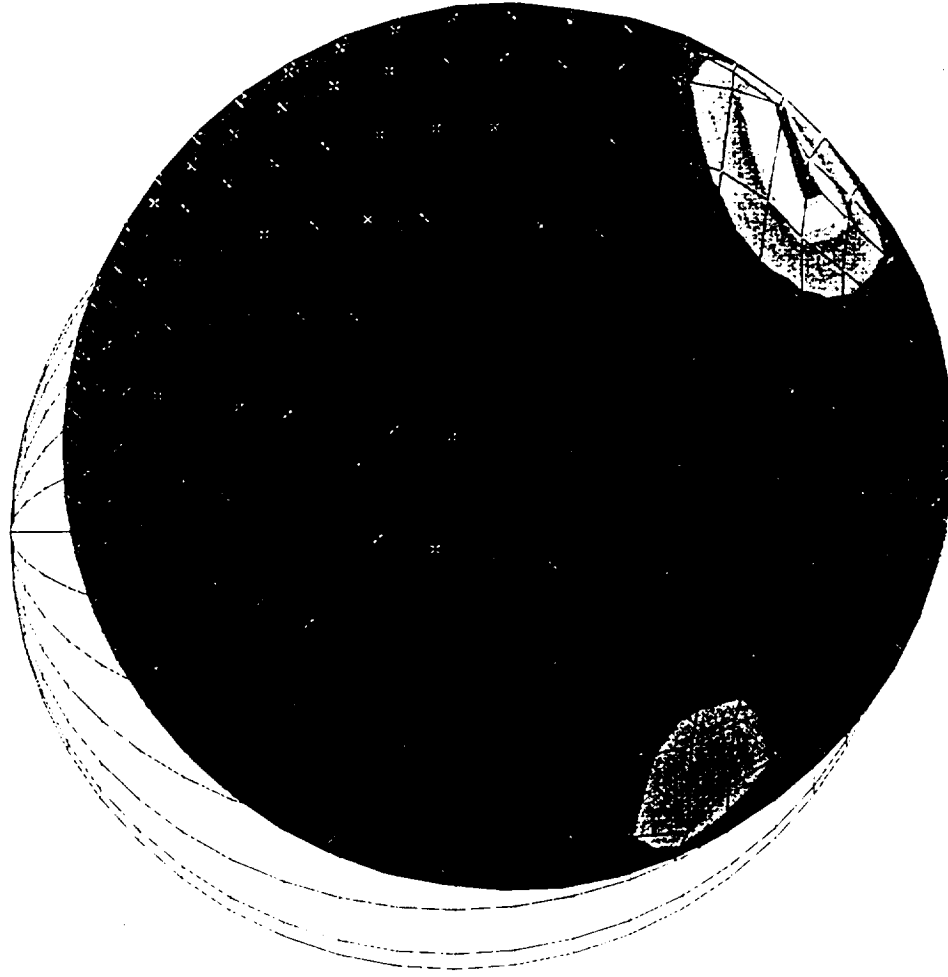
88084.
82638.
77192.
71746.
66300
60854
55408
49962
44516
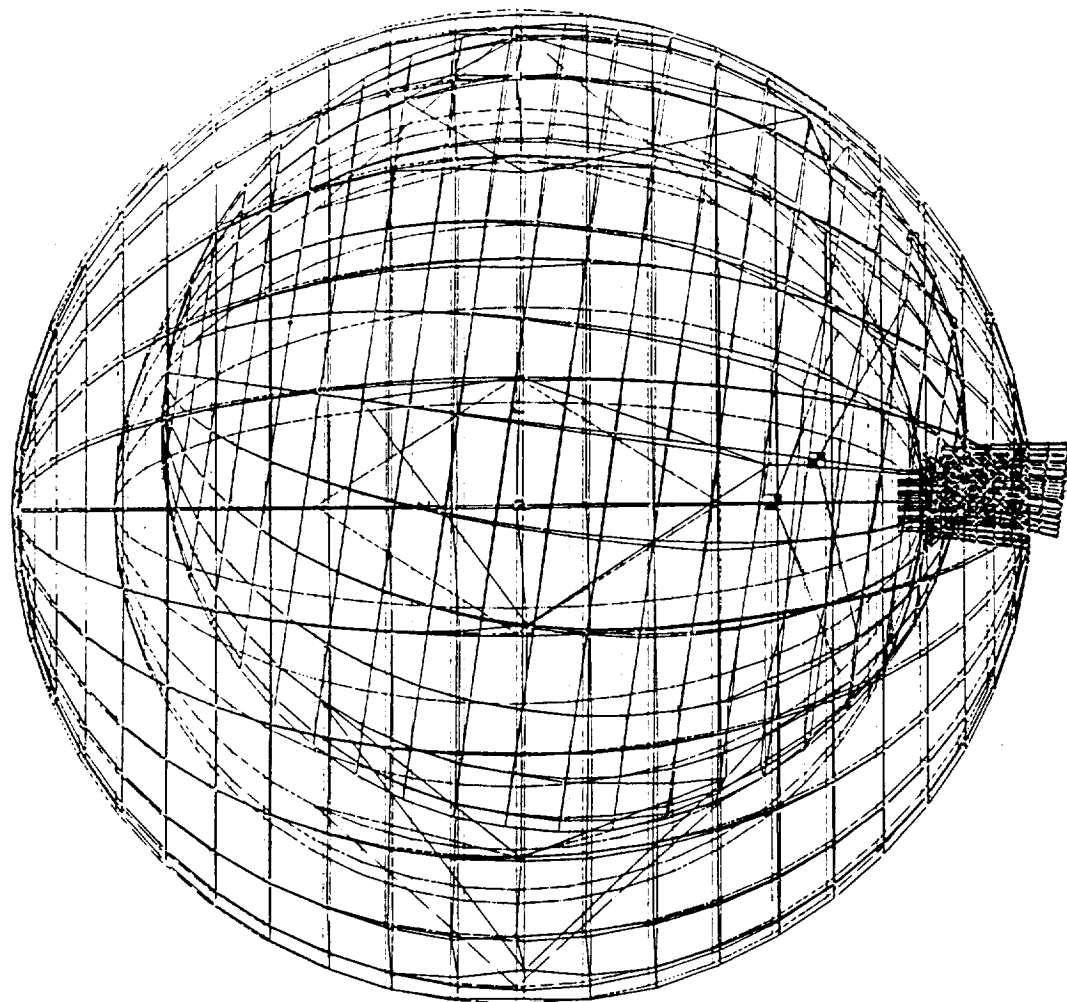39070
33624
28178
22732
17286
11840.
6394.
947.5
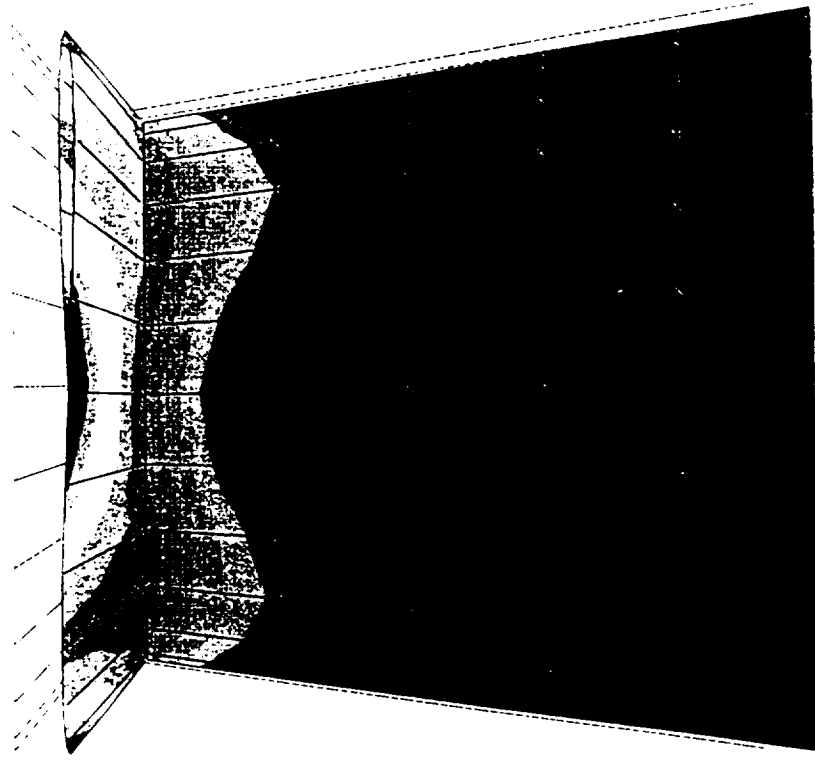
Z

Y   X

Output Set: UAI/NASTRAN Case 1
Deformed(0.114): Total Translation
Contour: Plate Bot VonMises Stress

Fig. 4i

500 g z tilt 15 deg in x,   vg1x1

2777.
2655.
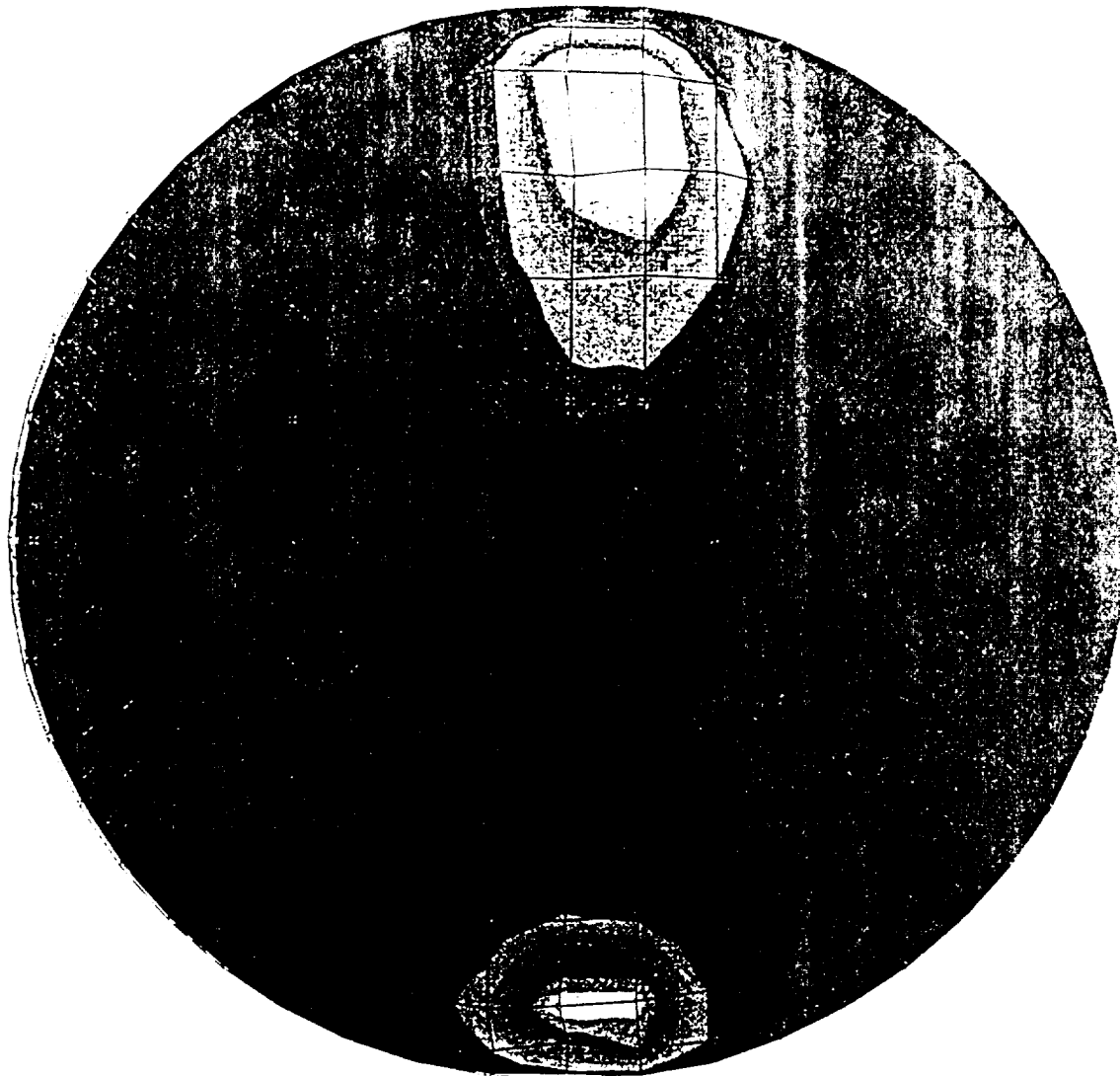2532.
2410.
2288
2166
2044
1921
1799
1677
1555
1433
1310.
1188.
1066.
943.7
821.5

V1
L1
C2
G13

Z

Y   X

Output Set: UAI/NASTRAN Case 1
Deformed(0.114): Total Translation
Contour: Plate Bot VonMises Stress

Fig. 4j

JET PROPULSION LABORATORY

INTEROFFICE MEMORANDOM
352G:96:150:MS

December 30, 1996

To: Ken Klaasen

From: Moktar Salama

Subject: Revised VASSIS Gondola Design

Reference: (1) The VASSIS Gondola Structural Design, IOM 352G:96:146:MS, Nov 6, 1996, to K. Klaasen from M. Salama.

BACKGROUND

In Reference (1), the possibility of excessive relative deformation of about 0.114 inch between the inner and outer spherical shells in the vicinity of the viewport / lens was identified as a deficiency in the VASSIS gondola design concept reported therein. Such excessive deformation could cause gapping at that junction and allow leaking of the outside atmosphere into the space between the two spheres. The purpose of this memorandum is to summarize the work done since then to resolve this problem.

Gapping could be avoided at the junction in question by implementing a number of design modifications which;
1. increase the stiffness of the support elements between the two spherical shells, thereby decreasing the deformation at the lens / viewport junction,
2. provide sufficient overlap between the various relevant elements at the junction,
3. design a resilient element in the junction between the two spherical shells so that no gapping develops.

In the following, two options are summarized which combine the above modifications into specific design changes. The first option is the one we recommend at the present time. It combines design modifications from 1, and 2 above. The second option combines modifications consistent with 1, 2, and 3. The second option is promising, but it will need further study and analysis before it can be declared flawless.

OPTION 1

The design changes recommended under this option are aimed at creating a stiffer interconnection between the outer and inner spherical shells, while allowing the camera lens to move laterally at its free end without being constrained by the conical viewport. The increased stiffness is implemented in the following areas, while still assuming the use of three pairs of tension bands as before:

1. Increase the cross section of the mid-ring on the outer spherical shell uniformly to 0.75 x 0.3 inch,
2. Reinforce the thickness of the outer spherical shell locally to 0.2 inch in the neighborhood of areas where the tension bands connect to the mid-ring,
3. Reinforce the thickness of the inner shell locally to 0.35 inch in the neighborhood of areas where the tension band connect to the inner shell,
4. Increase the thickness of the inner shell to a maximum thickness of 0.15 inch at the viewport junction, then taper this thickness away from the viewport over two inches to the uniform 0.05 inch thickness.

Additional design modifications include:

5. Increase the initial preload in the tension bands to 3100 LB tension. This will cause the bands to be taut at all times. Also, reduce the cross section diameter of the bands to 0.30 inch,

6. Allow for a 0.05 inch clearance between the outer end of the fused silica lens and the metallic cone / outer shell, so that the lens does not come in forced contact with the cone during expected maximum deformations between these elements at time of entry into Venus atmosphere.

7. Add a thin (0.02 inch) annular Ti cover plate (welded to the outer shell) over the .05 inch clearance to minimize entry and accumulation in the clearance area of unwanted atmospheric particulates.

8. Increase the overlap between the viewport cone and the ring at the inner shell

Some of the design changes listed above are indicated on Fig. 1, and have been implemented in a finite element analysis model of Fig. 2. Results of this analysis are shown graphically in Figs 3 through 18, and are also summarized in Table (1) below for two of the most critical loading conditions discussed previously in Reference (1). These two conditions are : (a) 500 G deceleration during entry, directed at 15 degree from the normal to the surface, and (b) 1450 psi pressure and 460 C degrees near Venus surface.

Table 1
Analysis Summary of Modified VASSIS Design (OPTION 1)

	Maximum Stresses (psi)			Rel Deform: Lens/Outer Shell (in)		
	Outer Shell	Inner Shell	Bands·	X-tangent	Y-tangent	Z-normal
Pressure and Thermal	69647	59474	65162	0.003	0.003	0.043
500 G/15 degree tilt in Y	35275	74405	95833	0.002	0.015	0.018

The pressure and temperature loading occurs near Venus surface, during which time the temperature of the outer shell will be at 460 C. The above figures present much greater improvement over the design of Ref 1. However, at 460 C temperature, stresses in the 60,000 psi range may be considered somewhat high for titanium's yield strength . But these stresses could be reduced considerably by:

1. Increasing the number of tension bands from three pairs to four or six pairs,

2. Refining details of the reinforcements discussed above, without necessarily increasing their thicknesses. These two changes are recommended for future studies.
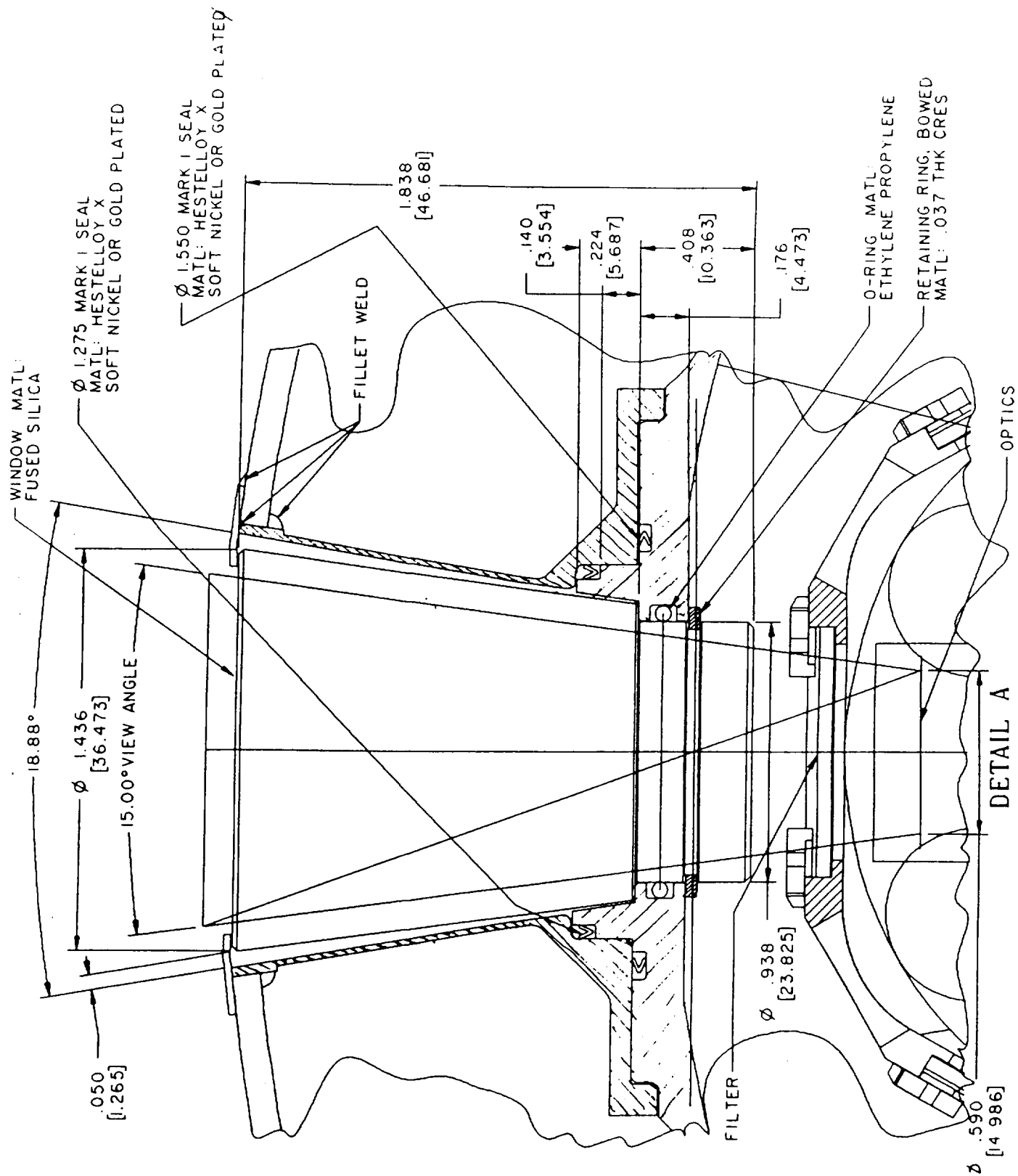
OPTION 2

In this option, increased stiffness of the components discussed in Option 1 are still included here as well. But in addition, the Ti conical viewport is made partly from resilient titanium corrugation (bellows) as shown in Fig. 19. The relative resilience of the corrugated part of the cone is intended to help in reducing or eliminating the tendency for complete separation (gapping) at the junction between the inner spherical shell and the conical viewport. This junction is secured only by a tight fit between parts, without fasteners or welds. Therefore, the stresses in the corrugated part are not expected to be high. In terms of the expected deformations and stresses, this configuration is more complex than the one in the first Option. However, no analysis was performed for it because of shortage of the remaining time and funds. Hopefully, future studies would allow for a more complete assessment of this design.

cc: G. Forsberg   S. Langenbeck   A. Vaughan
     J. Garba   P. Mac Neal   E. Villegas
     M. Heun   J. Jones
     L. Hulcy   D. Senske

p

WINDOW MATL.
FUSED SILICA

Ø 1.275 MARK 1 SEAL
MATL: HESTELLOY X
SOFT NICKEL OR GOLD PLATED

Ø 1.550 MARK 1 SEAL
MATL: HESTELLOY X
SOFT NICKEL OR GOLD PLATED

FILLET WELD

18.88°

Ø 1.436
[36.473]

15.00° VIEW ANGLE

.050
[1.265]

1.838
[46.681]

.140
[3.554]

.224
[5.687]

.408
[10.363]

.176
[4.473]

O-RING MATL.
ETHYLENE PROPYLENE

RETAINING RING, BOWED
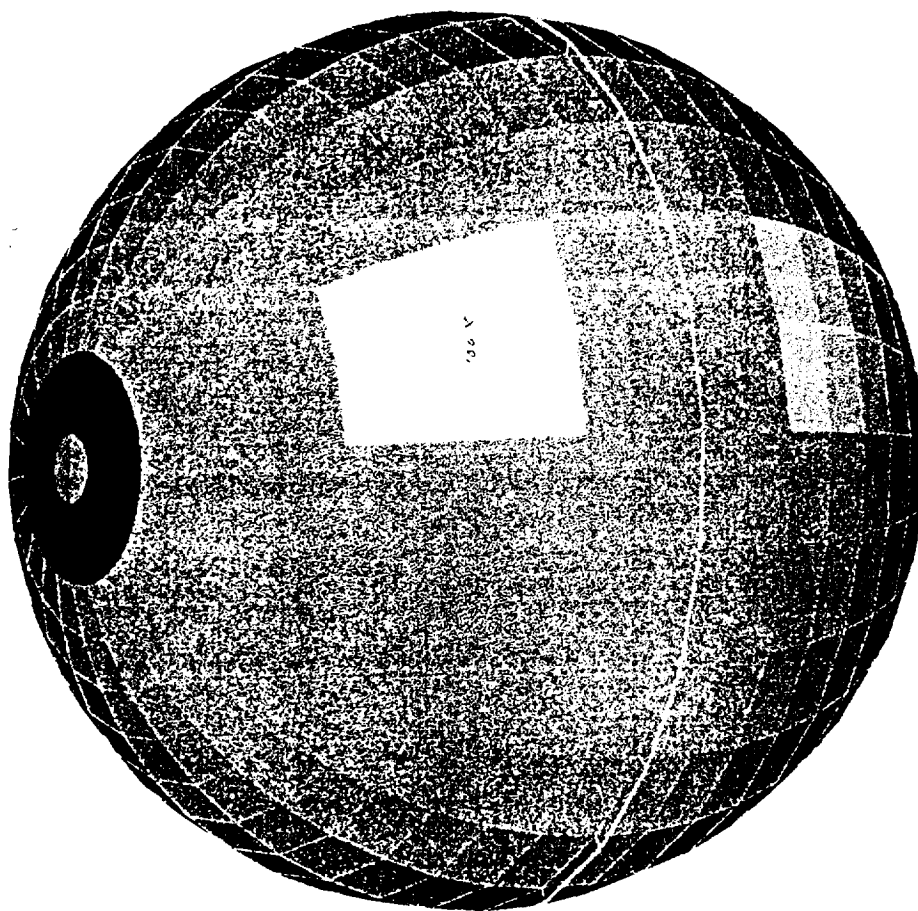MATL: .037 THK CRES

OPTICS

FILTER

Ø .938
[23.825]

D .590
[14.986]

DETAIL A
SCALE 4/1

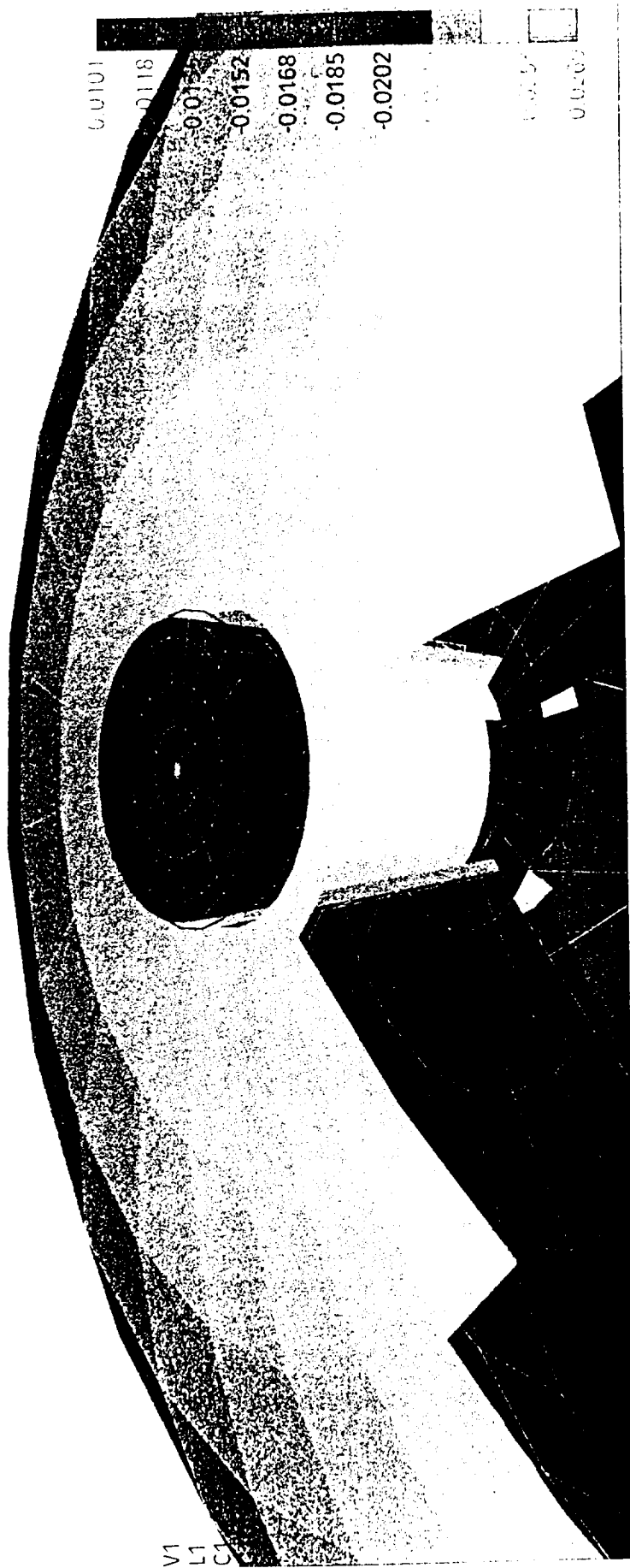Figure 1.

VENUS AEROBAT SURFACE SCIENCE IMAGING SYSTEM

INNER SPHERE WITH REINFORCEMENTS

Figure 2.

VENUS AEROBAT SURFACE SCIENCE IMAGING SYSTEM

Output Set: PRELOAD + 500 G'S IN Z
Deformed(0.0269): Total Translation
Contour: T3 Translation

0.0101
0.0118
-0.0152
-0.0168
-0.0185
-0.0202

0

Z DEFLECTIONS FOR -500 G LOAD

Figure 3.

VENUS AEROBAT SURFACE SCIENCE IMAGING SYSTEM

Output Set: PRELD; 492 G'S Z;87 G'S X
Deformed(0.0284): Total Translation
Contour: T1 Translation

0.0188

0.00751
0.0061
0.00451
0.00292
0.00181
-0.00181
-0.00343
-0.09502
-0.09661

X DEFLECTIONS FOR 10 DEGREE ANGLE OF ATTACK IN X

Figure 4.

VENUS AEROBAT SURFACE SCIENCE IMAGING SYSTEM

Output Set: PRELD: 492 G's Z; 87 G's X
Deformed(0.0284): Total Translation
Contour: T3 Translation

X
Y
Z

0.
-0.00998
-0.0116
-0.0133
-0.0166
-0.0183
-0.02
-0.0249
-0.0266

V1
L1
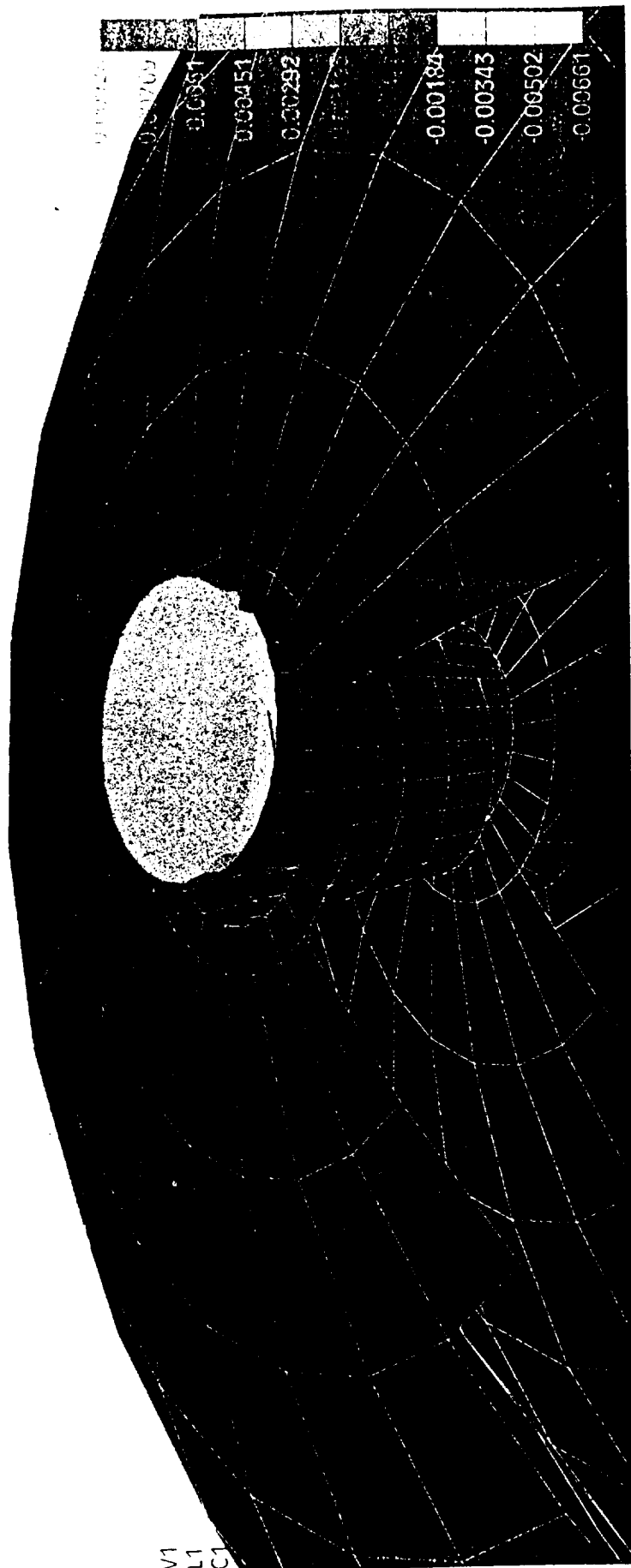C1
G10

Z DEFLECTIONS FOR 10 DEGREE ANGLE OF ATTACK IN X

Figure 5.

VENUS AEROBAT SURFACE SCIENCE IMAGING SYSTEM

Output Set: PRELD; 492 G'S Z;87 G'S Y
Deformed(0.0289): Total Translation
Contour: T2 Translation

0.0206

0.00724
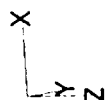0.00557
0.0039
0.00224
0.00112
0.00279
0.00447
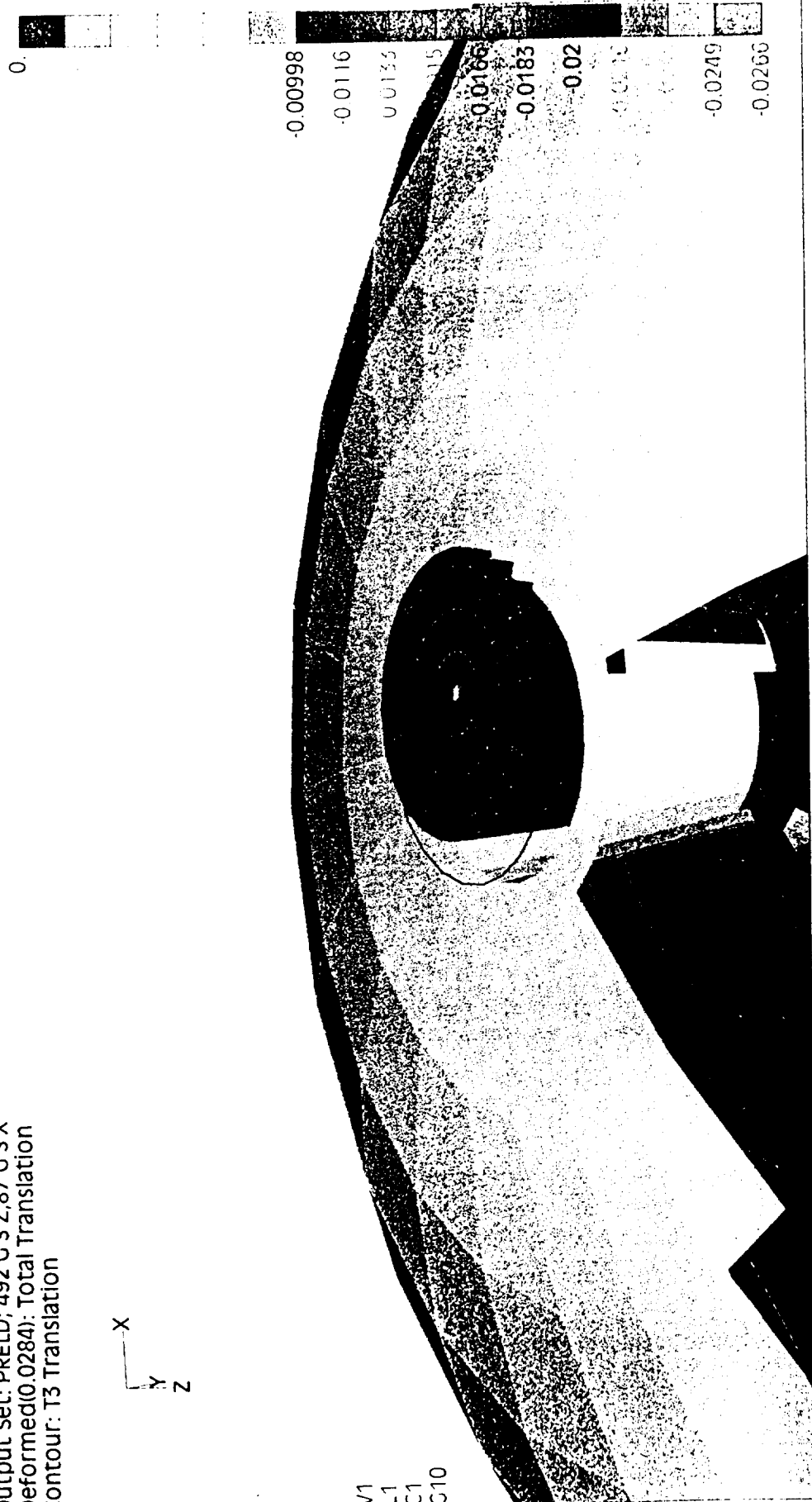0.00614

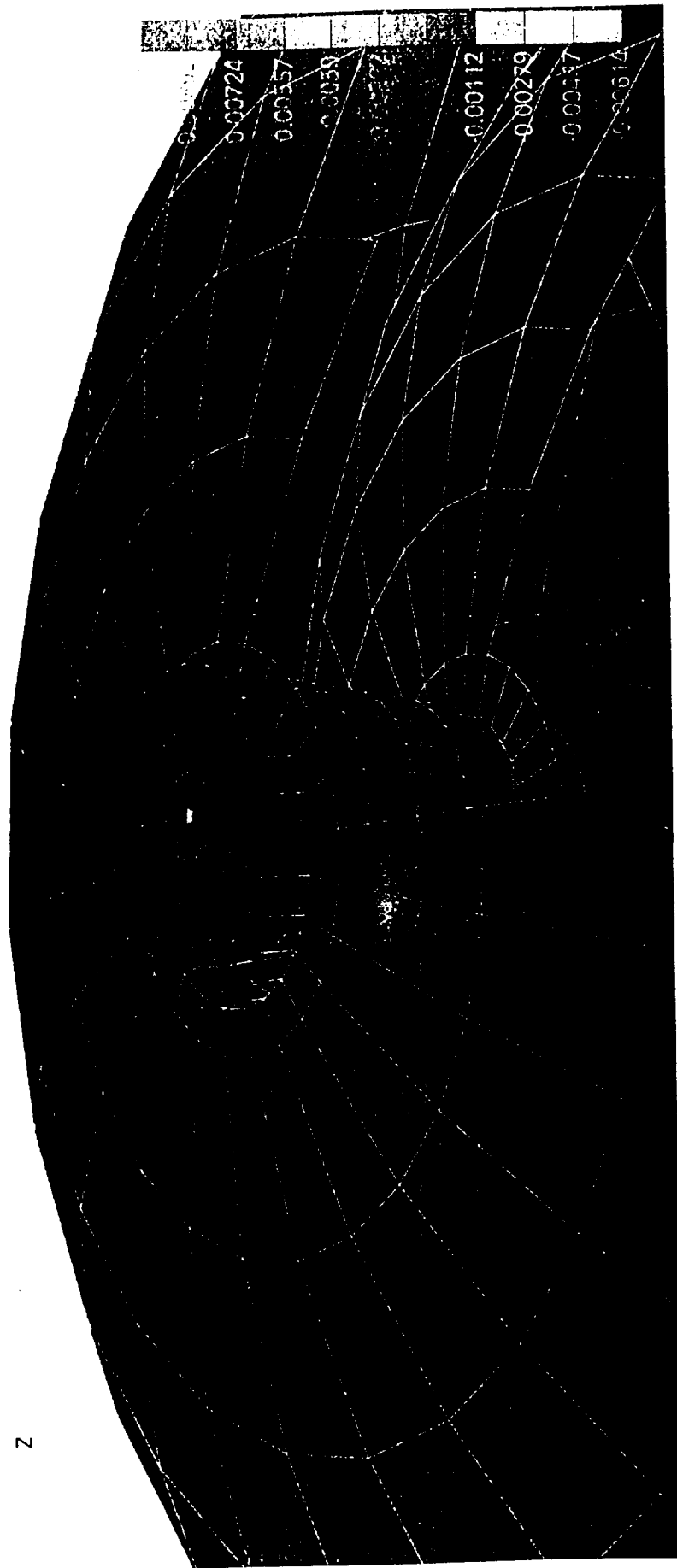Y DEFLECTIONS FOR 10 DEGREE ANGLE OF ATTACK IN Y

Figure 6.

VENUS AEROBAT SURFACE SCIENCE IMAGING SYSTEM

Output Set: PRELD; 492 G'S Z;.87 G'S Y
Deformed(0.0289): Total Translation
Contour: T3 Translation

-0.00998
-.0116
-0.015
-0.0166
-0.0183
-0.02

C1
C10

Z DEFLECTIONS FOR 10 DEGREE ANGLE OF ATTACK IN Y

Figure 7.

VENUS AEROBAT SURFACE SCIENCE IMAGING SYSTEM

Output Set: PRELD; 483 G Z;129 G Y
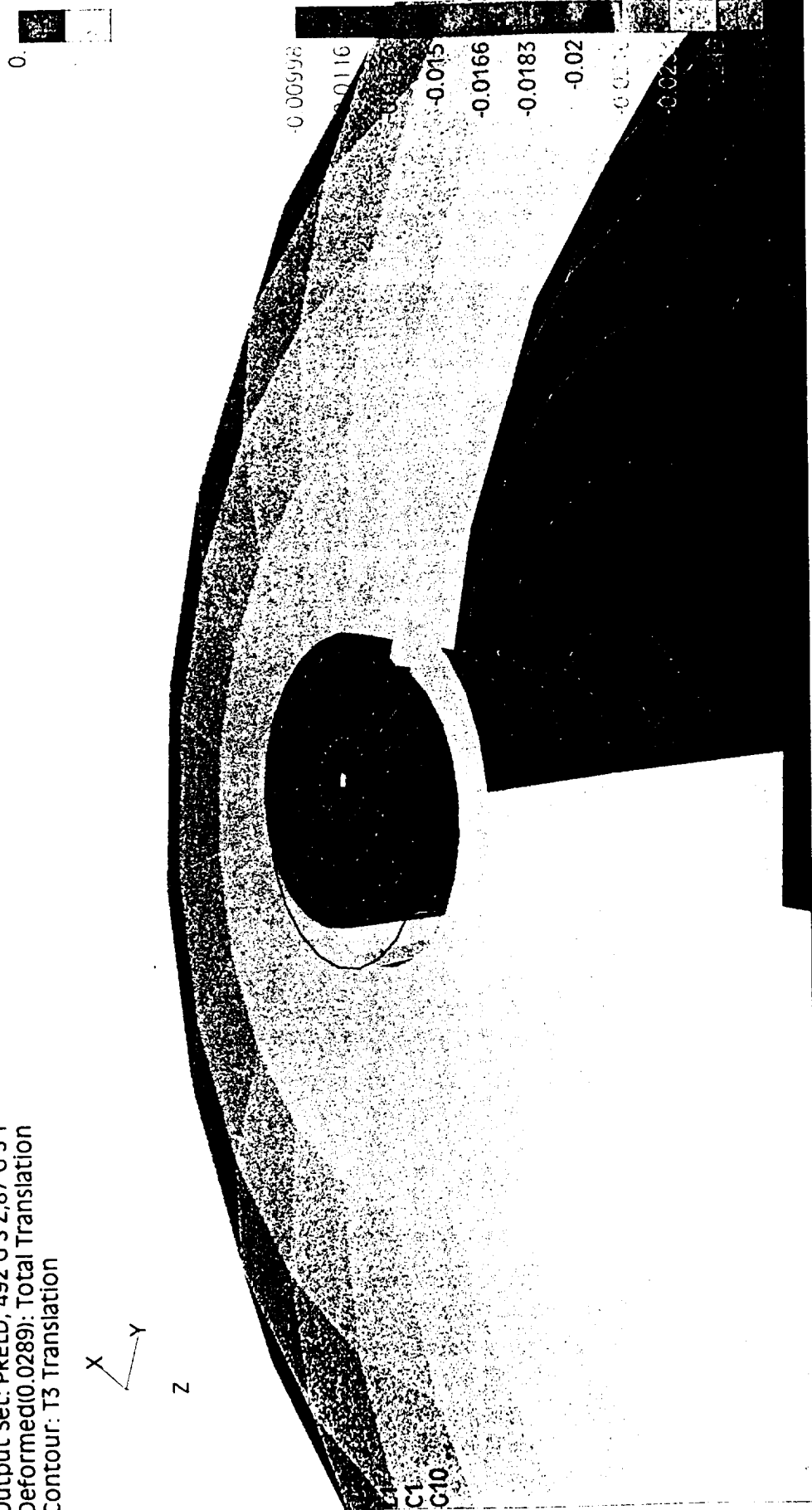Deformed(0.0308): Total Translation
Contour: T2 Translation

0.0234
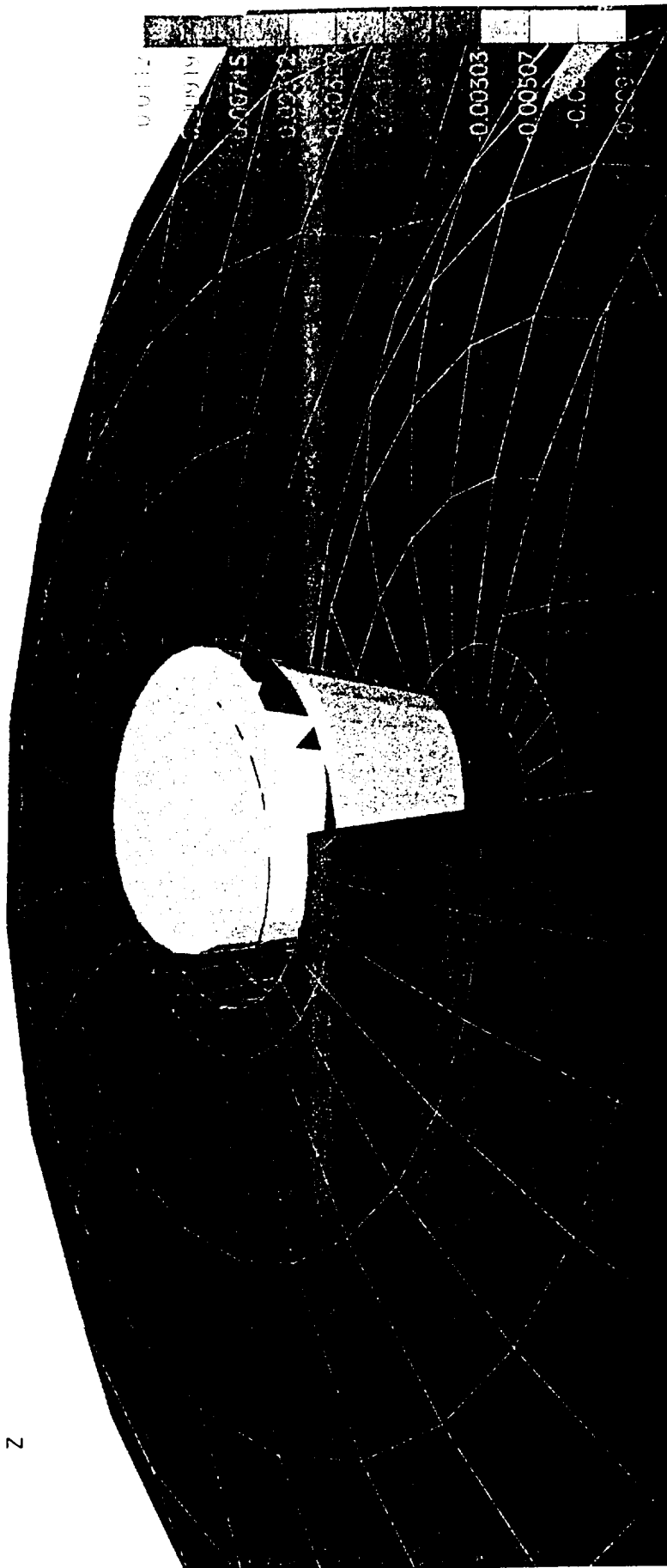
Y DEFLECTIONS FOR 15 DEGREE ANGLE OF ATTACK IN Y

Figure 8.

VENUS AEROBAT SURFACE SCIENCE IMAGING SYSTEM

Output Set: PRELD; 483 C Z;129 G Y
Deformed(0.0308): Total Translation
Contour: T3 Translation

0.000961

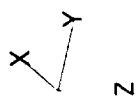-0.00922
-0.0109
-0.0126
-0.0143
-0.016
-0.0177
-0.0194
-0.0211
-0.022
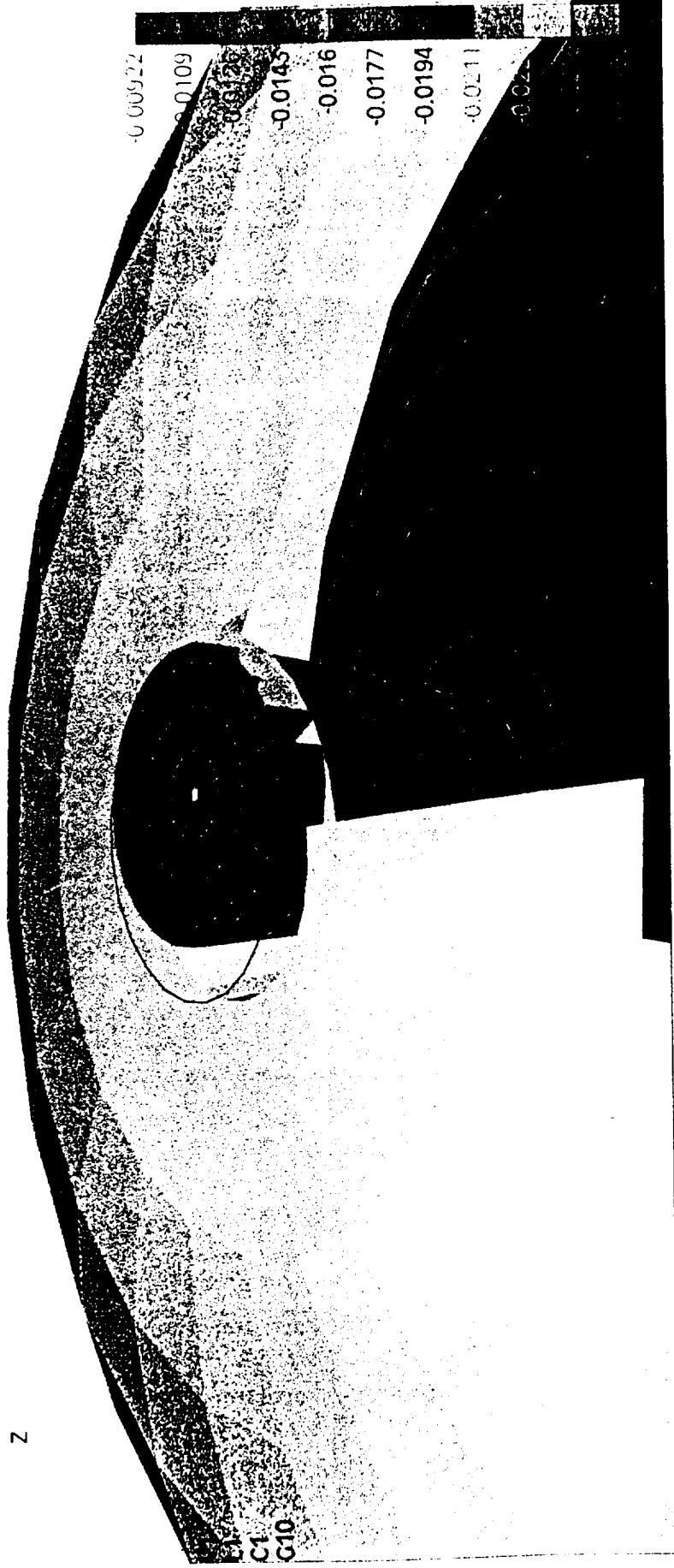
Z DEFLECTIONS FOR 15 DEGREE ANGLE OF ATTACK IN Y

Figure 9.

VENUS AEROBAT SURFACE SCIENCE IMAGING SYSTEM
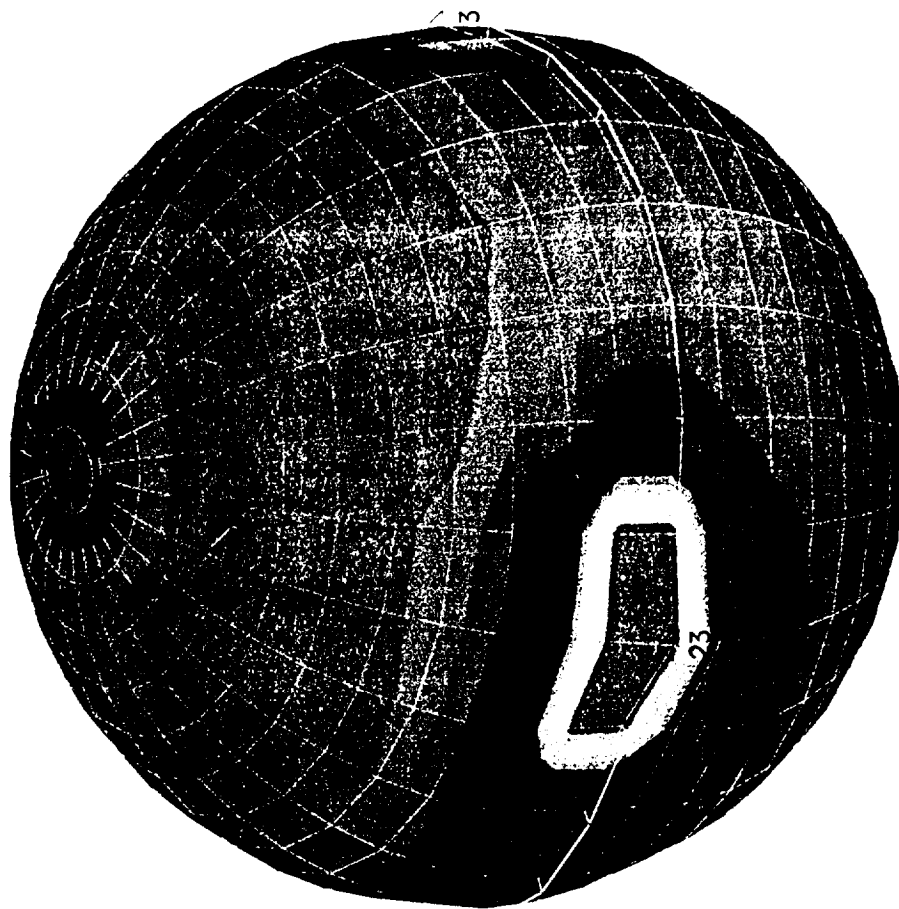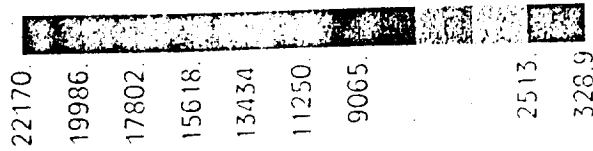
OUTER SHELL STRESSES DUE TO 15 DEGREE ANGLE OF ATTACK IN Y

Figure 10.

55275

22170.
19986.
17802.
15618.
13434.
11250.
9065.

2513.
326.9

V1
L1
C1
G2

Output Set: PRELD: 483 G Z;129 G Y
Deformed(0.0308): Total Translation
Contour: Plate Bot VonMises Stress

X
Y
Z

VENUS AEROBAT SURFACE SCIENCE IMAGING SYSTEM

74405.

47428.
42931.
38435.
33939.
29443
24947
20450

6962.
2465

Output Set: PRELD; 483 G Z;129 G Y
Deformed(0.0308): Total Translation
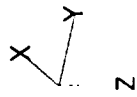Contour: Plate Bot VonMises Stress

X
Y
Z

V1
L1
C1
G11
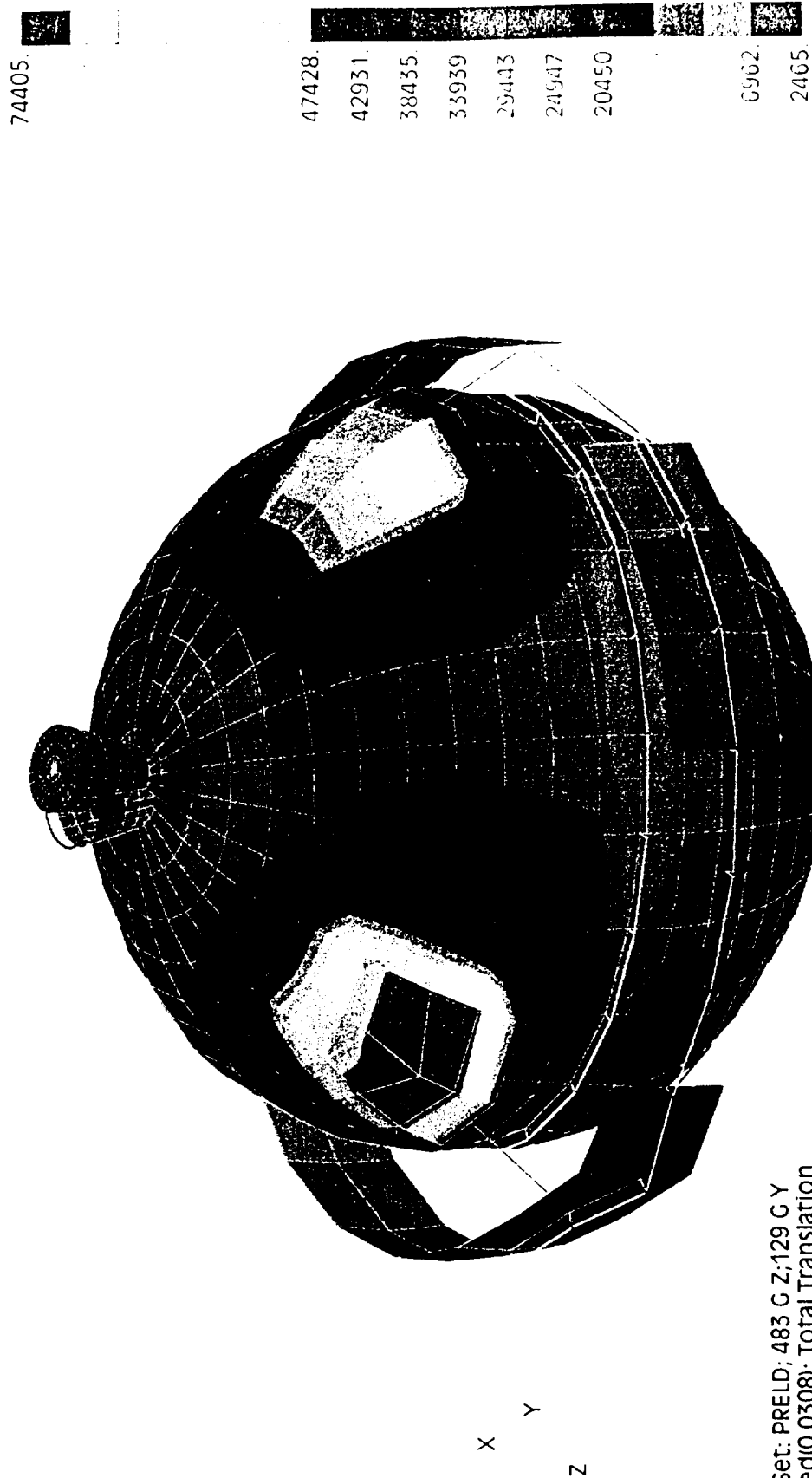
INNER SPHERE STRESSES DUE TO 15 DEGREE ANGLE OF ATTACK IN Y

Figure 11

VENUS AEROBAT SURFACE SCIENCE IMAGING SYSTEM

Output Set: PRELD: 483 G Z;129 G Y
Criteria: Beam EndA Axial Force
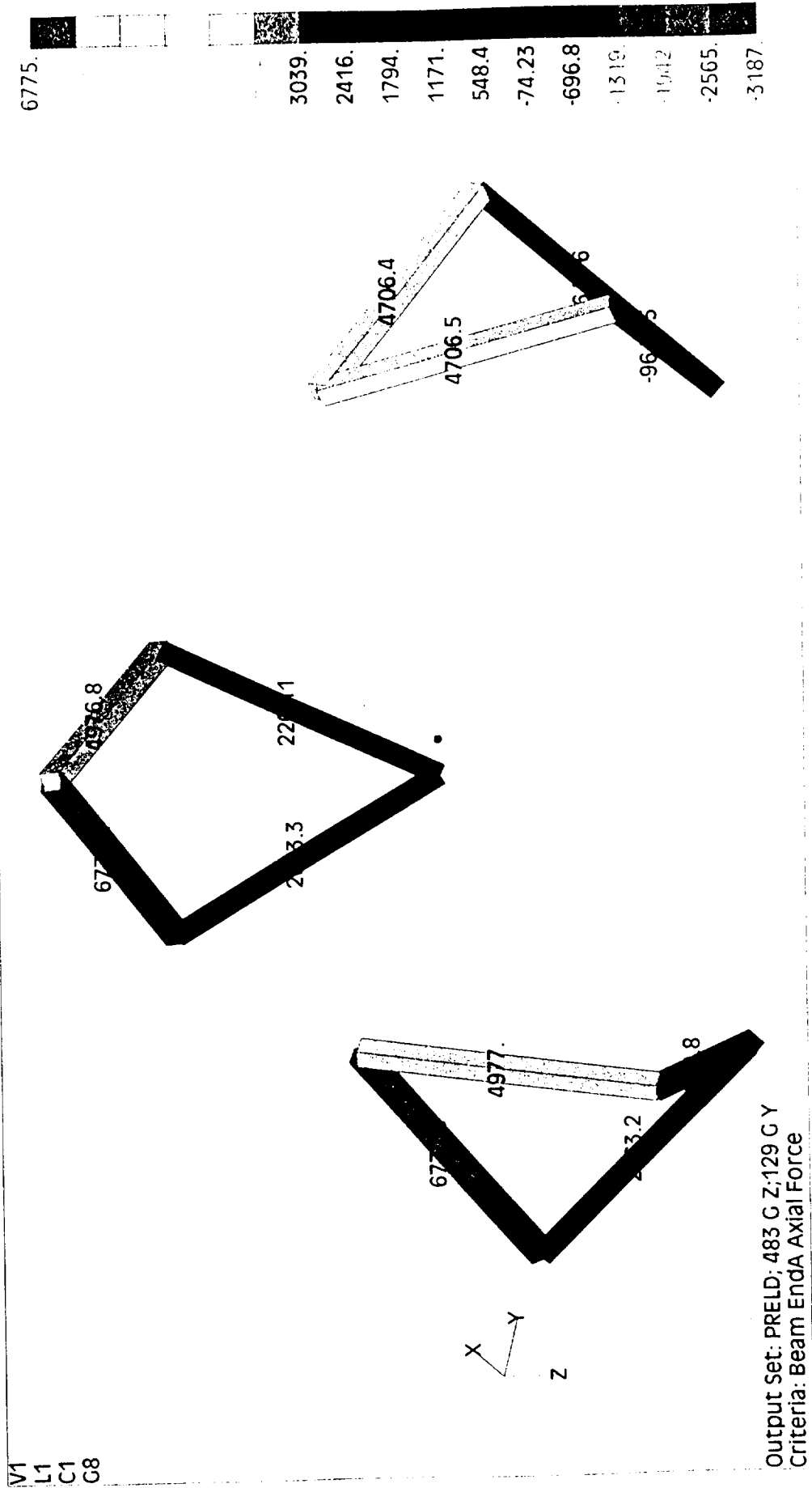
AXIAL LOAD IN STRAPS DUE TO 15 DEGREE ANGLE OF ATTACK IN Y

Figure 12

VENUS AEROBAT SURFACE SCIENCE IMAGING SYSTEM

4607.

-1095.
-2046.
-2996.
-3946.
-4897.
-5847.
-6797.
-7748.
-8698.
-9648.
-10599.

V1
L3
C1
G8
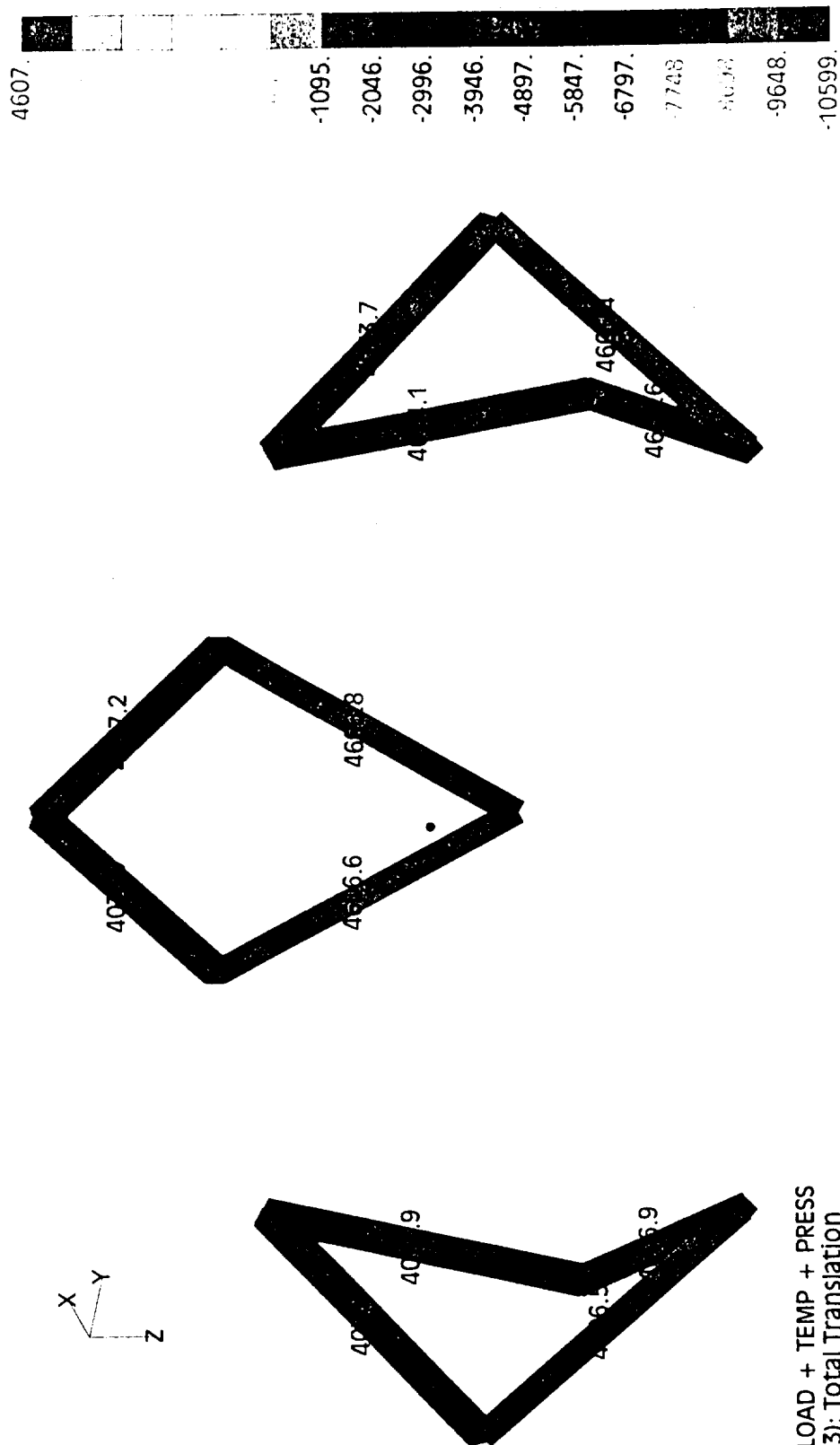
Output Set: PRELOAD + TEMP + PRESS
Deformed(0.0593): Total Translation
Criteria: Beam EndA Axial Force

AXIAL LOAD IN STRAPS (LBS) DUE TO PRELOAD + TEMP + PRESSURE

Figure 13.

VENUS AEROBAT SURFACE SCIENCE IMAGING SYSTEM
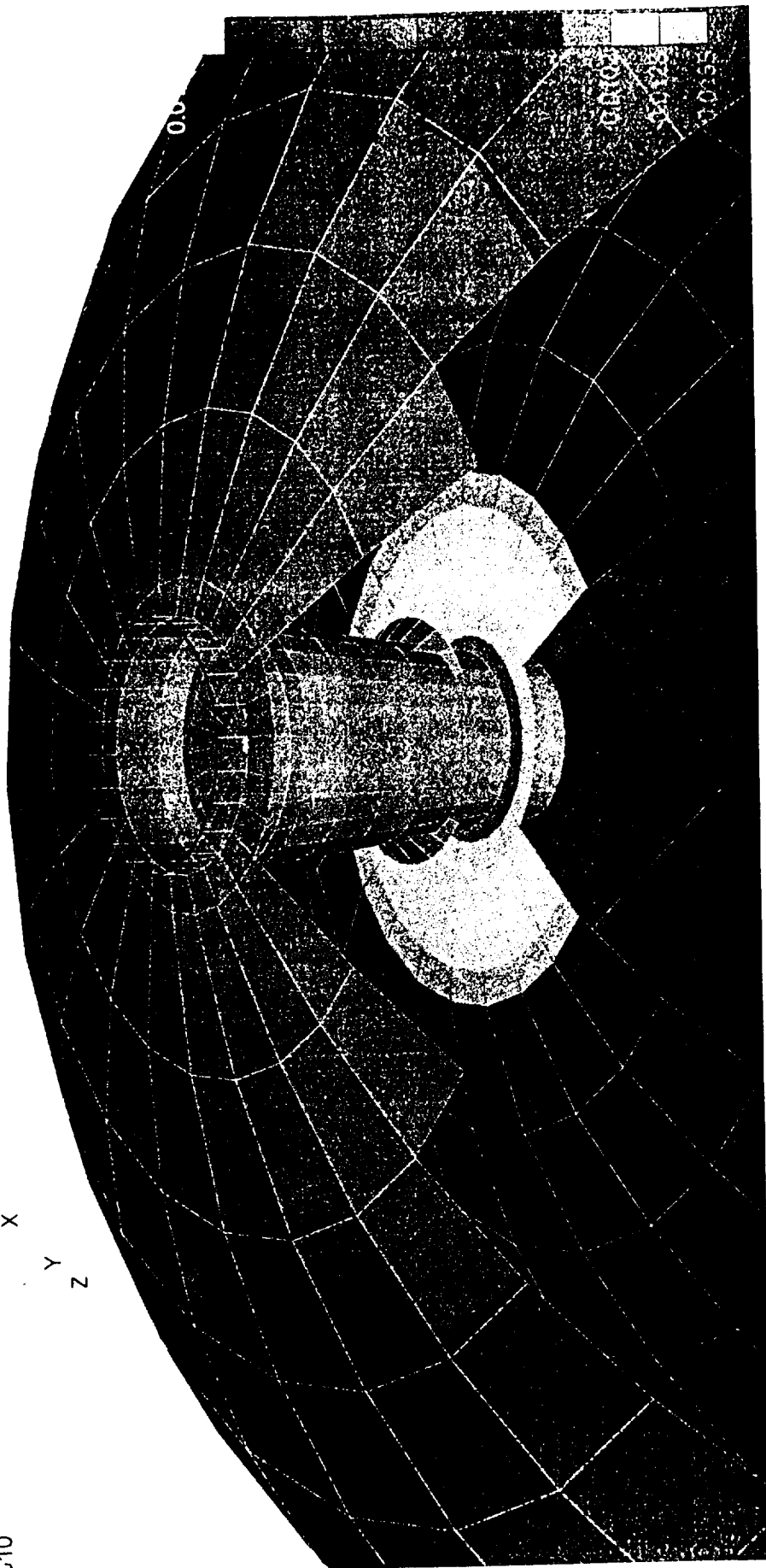
Z DIRECTION DISPLACEMENTS DUE TO PRELOAD + TEMP + PRESSURE

Figure 14

VENUS AEROBAT SURFACE SCIENCE IMAGING SYSTEM

59474
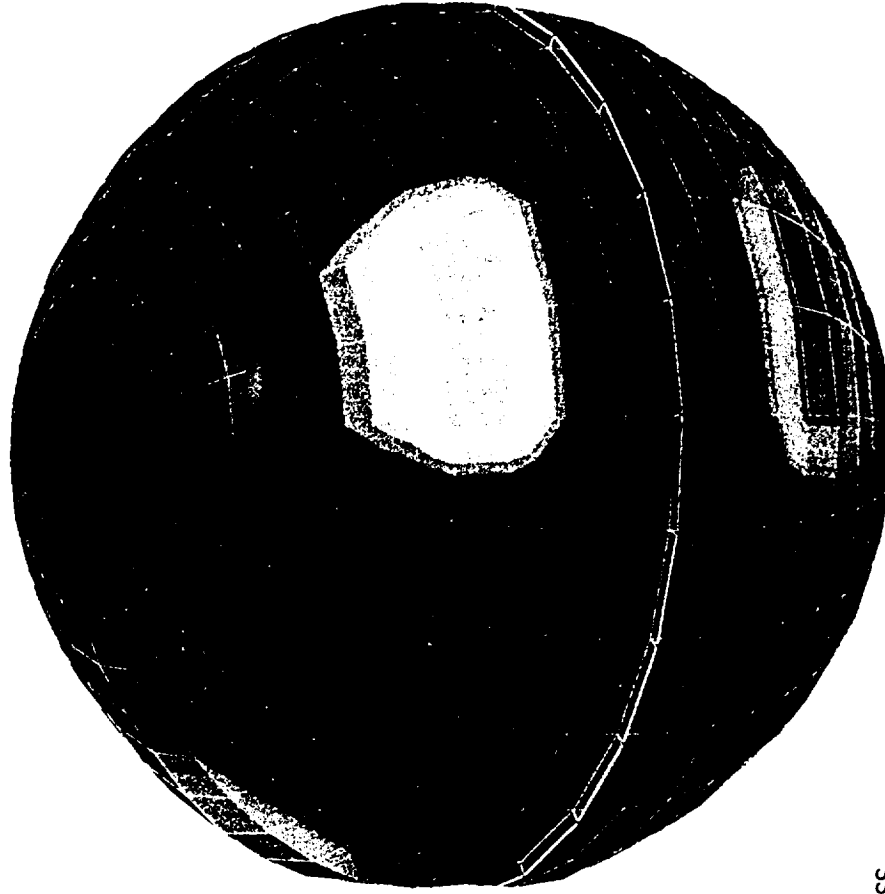
37921.
34329.
30736.
27144.
23552
19959.
16367.

5590.
1998

X
Y
Z

V1
L3
C1
G1

Output Set: PRELOAD + TEMP + PRESS
Deformed(0.0279): Total Translation
Contour: Plate Bot VonMises Stress

INNSER SPHERE STRESSES DUE TO PRELOAD + TEMP + PRESSURE

Figure 15

VENUS AEROBAT SURFACE SCIENCE IMAGING SYSTEM
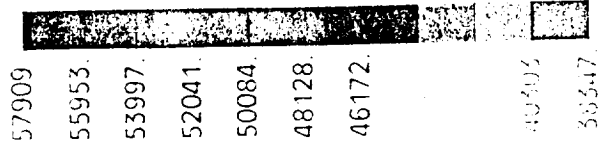
57909
55953.
53997.
52041.
50084
48128.
46172.

690.17

Output Set: PRELOAD + TEMP + PRESS
Deformed(0.0593): Total Translation
Contour: Plate Top VonMises Stress

OUTER SPHERE STRESSES DUE TO PRELOAD + TEMP + PRESSURE

Figure 16

V1
L3
C1
G2

X
Y
Z

VENUS AEROBAT SURFACE SCIENCE IMAGING SYSTEM

V1
L3
C1
G4

56801.

36894.
33576.
30258.
26940.
23622.
20304.
16986.

7033.
3715.

X
Y
Z
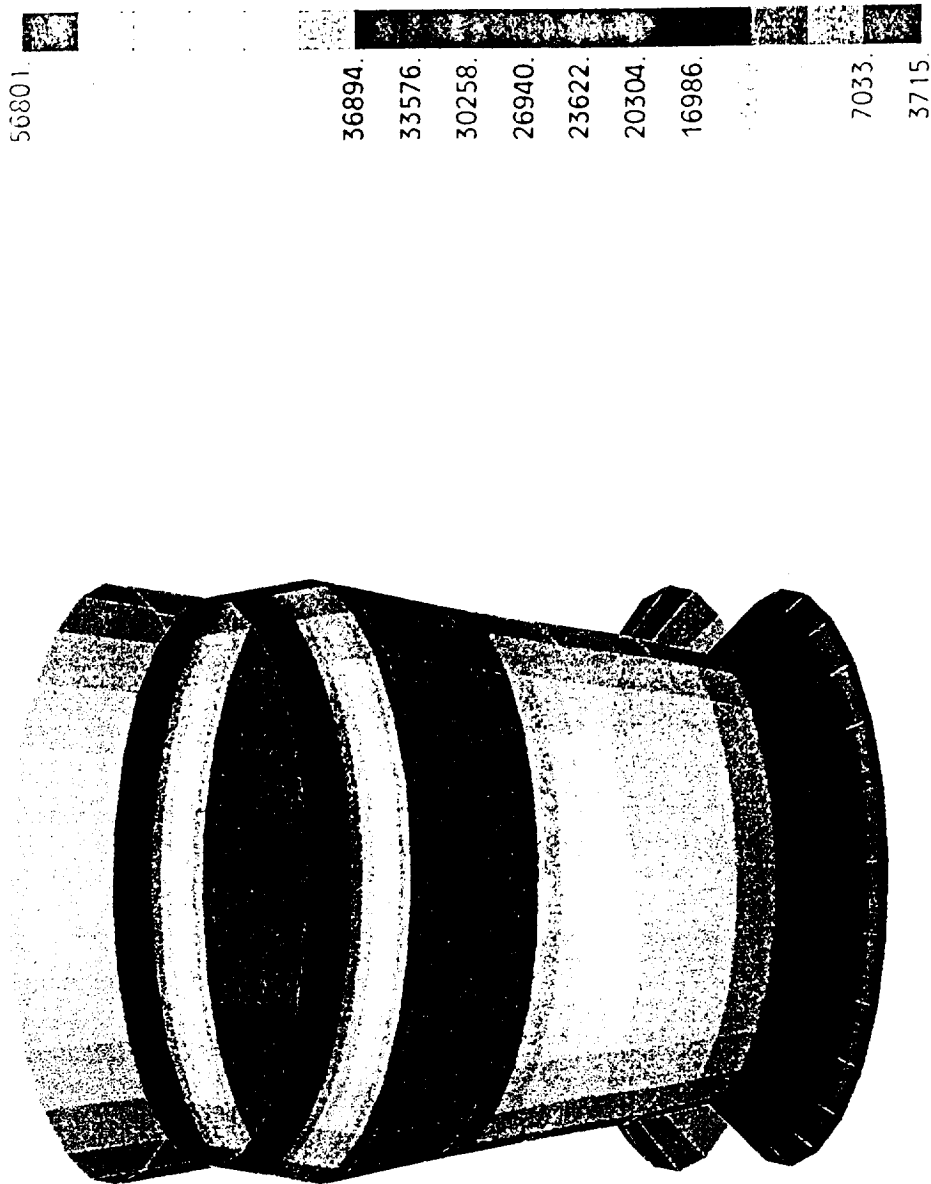
Output Set: 1450 PSI PRESSURE
Deformed(0.0527): Total Translation
Contour: Plate Top VonMises Stress

STRESSES IN APERTURE CONE DUE TO 1450 PSI PRESSURE

Figure 17

VENUS AEROBAT SURFACE SCIENCE IMAGING SYSTEM

V1
L3
C1
G1

24336.
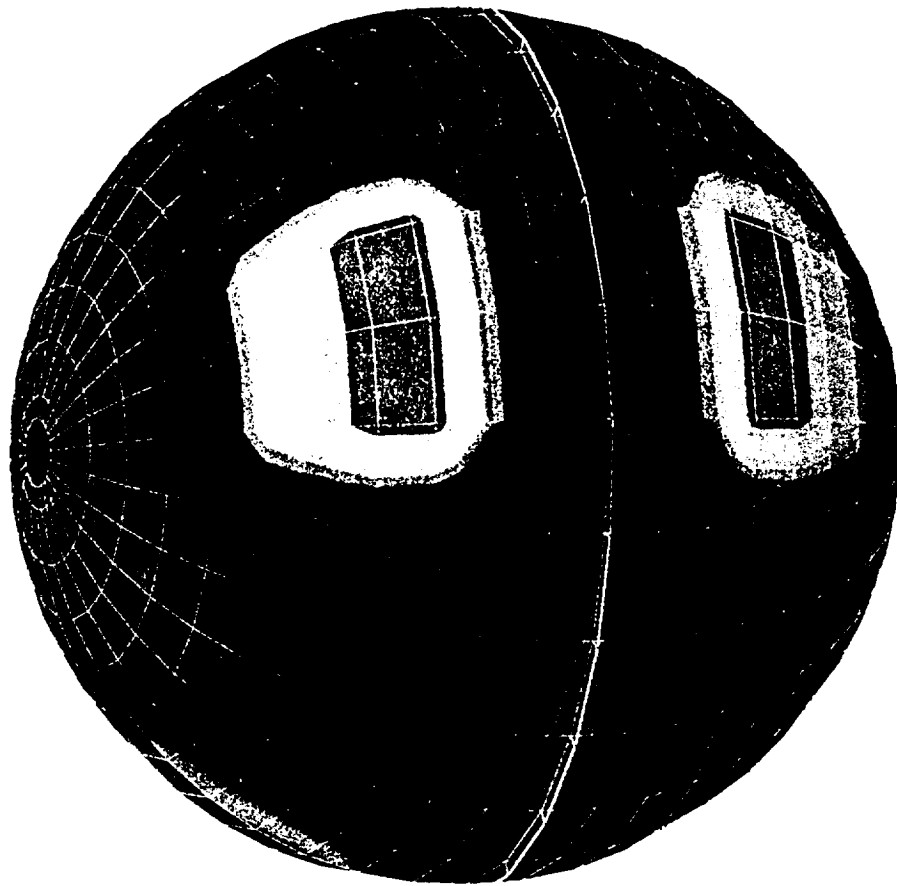
15491.
14017.
12543.
11069.
9594.
8120.
6646.

2224.
749.7

X
Y
Z

Output Set: HOT TEMPERATURE
Deformed(0.0345): Total Translation
Contour: Plate Bot VonMises Stress

STRESSES IN INNER SPHERE DUE TO HOT TEMPERATURE

Figure 18

WINDOW MATL: FUSED SILICA

Ø 1.420 MARK I SEAL
MATL: HESTELLOY X
SOFT NICKEL OR GOLD PLATED

Ø 1.550 MARK I SEAL
MATL: HESTELLOY X
SOFT NICKEL OR GOLD PLATED

Ø 1.550 MARK I SEAL
MATL: HESTELLOY X
SOFT NICKEL OR GOLD PLATED

FILLET WELD

1.838
[46.68]

.140
[3.554]

.224
[5.687]

.408
[10.363]

.176
[4.473]

O-RING MATL:
ETHYLENE PROPYLENE

RETAINING RING, BOWED
MATL: .037 THK CRES

OPTICS

Ø 1.436
[36.473]

15.00°

15.00° VIEW ANGLE

1° GREATING TO ALLOW
WINDOW MOVEMENT

19°

15°

.048
[1.210]

.040
[1.016]

.172
[4.356]

Ø .938
[23.825]

FILTER

Ø .590
[14.986]

DETAIL A
SCALE 4/1

Figure 19

AIAA

AIAA 98-0897

GONDOLA DESIGN FOR VENUS DEEP ATMOSPHERE AEROBOT OPERATIONS

Matthew Kuperus Heun, Jack A. Jones and Jeffery L. Hall

Jet Propulsion Laboratory
California Institute of Technology
Pasadena, California 91109

36th Aerospace Sciences
Meeting & Exhibit
January 12–15, 1998 / Reno, NV

GONDOLA DESIGN FOR VENUS DEEP-ATMOSPHERE AEROBOT OPERATIONS

Matthew Kuperus Heun, Jack A. Jones* and Jeffery L. Hall*
Jet Propulsion Laboratory
California Institute of Technology
Pasadena, CA 91109

Abstract

Aerobots are balloon-based AEROnautical RoBOTS with autonomous navigation capabilities. An aerobot mission has been proposed for exploration of the upper atmosphere through near-surface regions of Venus. The wide range of atmospheric conditions from the relatively benign upper atmosphere to the hot, high-pressure surface require thermal protection of the scientific instruments, and the mass constraints of a balloon system require that the thermal protection system be lightweight. To meet the thermal control challenges, we propose use of lightweight vacuum dewar technology combined with a phase-change material (PCM) thermal damper. For the proposed aerobot mission, the total thermal control mass is estimated to be 7.1 kg out of a total gondola mass of 25 kg. The design allows 7.3 kg for science instruments and communication hardware. Four kilograms of PCM are required to provide a repeatable 15-hour mission sequence that includes a 3.5-hour descent to the surface, 1 hour of surface operations, a 2.5-hour ascent to the cooler upper atmosphere, and 8 hours to refreeze the PCM.

Lastly, aerobot system design tradeoffs are discussed, and the extension of vacuum dewar/PCM technology to outer planet probes is briefly explored.

Introduction

In 1985 the Vega/Venera program, a French/Russian/US initiative, sent two balloons and two landers to Venus. The balloons floated for 1–2 days at 54 km and concentrated primarily on atmospheric science. The landers made a 60-minute descent to the surface where measurements were taken for about 2 hours. The landers focused on surface geoscience at single sites and had limited operational life due to the harsh surface environment at Venus. No subsequent *in situ* surface or atmospheric explorations of Venus have been attempted despite a strong scientific motivation to improve our understanding of Venusian volcanism, tectonic processes and atmospheric dynamics.[1] These issues would be ideally addressed by a vehicle with the capability for (a) repeated descents to the Venusian surface, (b) autonomous navigation toward specific targets of scientific interest, and (c) long-term *in situ* atmospheric measurements. One such vehicle is an autonomously navigated aerobot (AEROnautical roBOT) consisting of a instrumented gondola suspended below a zero-pressure balloon filled with a phase change buoyancy fluid. This concept is described below. Although there are many aspects of Venusian aerobot design, this paper focuses on the structure and thermal control strategies for the instrumented gondola to enable its survival during repeated descents to the surface.

Aerobots

Aerobots with surface descent capabilities provide a unique opportunity to advance our understanding of the surface *and* atmosphere of planets and moons with significant atmospheres. In particular, Venus, Earth and Titan have extensive tropospheric atmospheres that allow the use of balloons containing phase-change fluids (PCF) to provide altitude control capabilities.[2] By using knowledge of wind headings at various altitudes and on-board computer-based path planning algorithms, PCF balloons offer the possibility of zero-power autonomous navigation through these atmospheres. The only power required is for on-board electronics and scientific instrumentation.

Altitude control requires a PCF that exists as a vapor at warmer, low-altitude conditions and as a

---

* Senior member, AIAA.

liquid at cooler, high-altitude conditions. The aerobot's vertical motion is therefore caused by buoyancy modulation associated with balloon volume change as the PCF vaporizes or condenses. When mostly vaporized, the PCF provides enough buoyancy to move the aerobot upwards; when mostly condensed, the PCF provides insufficient buoyancy and the aerobot drops downwards. Note that this strategy only works in the tropospheric part of the atmosphere where the temperature decreases with altitude.

Figure 1 shows a Van't Hoff (vapor pressure) plot of several candidate PCFs along with the pressure curve for the Venusian atmosphere. The point at which any PCF line crosses the atmosphere line is the equilibrium altitude for an aerobot employing that particular PCF. When the PCF is above its equilibrium altitude it is a liquid, and when the PCF is below its equilibrium altitude it is a vapor. It is seen from the plot that there are many possible fluid choices depending on the details of the aerobot and mission design. For example, a mixture of water (H_2O) and ammonia (NH_3) has been proposed for use at Venus, where water would boil below 42 km and partially condense above 42 km.[3,4,5] Alternatively, a more recent study at JPL has suggested that a helium-water mixture would yield a lighter, more robust buoyancy system.[6] Whatever the final choice of fluids, the feasibility of the PCF balloon concept itself has been recently demonstrated in a successful campaign of flights over the Southern California deserts.[7]

A nominal Venus aerobot mission profile is shown in Figure 2. The alternating evaporation and condensation of the PCF causes oscillatory motion of the system about the equilibrium altitude. Note, however, that the aerobot does not require an on-board energy source to accomplish this vertical motion. Thermodynamically, the aerobot acts as a heat engine using the planet's natural atmospheric temperature gradient below the tropopause to drive the system's vertical motion in the gravitational field. The thermal energy absorbed by the PCF during evaporation at low altitudes is used to propel the aerobot upward. When the energy is released by the PCF during condensation at high altitudes, the aerobot descends and the thermodynamic cycle is complete.

The natural oscillating behavior of the aerobot can be altered by capturing the PCF liquid in a small reservoir, thereby delaying or preventing its vaporization. In this situation, the aerobot will descend deep into the atmosphere and potentially to the planet's surface. This will enable surface and near surface scientific examination of the planet or moon. Upon release of the liquid from the reservoir, the aerobot will re-ascend to the upper atmosphere.

The Venus Environment

The Venusian environment is challenging for *in situ* scientific exploration because of its dense, optically thick and corrosive atmosphere. The nominal flight profile (Figure 2) for a Venus Aerobot spans the range from 0 to 60 km altitude. On the surface, the temperature is 460 °C and the pressure is 92 atmospheres; at 60 km, the temperature is -10°C and the pressure is 0.24 atmospheres. The Venusian cloud layer extends from approximately 47 to 70 km with thick haze layers both below and above. Not only do these layers hamper visual observations, but the clouds also contain a significant amount of sulphuric acid droplets. Therefore, all exposed components of the aerobot must be resistant to sulphuric acid attack, as well as be compatible with the temperature and pressure extremes encountered during the flight profile. The remainder of this paper will focus on the design of a gondola that can safely house the onboard electronics and scientific payload in this environment.

Venus Aerobot Gondola Requirements

A recent JPL effort has examined low-power camera configurations and thermal control strategies for Venus aerobot operations. The Venus Aerobot Surface Science Imaging System (VASSIS) project began by deriving survivability requirements from the expected aerobot mission profiles and the Venusian environment. Table 1 summarizes preliminary Venus aerobot mission flight requirements, and Table 2 summarizes the Venus atmospheric parameters associated with the flight requirements.

It can be shown that each additional kilogram of mass carried on the gondola requires roughly a threefold increase in the overall system mass because the increased balloon volume required to carry the additional gondola mass. Thus, the primary gondola design challenge is to provide pressure and thermal protection, provide an optical viewport, and allow external data communications with a minimum amount of mass. The following section describes a gondola design that meets the VASSIS requirements.

VASSIS Gondola Design

Pressure Vessels

A schematic of the VASSIS gondola is shown in Figure 3. It's a concentric sphere design employing both passive and active thermal control devices. The central spherical instrument housing is 30.5 cm (12 in.) in diameter and is surrounded by multi-layer

insulation (MLI) in a vacuum. The proposed MLI is 15 to 20 layers of doubly-aluminized Kapton with fiberglass spacers. In addition, a couple of layers of aluminum or gold foil will be required next to the outer shell because Kapton starts to degrade in the range of 430 to 450 °C.[*] Note that this inner vessel is not subjected to Venusian atmosphere pressure loading and therefore is only 0.75 mm thick. In contrast, the outer pressure vessel is a spherical titanium shell that is 4.0 mm (0.16 in.) thick. It is designed to withstand the Venus surface conditions of 460 °C and 92 bar, as well as atmospheric entry force loads of up to 500 g.[9,10] The central instrument housing is held in place by a series of tension bands (Figure 4) fabricated from braided polybenzoxazole (PBO) fiber material.[†] Despite the mechanical complexity of using tension band supports, PBO's high strength and low thermal conductivity make it an attractive choice for minimizing heat conduction from the hot outer shell to the cool inner shell in the lower atmosphere.[‡]

Gettering material will be placed in the annulus between the two shells to help maintain the vacuum. One material being tested at JPL is the zirconium-based getter St707 manufactured by SAES getters.

Phase-change Material (PCM) and Heat Pipe

A heat sink is used in addition to the MLI to provide temperature control for the instrument housing. It consists of a high heat of fusion phase-change material (PCM), $LiNO_3 \cdot 3H_2O$, that absorbs 296 kJ/kg of heat conducted through the MLI. Note that this phase change material is different than the phase change fluid used as a buoyancy gas inside the balloon. The melting temperature of $LiNO_3 \cdot 3H_2O$ is 30 °C; therefore, during descents into the hot lower atmosphere, the PCM will maintain a 30 °C internal temperature until it is completely melted. Upon re-ascent to a 55 km altitude, the PCM will begin to freeze again as it dumps heat to a now cooler than 30 °C atmosphere. A simple, hollow stainless steel tube, 1.27 cm (0.5 in.) diameter, partially filled with ammonia, is the means by which heat is transferred from the PCM in the central instrument housing to the outer pressure vessel and atmosphere. When the

pressure vessel is cooler than the instrument housing, ammonia will condense in the pipe near the pressure vessel wall and will fall by gravity to the inner instrument housing. The liquid ammonia will absorb heat from the PCM as it boils. The vapor returns to the outer pressure vessel and condenses again on the cooler surface, thereby transferring energy to the environment and completing the cycle.

The heat delivered to the outer pressure vessel by this gravity-fed diode heat pipe (also known as a reflux boiler) transfers conductively through the titanium pressure vessel to a second, external heat pipe circuit, without the necessity of transferring the ammonia itself through the pressure vessel wall. This outer, secondary heat pipe circuit (Figure 5) is fashioned similarly as a gravity-fed, 1.27 cm (0.5 in.) OD hollow tube, wherein ammonia is condensed in an upper finned heat transfer matrix and falls by gravity to the outer pressure vessel wall area where it boils.

Note that when the outer shell is hot in the lower atmosphere, the ammonia does not condense on it and therefore does not transfer a significant amount of heat between the vessels. The one-way nature of the heat transfer is why it's called a *diode* heat pipe.

Gondola Thermal Performance

To evaluate the thermal performance of the system, it was necessary first to estimate the balloon ascent and descent velocities. A transient thermal model was constructed for a 25 kg gondola with a balloon that was fabricated from 0.05 mm (0.002 in.) PBO film. At an altitude of 56 km, the balloon is 2.5 m diameter and 25 m long, and it is filled with PCF mixture of 50 % ammonia and 50 % water. The total floating mass of this system is about 100 kg (25 kg ammonia, 25 kg water, 25 kg payload, 15 kg balloon material, and 10 kg structure and miscellaneous). Figure 6 shows the altitude profile for the aerobot, and Figure 7 shows the velocity profile for the aerobot. (The secondary effects of atmospheric thermal radiation were not included in the simplified aerobot trajectory analysis.)

As shown in Figure 7, the initial descent velocity is 12 m/s, but this slows to a nearly steady value of 3 m/s from 30 km down to near the surface. Total descent time is calculated to be 3.5 hours, while total ascent time is slightly less than 2.5 hours. These calculations assume only balloon drag is important, with a descending coefficient of drag of 0.8 and an ascending coefficient of drag of 0.4, as has been estimated for similar Earth balloon systems.[12] Also, balloon heat transfer rates are assumed to be infinite so

---

[*] unpublished JPL data.

[†] This material is also being investigated for use as the primary Venus balloon material.[11]

[‡] However, current experimental work at JPL is using an alternative design based on rigid Ti-6Al-4V struts

that all balloon water vapor is condensed quickly at altitude and boiled quickly near the Venus surface when ascent is initiated.

A thermal model of the VASSIS gondola has been constructed in parallel with the above trajectory model. The resulting heat loads are shown in Figure 8 as a function of altitude. The problem of calculating heat transfer rates through the MLI was finessed by simply assuming that the total effective radiative emissivity (ϵ) between the concentric spheres is 0.01. This value is somewhat lower than achieved on typical spacecraft instruments (for which $\epsilon \sim 0.03$) but is believed to be achievable with careful design and installation of the MLI. Note that extremely low power dissipation rates (< 1 W average) are expected for the science instruments during low-altitude operations. The above assumption is reasonable because a communication system would be used only during upper-atmosphere operation. Thus, no internal electronic power dissipation is shown in Figure 8.

At altitudes below about 10 km. the radiation heat leak between the spheres dominates conduction heat leaks from the PBO band supports and the combined conduction and radiation at the camera window (constructed from fused silica glass). Total heat load at the surface is roughly 85 W. Approximately 1.5 kg of PCM mass is necessary to absorb the integrated descending heat load (Figure 9), a further 1 kg of PCM is required to absorb the heat load from 1 hour of surface operations, and another 1 kg is required to absorb the integrated ascending heat load. The nominal design includes an additional 0.5 kg of PCM for margin.

An estimate has been made of the time required for PCM cooling when the balloon bobs between 56 km and 40 km during alternate condensation and boiling of the water in the water/ammonia balloon. The model shows that two hours of bobbing time (about two full round trips) is required for each kilogram of PCM to be re-frozen. Thus, one repeatable mission scenario could consist of a 3.5-hour descent, 1 hour on the Venus surface, a 2.5-hour ascent, and 8 hours bobbing time for a total of 15 hours if 4 kg of PCM is used. Significantly longer low-atmosphere hover times could be achieved if the aerobot did not descend all the way to the surface due to the compounding effect of rapidly increasing heating rates and transit times at the lowest altitudes.

Table 3 presents a mass breakdown of the thermal control system. The PCM and the two ammonia heat exchangers comprise the bulk of the 7.1 kg total. Table 4 presents a mass breakdown for the entire gondola.

The thermal control system comprises 28%, the outer titanium shell 34%, and the onboard electronics and science payload 29% of the 25 kg total.

Venus Aerobot Thermal/System Design Issues

There exist many interesting design issues and tradeoffs with the gondola thermal design and its interaction with the overall Venus aerobot balloon system design. First, it must be realized that because the aerobot is a floating system, small increases in insulation or PCM mass lead to large increases in total system mass. This drives the need for highly efficient insulation (MLI) to minimize the heat leak into the instrument container and hence minimize PCM mass. Similarly, if the heat of fusion of the PCM were to be larger, then less would have to be carried and the overall system mass would shrink. Alternatively, higher heat of fusion PCMs would enable longer hover times near the surface for the same mass.

Another interesting tradeoff concerns the choice of melting temperature of the PCM. The lower the PCM melting temperature, the higher the aerobot must fly to refreeze the PCM after surface operations. Higher altitudes require larger (and heavier) balloon systems and therefore heavier cruise and entry systems. On the other hand, higher melting temperature PCMs lead to higher operating temperatures for the onboard electronics and science instruments. This can be a particular problem for imaging systems where the signal to noise ratio is a strong function of temperature.

Another design tradeoff involves the shape of the balloon and the PCM mass. To limit transit time between the upper, cooler atmosphere and the lower, hotter surface (and therefore reduce the amount of PCM necessary), the balloon should present a small frontal area to minimize drag. To achieve reduced frontal area for a given volume, a cylindrical balloon with large aspect ratio (length/diameter) can be used. (The balloon used herein for the gondola design has a rather large aspect ratio of 10.) But, because of high surface area to volume ratios, high aspect ratio cylindrical balloons are relatively massive compared to cylinders (or spheres) with near-unity aspect ratios. The minimum mass design for the overall system must therefore balance these conflicting trends.

Applications for Outer Planet Exploration

The vacuum dewar, PCM gondola concept can also be used for deep atmospheric exploration of all the gas giant planets. Although the thermodynamic profiles vary from planet to planet, all feature high pressure, high temperature environments similar to

that of Venus at sufficiently low altitudes. A very preliminary evaluation has been performed by considering a point design for a deep-Jupiter probe that would make only one descent.

The non-repeating nature of this Jupiter design means that an atmospheric cooling heat exchanger is not required. Therefore the gondola/probe can be streamlined to increase the drop velocity and allow deeper penetrations for a given thermal design. With an aerodynamic tear-drop shaped inconel shell instead of a spherical titanium shell, a 50-kg, 38-cm diameter gondola would take approximately 1.5 hours to descend 414 km from the anticipated Jovian water clouds (5.0 bar, 0 °C) to about 500 bar pressure and 806 °C. Less than 2 kg of water serving as the PCM would be required to maintain all science instruments at 0 °C for the entire descent. For comparison, the 118 kg Galileo descent module only returned data from roughly the 20 bar (70 km) level.

Conclusion

This paper presents a design for a low-mass, thermally protective gondola that can be used for Venus aerobot operations near the surface. The proposed aerobot mission scenario involves descent to the surface followed by re-ascent to the upper, cooler altitudes of Venus on a 15-hour repeatable cycle. Vacuum dewar technology with multilayer insulation is used to protect the science instruments and communication hardware during excursions into the hot lower atmosphere. A phase change material is also used as a heat sink to help limit the temperature increase inside the gondola. Four kilograms of phase-change material will enable a mission sequence comprised of a 3.5-hour descent to the surface, 1 hour of surface operations, a 2.5-hour ascent to the upper atmosphere (about 56 km), and 8 hours to freeze the phase-change material. Total aerobot mass is 100 kg. The gondola mass is 25 kg with 7.3 kg available for science instruments and communication hardware.

The basic configuration of outer pressure vessel, inner evacuated MLI region, and inner science vessel with PCM has potential uses for deep atmospheric studies of not only Venus but also for Jupiter and the other, somewhat cooler, gas giant planets of Saturn, Uranus, and Neptune.

References

1. Gilmore. M.S., et al. "Investigation of the Application of Aerobot Technology at Venus: Scientific Goals and Objectives of the Proposed Balloon Experiment at Venus (BEV) and Venus Flyer Robot (VFR)—Final Report". Brown University Department of Geological Sciences. 1 June 1996.

2. Nock, K.T., J.A. Jones, & G. Rodriguez. "Planetary Aerobots: A Program for Robotic Balloon Exploration". 34th AIAA Aerospace Sciences Meeting and Exhibit. 15-18 January 1996, Reno, Nevada. paper number AIAA 96-0355.

3. Moskalanko, G.M. "Mekhanika Poleta v Atmosfere Veneny". Mashinosteroenie Publishers. Moscow, 1978.

4. Moskalanko, G.M. "Two Component Working Material for a Floating Probe in the Atmosphere of Venus", Proceedings, High Temperature Electronics and Instrumentation Conference, December 1981.

5. Moskalanko, G.M. "Dirizhabl' dlya Veneny". Nauka Zhizn. No. 9, September 1981, pp. 85-87.

6. Nock, K.T. et al. "Venus Geoscience Aerobot Study (VEGAS) Report", unpublished JPL report, 28 July, 1997.

7. Nock, K.T., et al. "Balloon Altitude Control Experiment (ALICE) Project". 11th AIAA Lighter-Than-Air Technology Conference, 16-18 May 1995, Clearwater, Florida.

8. Klaasen, K. "VASSIS Camera SNR Analysis as a Function of Wavelength, Altitude, and Sun Angle", unpublished JPL report, 2 July 1996.

9. Salama, M. "The VASSIS Gondola Structural Design", JPL Internal IOM 352G:96:146:MS, 6 November 1996.

10. Salama, M. "Revised VASSIS Gondola Design", JPL Internal IOM 352G:96:150:MS, 30 December 1996.

11. Yavrovian, A. et al., "High Temperature Material for Venus Balloon Envelopes", 11th AIAA Lighter-Than-Air Technology Conference, 16-18 May 1995, Clearwater, Florida.

12. Wu, J.J. & J.A. Jones. "Performance Model for Reversible Fluid Balloons", 11th AIAA Lighter-Than-Air Technology Conference, 16-18 May 1995, Clearwater, Florida.

Table 1. Venus aerobot mission flight requirements.

Parameter	Requirement
Mission duration	30–90 days
Maximum atmospheric entry deceleration	250–500 g
Estimated descent, ascent, and float periods	Descent: 3.5 hr, Ascent: 2.5 hr, Float: 0–1 hr
Flight altitude	surface < z < 60 km

Table 2. Venusian environment parameters corresponding to flight requirements.

Parameter	Value
Atmospheric temperature range	$-10\ ^\circ C < T < 460\ ^\circ C$
Atmospheric pressure range	$0.25\ atm. < P < 92\ atm.$
Atmospheric corrosives	Sulfuric acid
Solar flux	$40\ W/m^2$ (diurnal average)
Length of day as seen by aerobot	~ 96 hours
Length of night as seen by aerobot	~ 96 hours

Table 3. VASSIS temperature control mass summary.

Component	Mass (kg)
Phase-change Material (PCM)	4.0
PCM Heat Exchanger (Inside Gondola)	1.5
MLI	0.2
Internal Gravity-fed Heat Pipes	0.3
External Heat Exchanger (Beryllium Fins)	0.9
Getters	0.2
Total	7.1

Table 4. VASSIS gondola mass summary.

Component	Mass (kg)
Temperature Control	7.1
Outer Titanium Shell	8.6
Inner Titanium Shell	1.0
Tension-band Supports	0.5
Miscellaneous	0.5
Science Instruments and Communication	7.3
Total	25.0
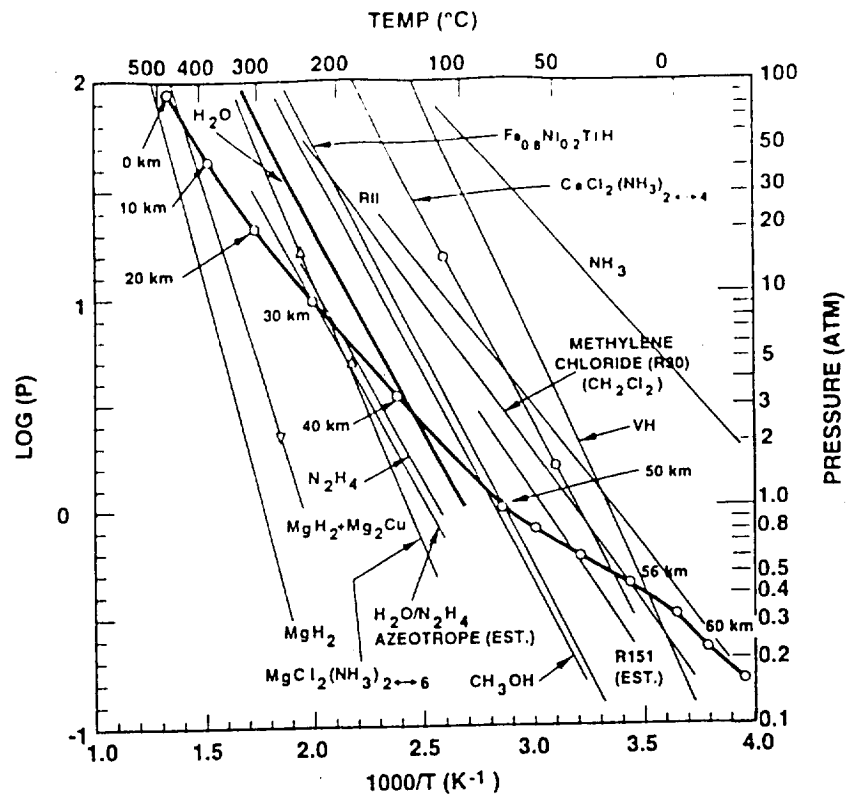
Figure 1. Van't Hoff plot for Venus atmosphere and candidate PCFs.
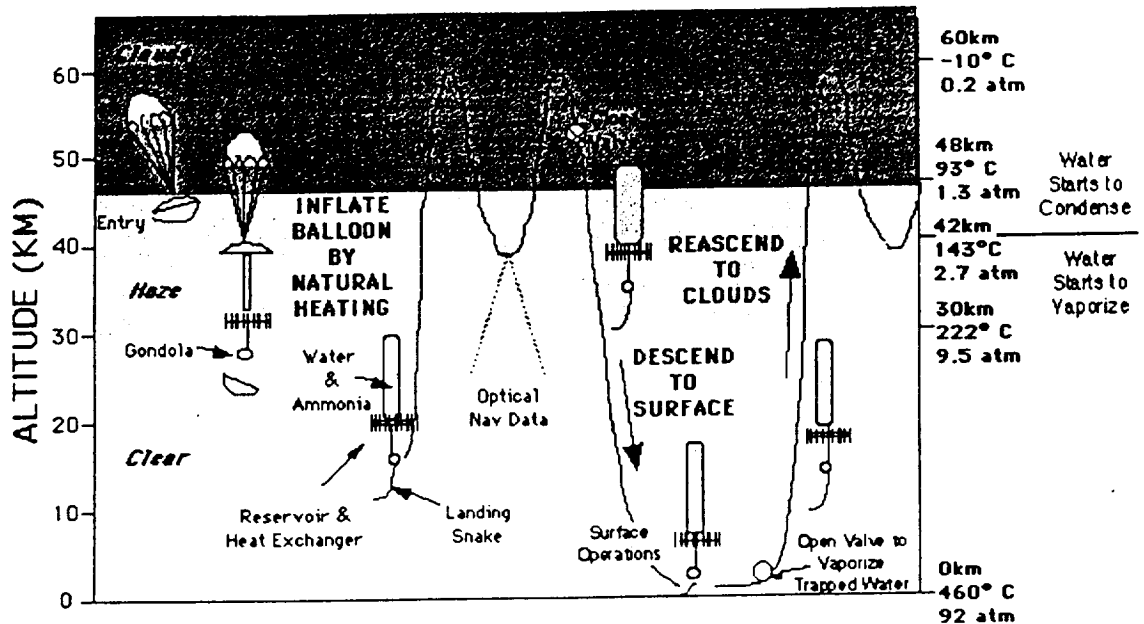
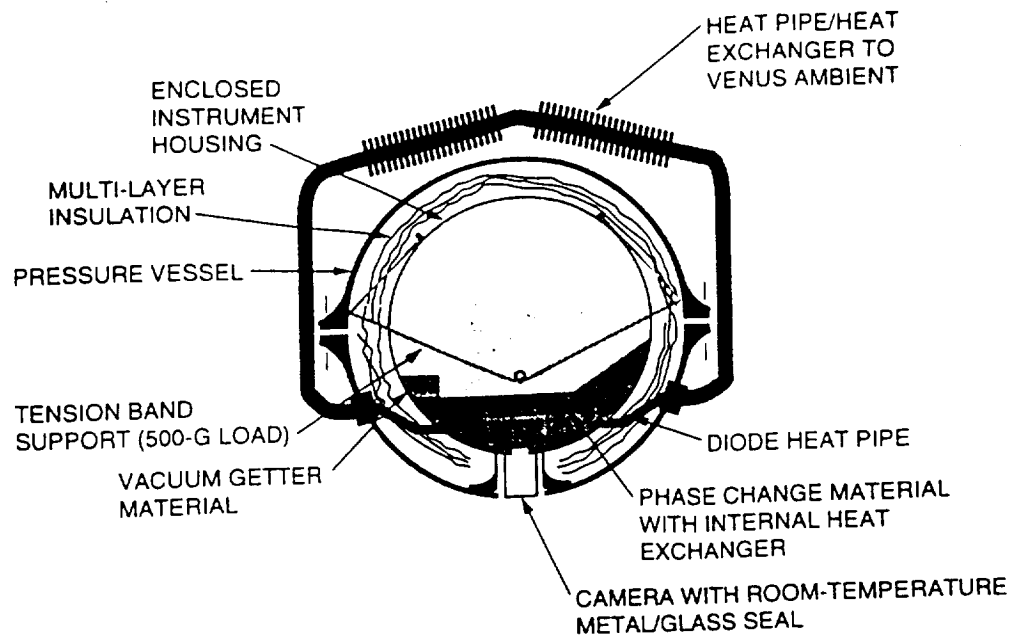Figure 2. Venus aerobot mission profile with surface descent capabilities.

HEAT PIPE/HEAT
EXCHANGER TO
VENUS AMBIENT

ENCLOSED
INSTRUMENT
HOUSING

MULTI-LAYER
INSULATION

PRESSURE VESSEL

TENSION BAND
SUPPORT (500-G LOAD)

VACUUM GETTER
MATERIAL

DIODE HEAT PIPE

PHASE CHANGE MATERIAL
WITH INTERNAL HEAT
EXCHANGER

CAMERA WITH ROOM-TEMPERATURE
METAL/GLASS SEAL

Figure 3. VASSIS gondola temperature control schematic.
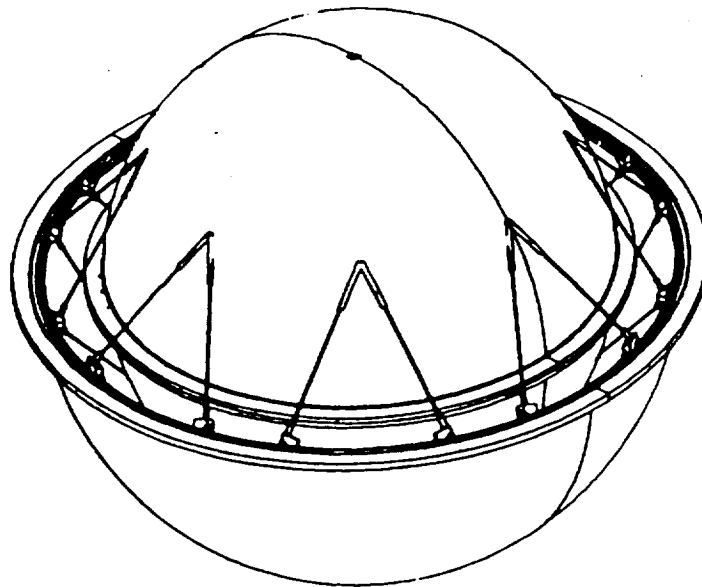
Figure 4. PBO Tension-band support system.
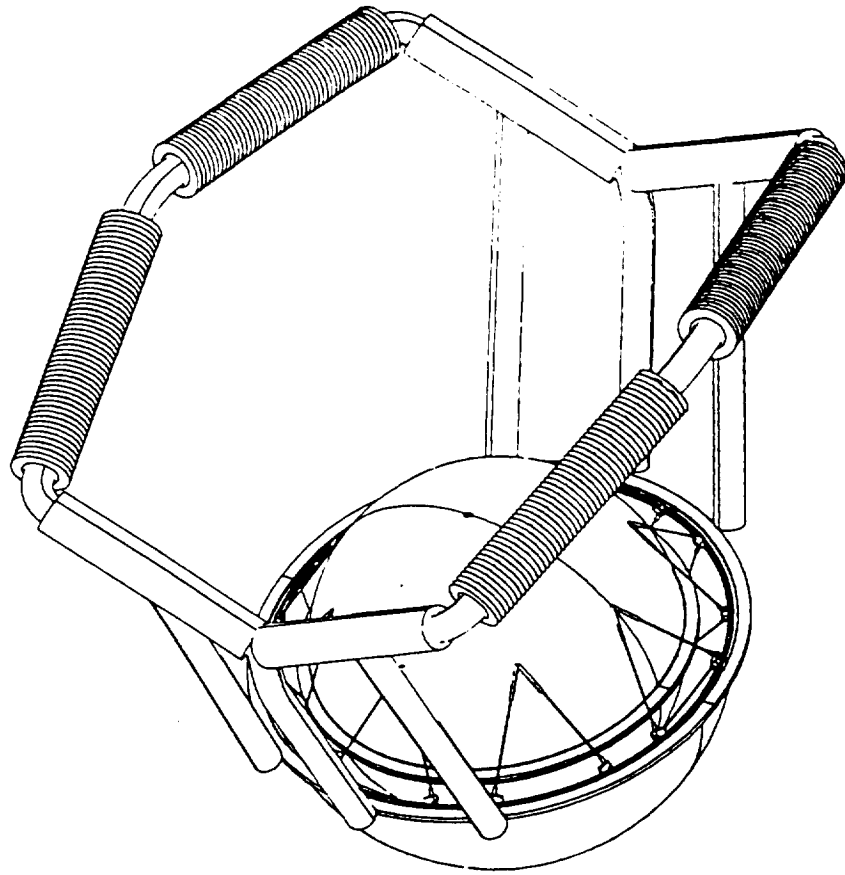
Figure 5.   Heat exchanger configuration.
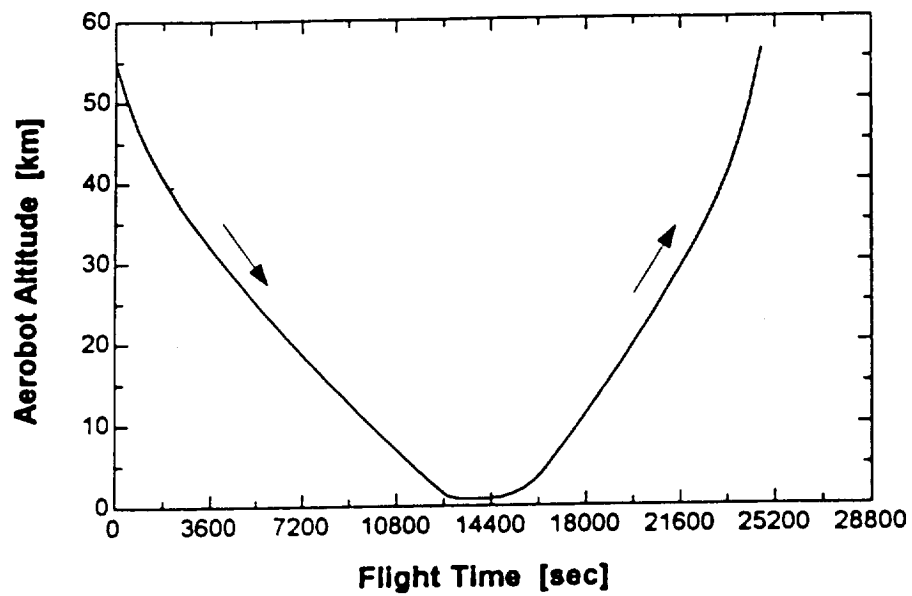
Figure 6.   Acrobot altitude profile.
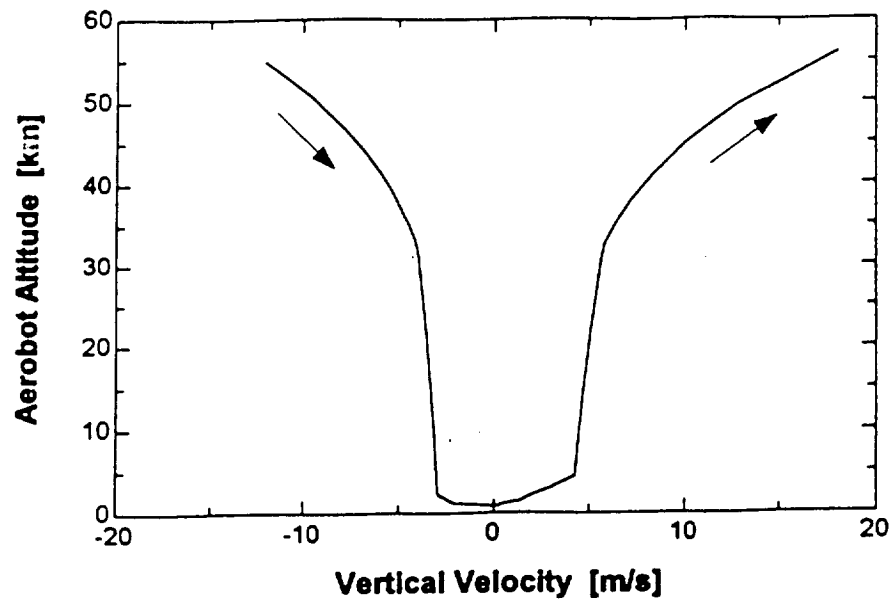
Figure 7. Aerobot descent velocity profile.
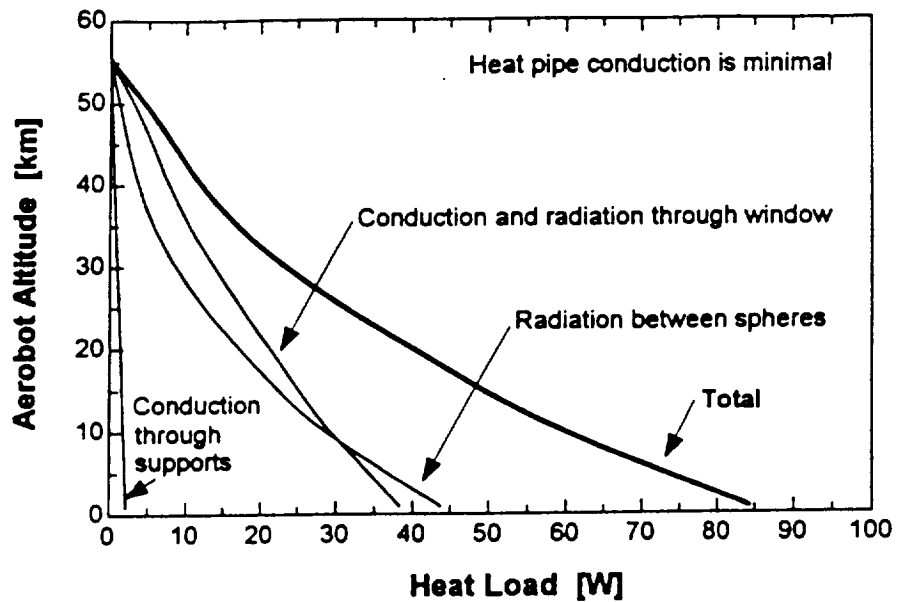
Figure 8. VASSIS gondola heat loads.
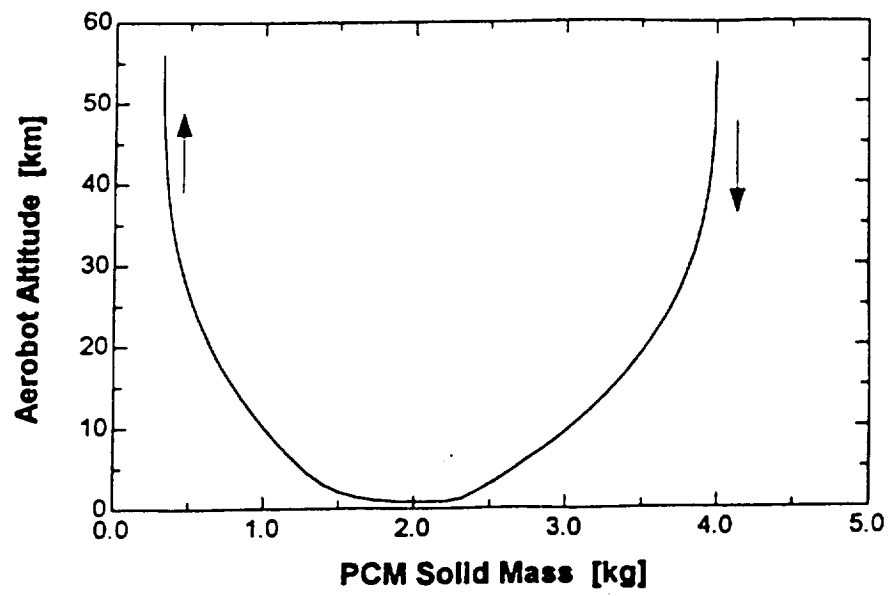
Figure 9. PCM solid mass during flight.

VASSIS PROTOTYPE CAMERA AND GSE FUNCTIONAL REQUIREMENTS

1. The VASSIS prototype camera system shall consist of a camera head including APS detector, lens, filter, shutter, and viewport window, attached by means of brackets to a 12-inch square x 3/8-inch thick aluminum base plate.

2. The VASSIS camera shall use a spare STRV-2 Active Pixel Sensor (APS) detector as a baseline. This detector has the following characterisitcs:

        256 x 256 array size
        Photogate pixels
        20.4 x 20.4 um2 pixels
        Fill Factor ~20%
        On-chip: Timing, control, CDS
        Conversion Gain ~10 uV/e-
        Full well saturation at ~750 mV
        Read noise ~13 e- rms
        Dynamic range ~76 dB
        Power requirement ~5 mW
        Dark current generation rate ~12 mV/sec (at T = +24°C)

3. The number of inoperative pixels in the detector array shall not exceed 40.

4. The detector shall exhibit response uniformity across all pixels of <3%.

5. The camera shall operate at room temperature (~22°C) under normal ambient laboratory conditions.

6. A temperature sensor (LM335) shall be located on the APS detector for telemetry.

7. The camera readout noise floor shall be <0.05% of the detector full-well level.

8. The system response shall be linearly related to the incident light level to <1% over its entire dynamic range.

9. Signal saturation in one pixel shall not affect any other pixel.

10. The APS operation shall be controlled by an FPGA controller chip.

11. The prototype camera head shall be fabricated using commercial grade parts (0 to +70°C) or better.

12. The camera shall operate using 5 vdc and ±12 vdc input power.

13. The APS shall operate within specification over operating voltage settings that vary as much as 0.2 v from their nominal values.

14. The VASSIS camera head shall accept, with no more than a change to an external jumper, the substitution of a Vigilante-type APS photodiode detector (256x256, 20 um pixels) in4place of the baseline STRV-2 photogate APS.

15. The camera gain shall be set to approximately 20 electrons/DN for the baseline photogate APS device (i.e., 200 uv/DN). A gain switch shall be provided that yields a gain of approximately 100 electrons/DN for the photodiode APS device (i.e., 350 uv/DN).

16. The output signals from the APS detector shall be digitized linearly to 12 bits.

17. The output data rate from the detector shall be >16 kpixels/sec or >200 kbps into a full-frame buffer (0.8Mb) included in the camera head.

18. The total camera head mass shall be <250 gm.

19. The camera head volume shall not exceed 2x2x2.5 in.

20. The operating power consumed by the camera shall be <2 watts.

21. The GSE shall be able to acquire, store, and display images from the VASSIS prototype camera.

22. The GSE shall command and control the camera head in a manner consistent with the camera logic design and shall command and control the shutter in a manner consistent with its control electronics.

23. The camera frame cycle timing shall begin on receipt of an imaging command from the GSE. The frame cycle shall include a 2-sec exposure window during which the APS detector is set to its signal integration state.

24. A high-speed erasure of the APS device shall be commanded just prior to the opening of the exposure window during each frame cycle.

25. The GSE shall synchronize the mechanical shutter operation with the camera frame cycle and APS clock operation.

26. The data transfer rate from the camera head frame buffer to external memory (i.e., the GSE) shall be >115 kbps.

27. Communication between the camera head and the GSE shall be via a RS-232 serial interface.

28. The camera's frame repetition time shall be <10 sec.

29. The GSE shall collect and display APS temperature at least once per frame cycle and shall append this data to the image file along with any operator input comments and an automatically generated unique frame ID.

30. The camera lens shall be a commercially available off-the-shelf air-spaced lens providing a nominally flat focal surface at up to 15-deg full field of view.

31. The lens focal length shall be nominally 20 mm. However, a focal length of 25 mm shall be acceptable in the prototype camera.

32. The lens shall have a fixed aperture, which shall provide a focal ratio of f/1.9 or faster (if possible, f/0.95 shall be provided).

33. An unobscured view into an f/0.95 light cone (28° half angle) from every pixel in the detector array shall be provided.

34. The lens mounting shall permit the distance from the lens to the APS to be adjusted by shims or slotted holes for optimum focus.

35. Some degree of focus adjustment (planarity) shall be provided on the camera head using Belleville washers in four locations.

36. The lens and APS mountings shall provide a minimum of 3 mm clearance to accomodate the blade of a rotating shutter wheel bwtween the lens and the camera head.

37. The shutter wheel blade shall, if possible, be spaced not more than 0.5 mm from the APS surface, or to a minimum spacing allowed by the depth of the APS in its housing.

38. The shutter shall be controllable in such a way as to provide exposure times ranging from 1 to 2000 milliseconds, via control of the limits of motion and speed of rotation of the shutter wheel and the dimensions of the open slits in the shutter wheel blade.

39. The exposure shall be triggered by a signal from the camera electronics.

40. The mode of setting the starting position and logging the shutter-open time is TBD depending upon the motor and motor controller selected. The starting shutter position shall be achieved with the APS in a non-integrating state prior to the pre-exposure APS erasure during each frame cycle.

41. The prototype camera shall provide a fixed mounting for manually interchangeable spectral filters of standard size (2x2 inch square, maximum 1/4-inch thick).

42. The viewport window shall be schlieren-grade fused silica of nominal thickness 46.68 mm, with optically polished faces to 1/20-wave rms flatness.

43. The viewport window faces shall be quarter-wave A/R coated for wavelengths in the range 500-1100 nanometers.

44. The viewport window shall provide sufficient aperture for the f/0.95 lens and 15-degree unvignetted full field of view.

45. The viewport window mounting shall be as shown in JPL Dwg. E10170667 (Camera Layout, VASSIS Gondola) utilizing a bowed retaining ring.

46. X,Y,Z positioning of the camera shall be implemented by mechanical adjustments and shimming on the camera base support plate.
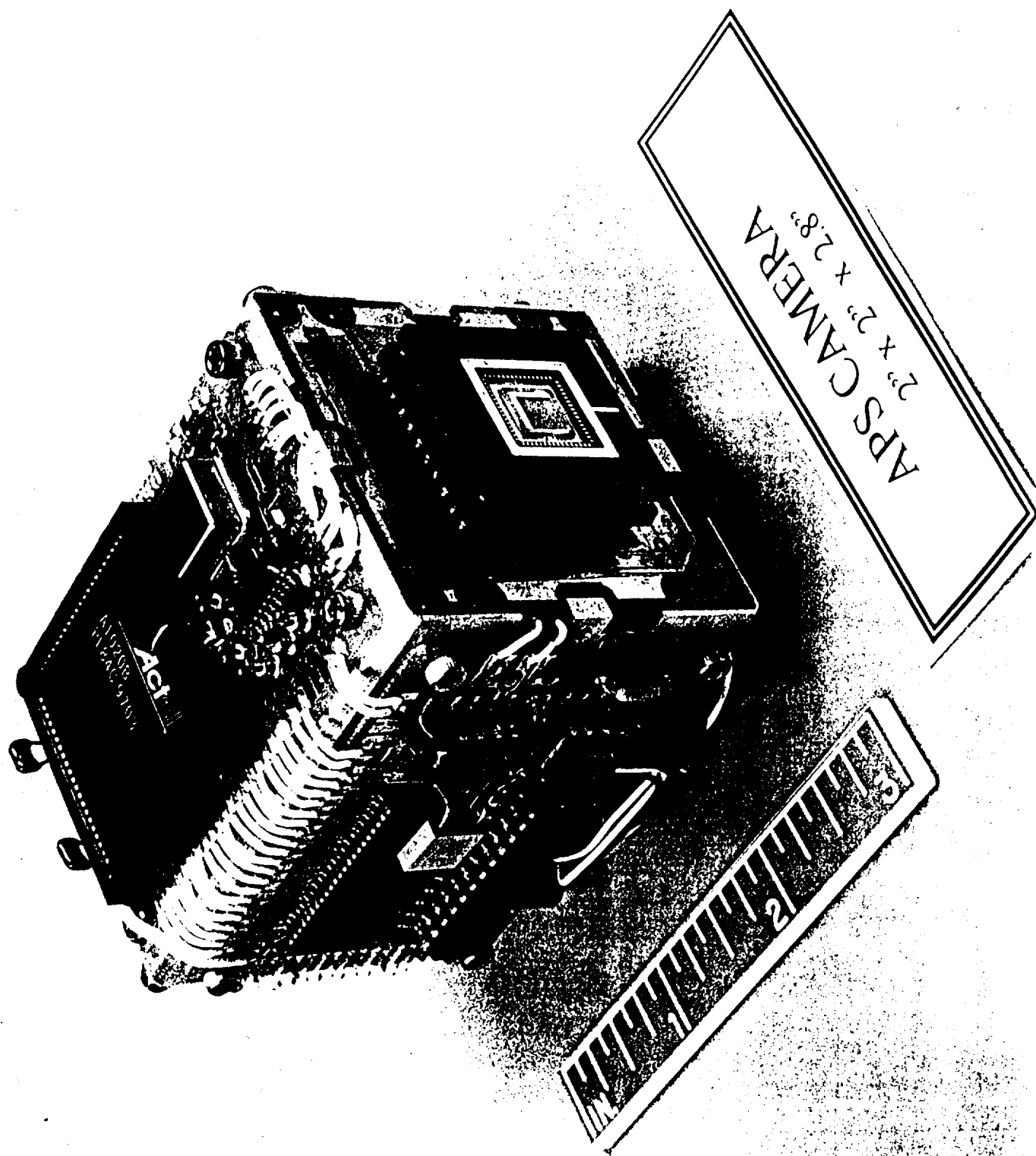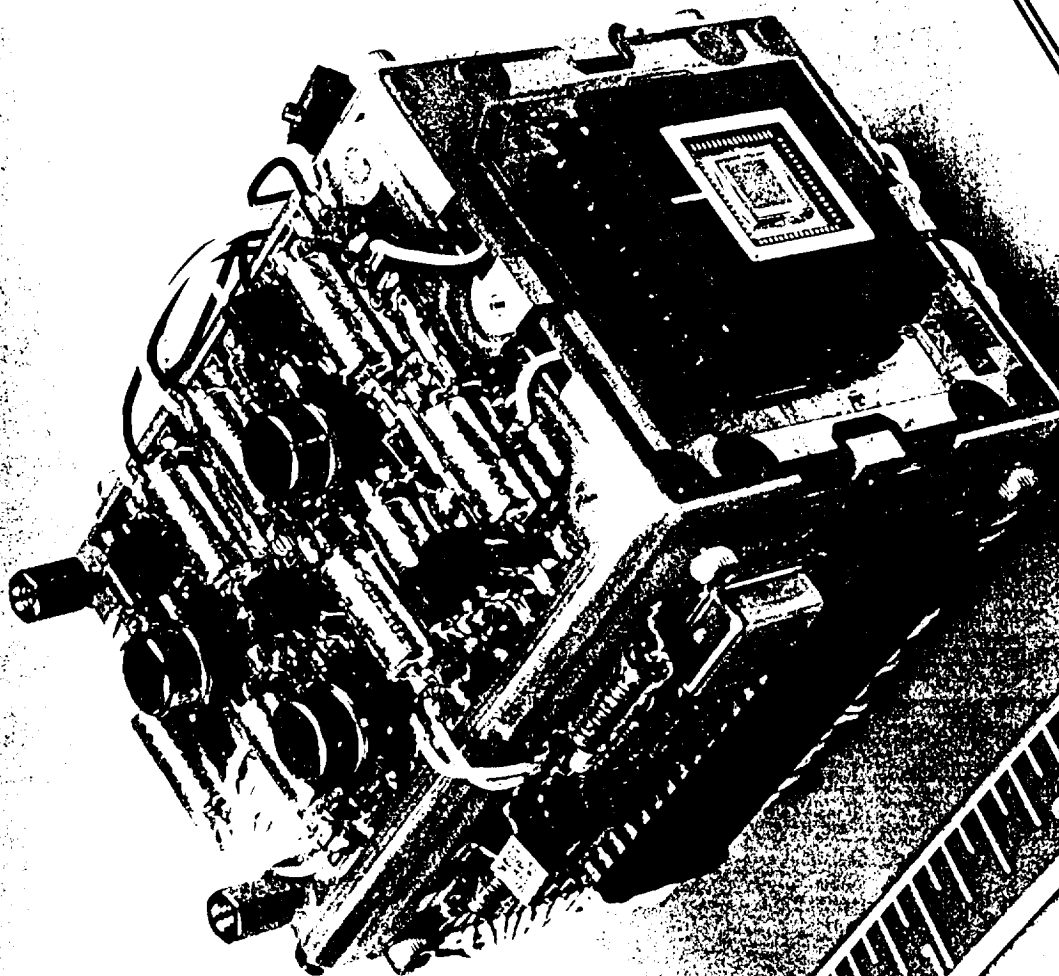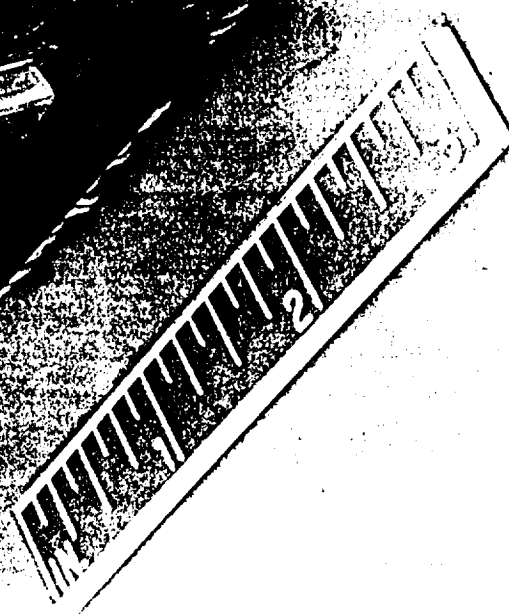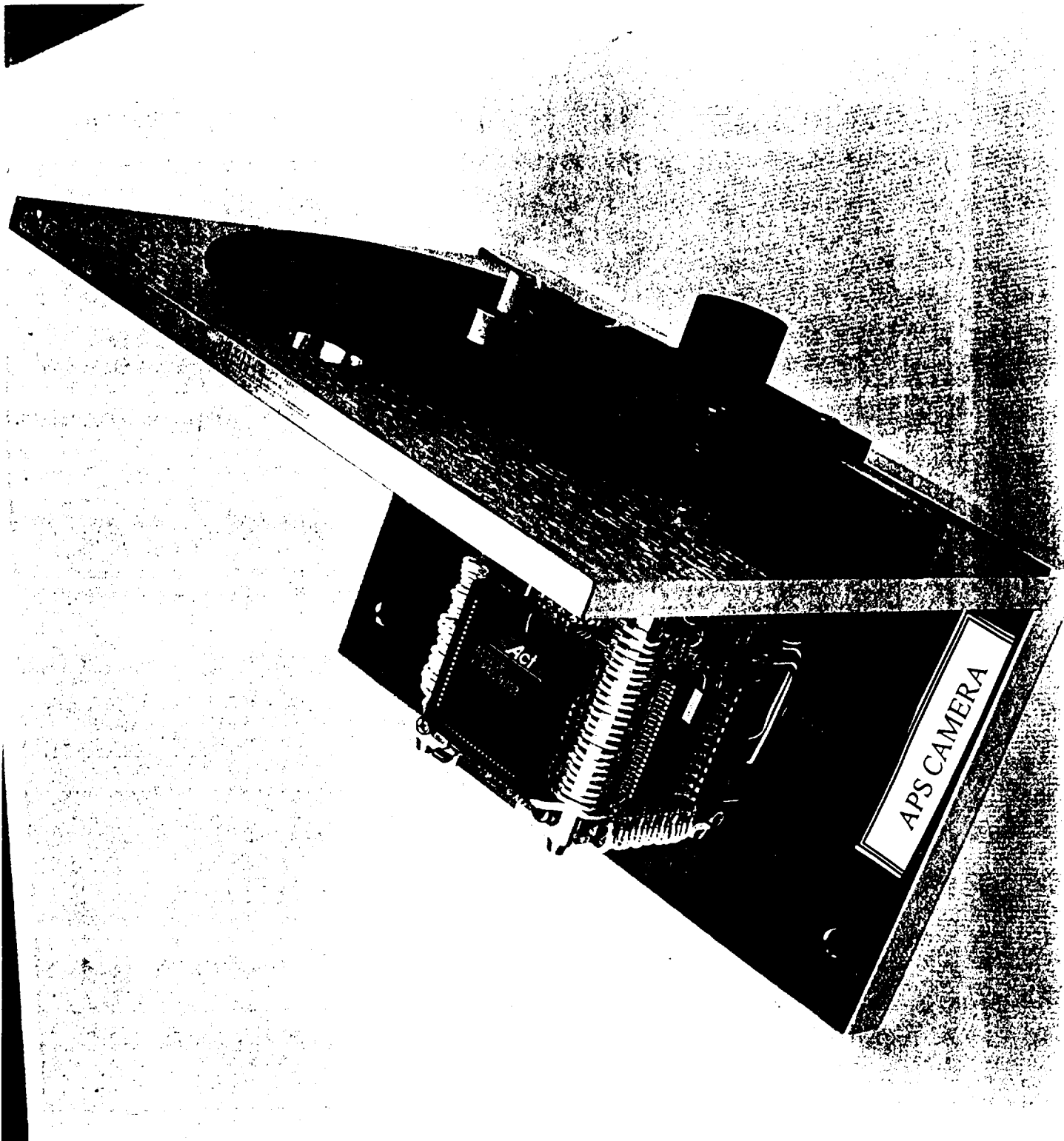
FIGURE 1. Front and side view photograph of the VASSIS APS camera. Note the APS detector on front board and FPGA on the top board. The ADC and the SRAM memory appear on the side board and not shown are the boards with the micro-D connector, the UART chip and the voltage regulators.

APS CAMERA
2" x 2" x 2.8"

APS CAMERA
2" x 2" x 2.8"
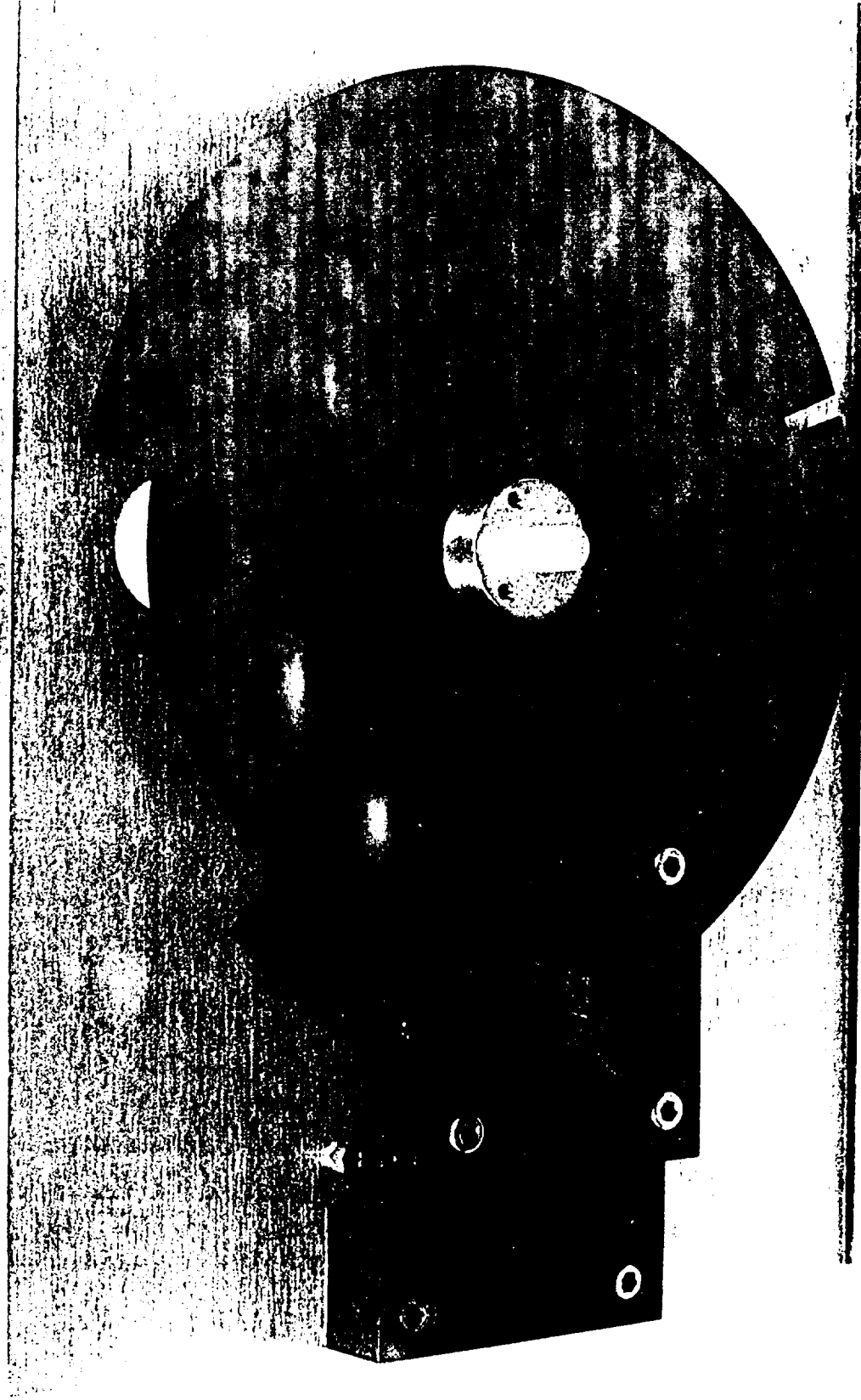
APS CAMERA

APS CAMERA

JET PROPULSION LABORATORY   **INTEROFFICE MEMO**

January 20, 1998
APSCAM001.doc

TO: Ken Klassen
FROM: Enrique Villegas
SUBJECT: **VASSIS APS Camera**
CC: Valerie Duval, George Fraschetti, Chris Stevens, Art Vaughn, Stan Soll

This memo is to document the performance results of the completed VASSIS APS camera. This report is limited to the camera alone, excluding the optics and the mechanical shutter and their associated performance contributions. While much information was gained in the performance of these camera tests, several questions arose in the process. Questions with respects to the linearity of the system in particular are still not yet resolved. However, in other areas the camera functions well. No data with respects to the Quantum Efficiency of the APS chip were collected.

The VASSIS (Venus Aerobot Surface Science Imaging System) camera is a prototype miniature camera to study the feasibility of utilizing it as the science instrument for a Balloon mission to Venus. The camera would be contained within a pressure vessel (two nested spheres) with a window looking down to the surface of Venus. The performance results of the camera system will be used to improve the proposed design of the mission.

The camera was built and assembled using off the shelf commercial parts and no particular attention was paid to using space quality components due to the budgetary constrains. Furthermore the camera design is a clone of a camera built for the ROCKY-7 prototyping activity. Hence, the camera performance was constrained to the specifications imposed by the original sponsor ROCKY-7. The added requirements levied on the already mature design were the incorporation of a mechanical shutter and its associated motor and driver/controller electronics. The added mechanism also required additional software design.

CAMERA DESCRIPTION
A photograph of the VASSIS APS camera is shown in figure 1. Note that a Printed Circuit Board(PCB) is mounted in each of the faces of the chassis. This arrangements was designed in order to maximize the heat dissipation of the camera. The camera has only one small micro-D connector on the rear looking PCB. The camera communicates and receives the power lines through this connector. No other electrical connections are required. The shutter motor and its associated electronics are a separate item from the camera thus they wont be covered here.

The camera is operated at room temperature and no provisions were made for cooling the detector other then by radiation and conduction for heat dissipation. It is expected that the camera would be operated at +40°C in the actual mission. One temperature sensor is imbedded right under the detector in intimate contact with the pin grid array that holds the detector.

The following is a list of the features of the cameras, excluding the optics:

1. CC256C' APS Photogate detectors (20.4 μm pixels with ~21% fill factor)
2. 1 Mbit SRAM memory (1 image)
3. RS-232 Serial interface @ 115Kbps
4. 12 bit ADC
5. Control Logic designed in an Actel 1020B FPGA
6. Voltage regulators (LM317,LM337)
7. LM 335 Temperature sensor
8. Jumpers for configuring camera to operate PhotoDiode APS detectors
9. Jumpers for configuring camera to operate 3.5 Volt APS detectors.
10. One Micro-D 25 pin PCB mount connector.

The detector is operated at 250Kpix/sec so that it takes approximately 300msec to read out an image into the cameras SRAM memory. However, since the image is then transferred serially to the computer it takes an additional 12 sec. With all the overhead timing it takes about 13 seconds to complete an image acquisition.

The camera was designed to operate with either a Photogate or Photodiode APS detector. It can also be configured to operate +5V or +3V versions of the detectors. The particular configuration is accomplished via a set of jumpers.

CAMERA PERFORMANCE

The camera's performance has been characterized although some results are not yet satisfactory. It is expected that additional characterization will take place when the shutter and associated electronics and s/w are completed. Further data will be taken then to address some of the open questions that remain. The following are some of the operating features and performance highlights of the camera:

1.	Power required:	1.5 W	:from +5V and ± 15V supplies
2.	Camera Weight:	182 grams	:excluding optics, shutter, motor
3.	Camera envelope:	5.6cm x 5.6cm x 7cm	:includes component heights
4.	Variable Integration:	.288 to 33 sec in 2msec steps	
5.	Noise (rms)	$\approx$ 48 e-	
6.	System gain	$\approx$ 24 e-/DN	
7.	Dynamic range	$\approx$ 64 dB	
8.	Linearity % $\approx$	TBD	:Issued will be studied further
9.	Dark Current rate:	8.5 mV/sec = 150 pA/cm^2	;Measurements appear suspect
10.	Fullwell capacity (e-):	$\approx$ 80,000 e-	
11.	Blooming characteristics;	TBD	;Data may be taken in future tests
12.	Quantum Efficiency (%):	Not in plan to perform	

In the case of the VASSIS camera, it is desired to have integration times of 2msec up to several msec. The way that is accomplished is by using the mechanical shutter wheel as the integration control. The shutter aperture will determine the duration of the exposure by nesting the its

exposure window within a larger fixed integration time set up for the detector as shown in the following diagram.

Detector integration:
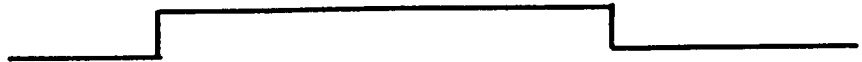
Shutter exposure:

A plot of a well behaved light transfer curve is shown in figure 2. Note that these data were collected by holding the integration exposure time fixed while the intensity of the light source (flat field) was slowly increased. Similar well behaved curves could not be obtained by performing the test by having a fixed light source and varying the integration time. The results of one such test are shown in figures 3 and 4. This plot shows a linear response of better than 5% for the low level signal case spanning about 75% of the dynamic range. The plot for the high signal level appears to have a larger linear range, however, the data does contain several outlying data points that must be ignored. To complicate the problem further these bad data points appear to be periodic and also signal level dependent since they don't correlate to the same integration times for he lower signal level plot. Thus the problem appears to have some signal level dependence that gets worst for higher intensity levels. This result can be attributed to either a problem with the camera electronics or with the detector but it is not clear which. I have taken other data on a completely different system for these particular detectors with similar but not identical linearity results. Ultimately there may exist a problem in both areas that only more detailed testing and analysis can conclusively determine. More work needs to be done in this area.

The dark current measurement is also suspect and further tests may be required to give conclusive results. I believe that the dark current generation rate of 8.5 mV/Sec as measured is too low, most of the APS devices of this type exhibit dark current rates of approximately ≈ 30 mV/Sec or higher. A plot of the dark current generation is shown in figure 5.

IMAGING QUALITY
No formal imaging tests have been yet performed. However, some crude targets have been set up and imaged through the lens onto the detector and recorded by the camera. An image taken with the camera is shown in figure 6. Further tests need to be performed to ascertain the Imaging qualities of the device. Parameters such as blooming, residual image and charge transfer issues can then be evaluated.

CAMERA CONTROL (GSE)
The camera is controlled from a PC computer via an RS-232 serial port operating at 115Kbps. The controlling software was written using Labview 4.0 running under windows 95. The operation of the camera is rather simple, a front control panel allows the user to enter the integration time desired and commands start of acquisition. An image is returned to the display at end of the transfer. The panel also displays the signal mean, high and low pixel values as well as the variance for that image. The user can then enter a text description of the image parameters into the header and then save file to the data directory. This file is stored as a Binary file that can then be analyzed by an image analysis program of choice.

FUTURE WORK
The complete characterization of the camera yet remains to be performed with all the elements in place. Presently the motor controller is at the vendor (Aerotech) for repair. The system including the camera, lens, and shutter need characterization to obtain the end to end performance results. To get to this point the shutter and associated electronics must be integrated to the existing camera. This requires completion of the repairs to the motor controller and completion of the s/w modifications necessary. Then the work of system characterization can be performed.

CONCLUSION
The VASSIS APS camera is completed and the several of the goals have been met. The camera weights 182 grams which is under the 250grams originally estimated. The 1.5 Watt power estimate was right on the estimated number. The envelope of the camera of 5 x 5 x 7 ccm also came in well under the original estimate. Some unexpected results have also been shown with respect to the linearity of the camera. Additional work would be required to study and resolve this problematic issues.

Figure 2. A plot of the VASSIS APS camera transfer curve. These data was collected with a fixed integration time of 383 msec and by slowly increasing the illumination source intensity.
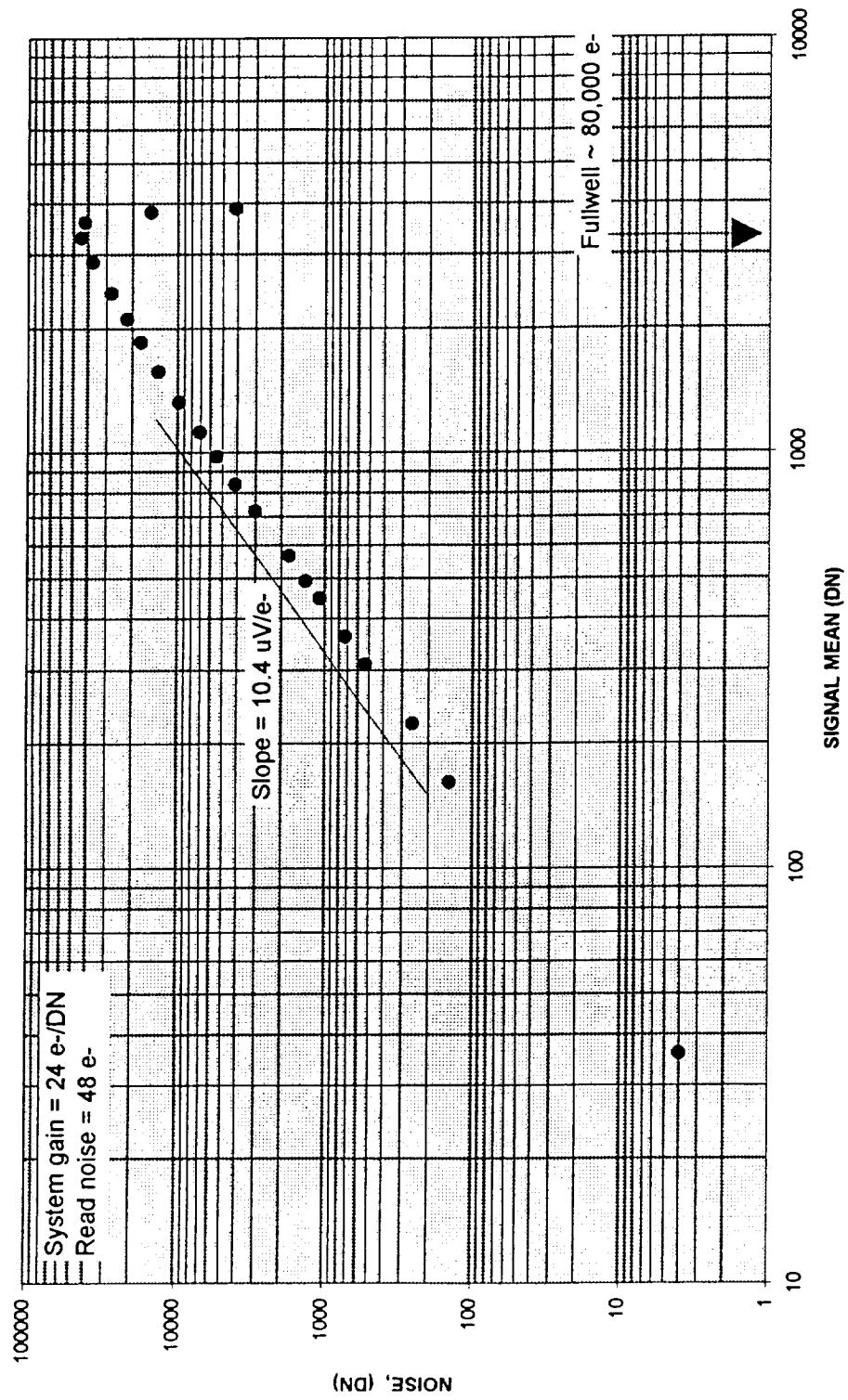
Figure 3. Plot of two transfer curves taken at two different fixed light levels and by gradually incrementing the integration time. Note that both curves exhibit some anomalies.
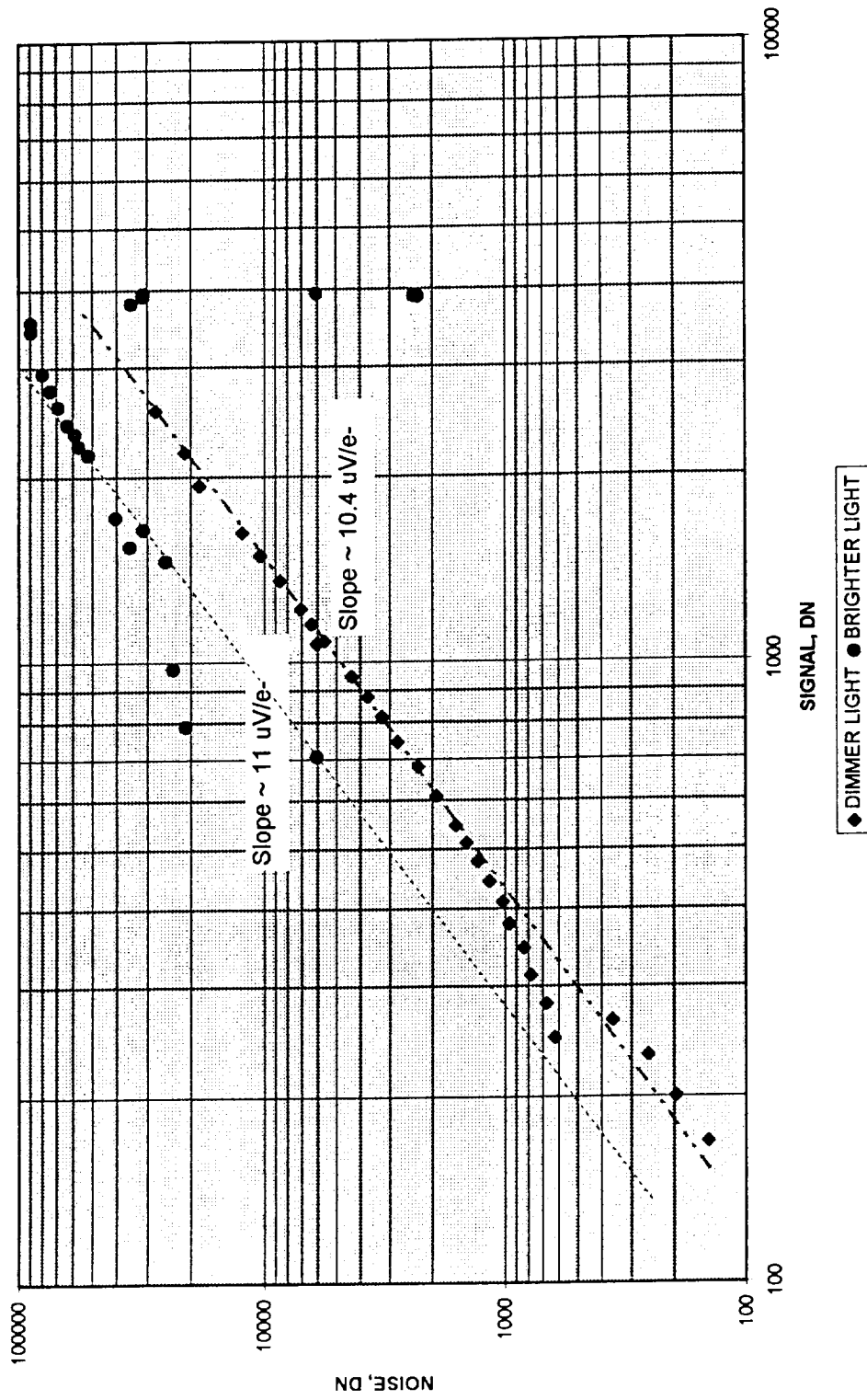
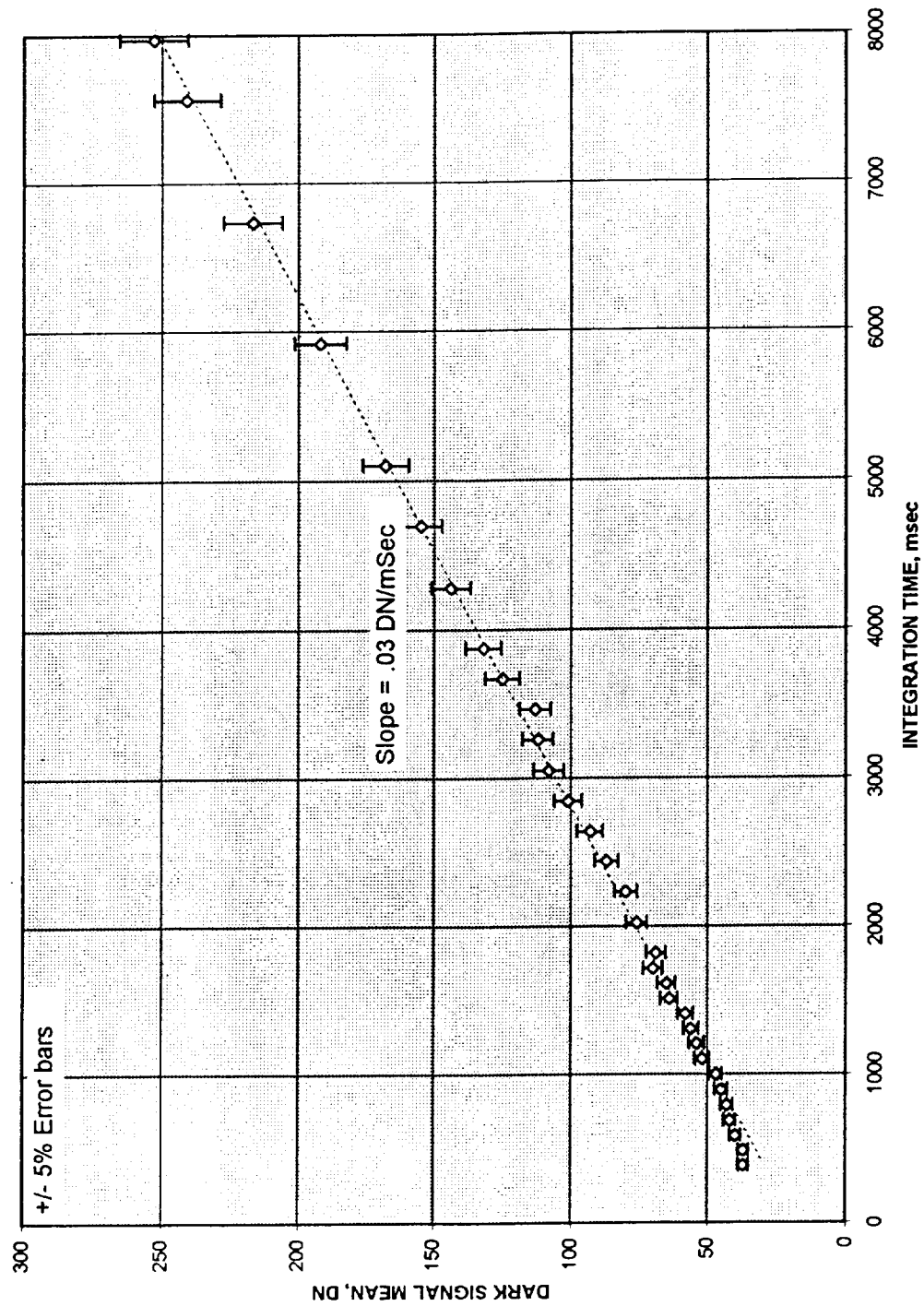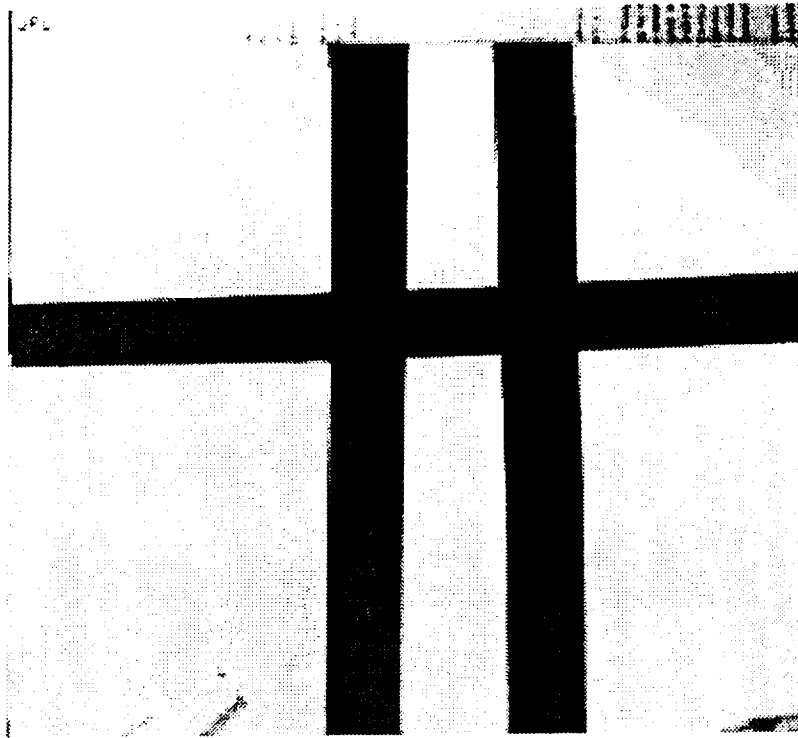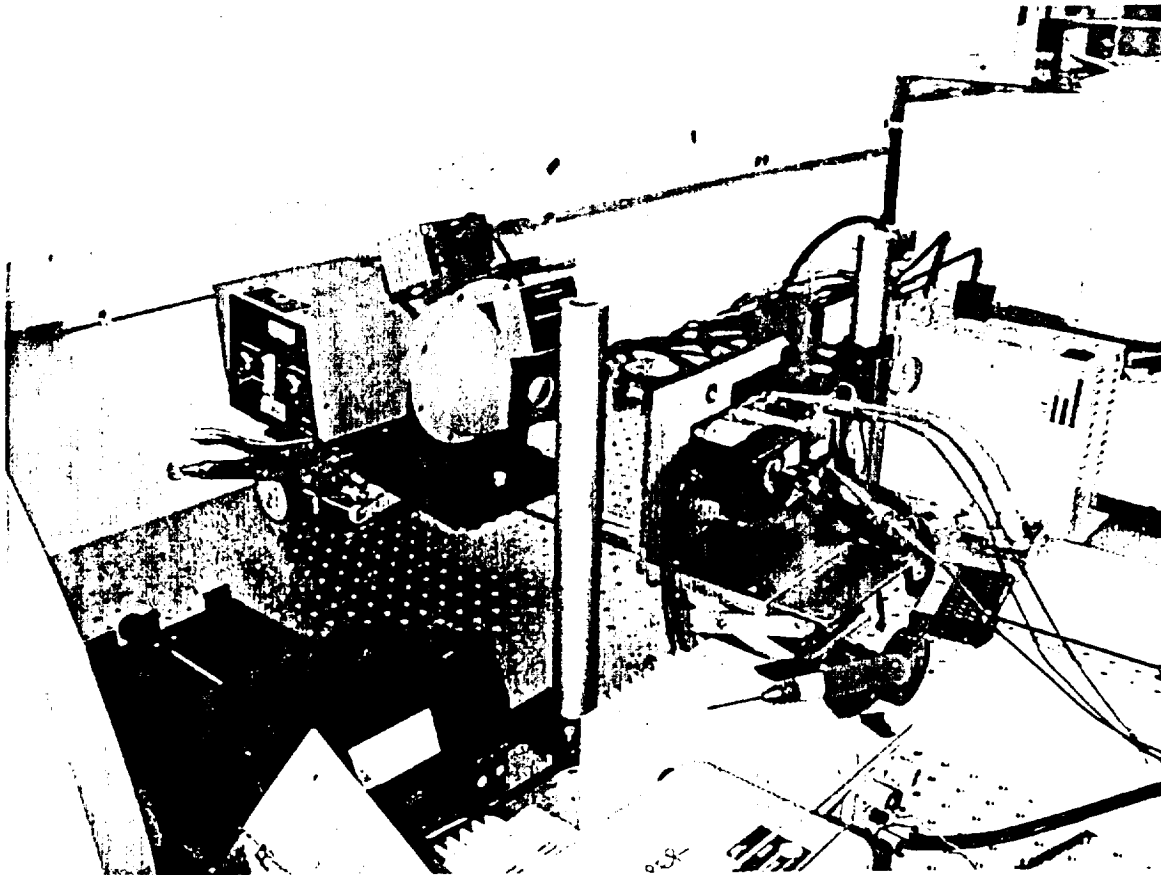## Figure 4. Linearity Plots of the same data presented in figure 3.
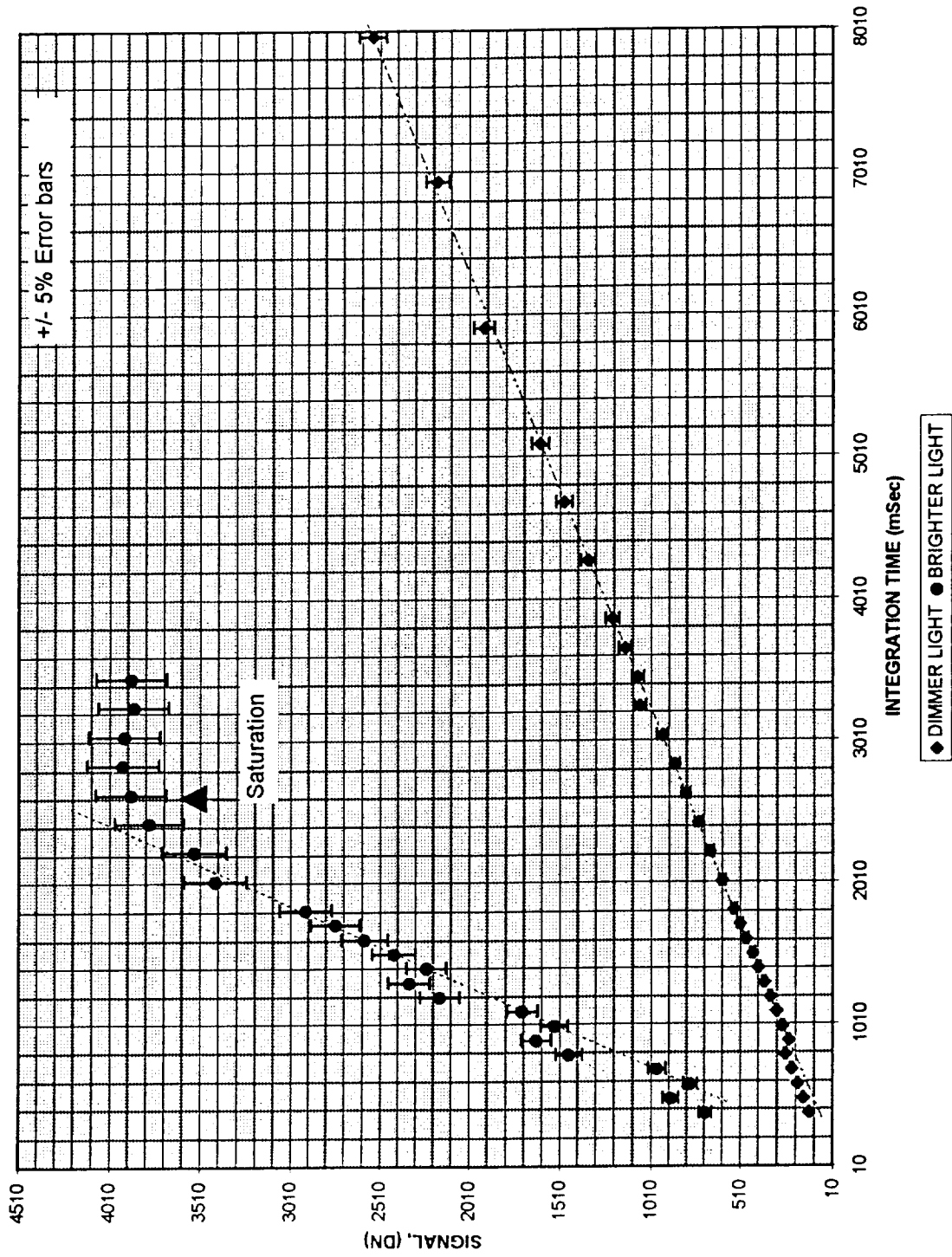
Figure 5. Plot of dark current vs. integration time, data collected at room temperature ~+ 18C.

FIGURE 6. Image of target taken using the VASSIS camera with attached lens
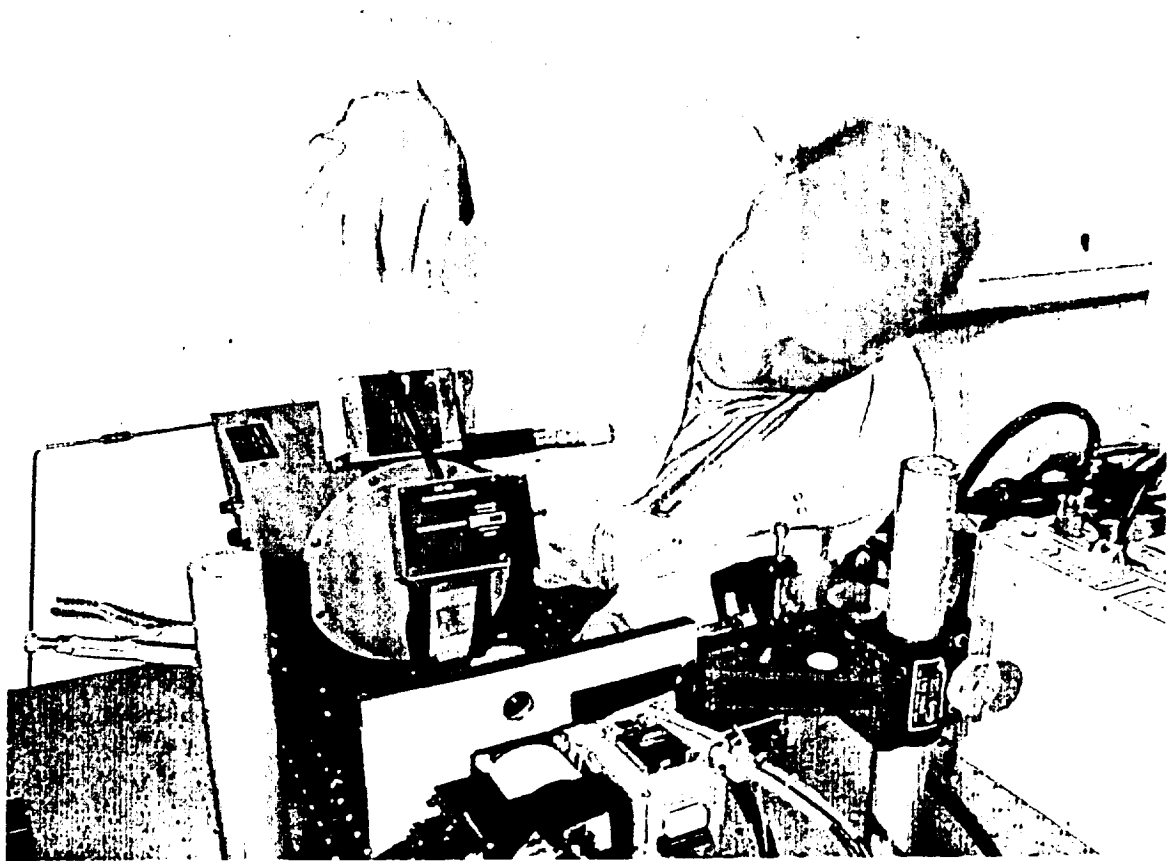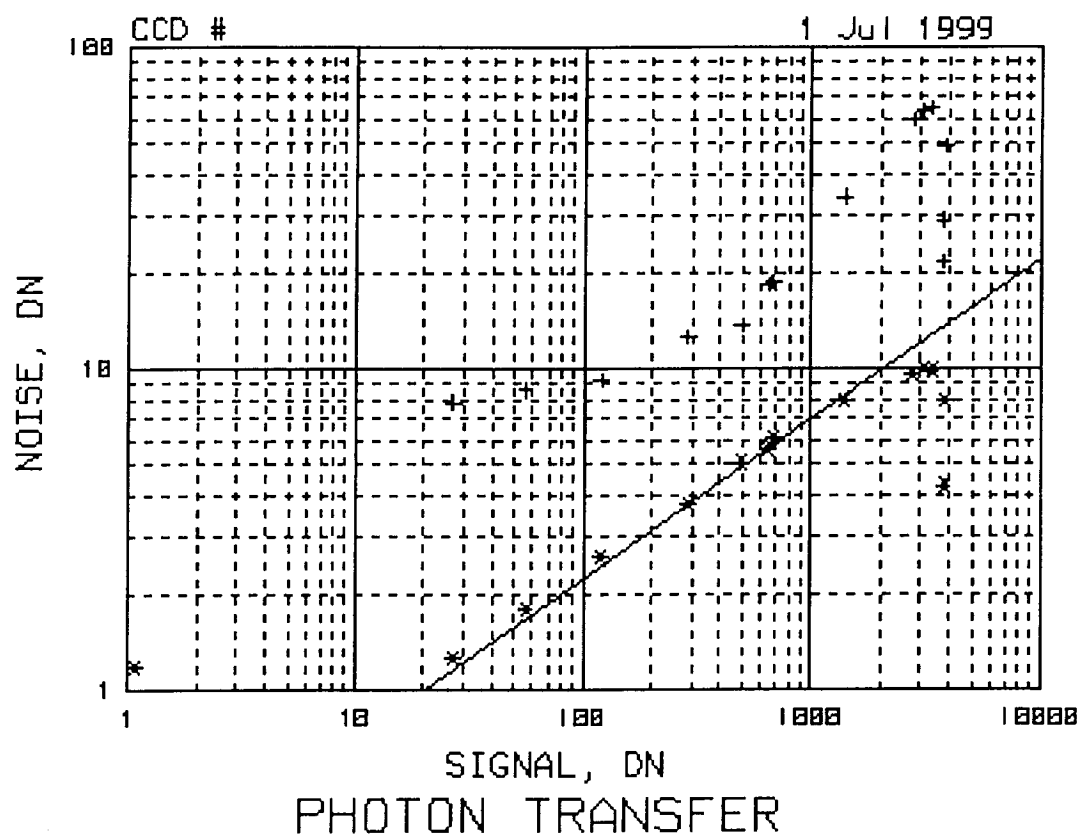
PHOTON TRANSFER

AREA LOCATION: X 50   Y 176
AREA SIZE: 30 x 30
e-/DN= 20.6

1 Jul 1999

LINEARITY CURVE
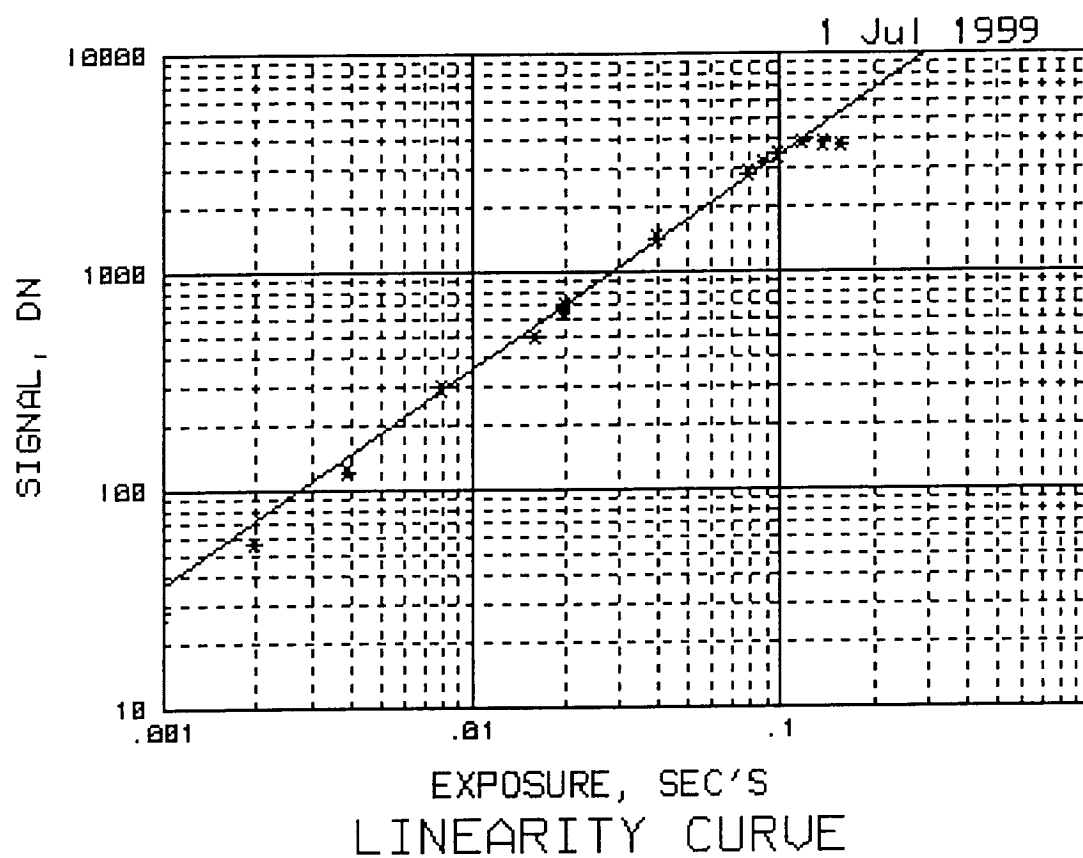
AREA LOCATION: X 50   Y 176
AREA SIZE: 30 x 30
e-/DN= 20.6

File#212733   1 Jul 1999
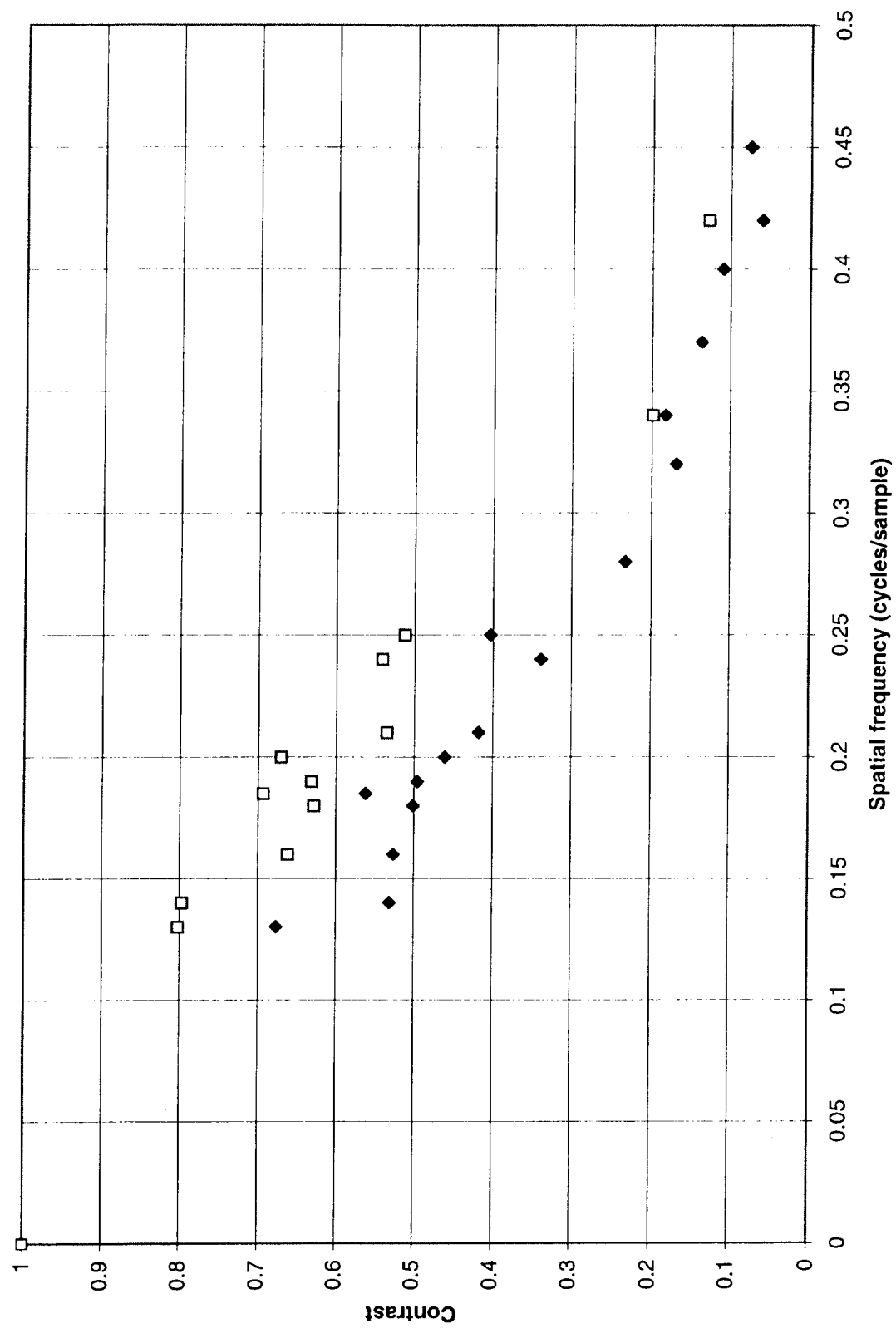xmin= 0 DN
xmax= 1000 DN
Resolution target
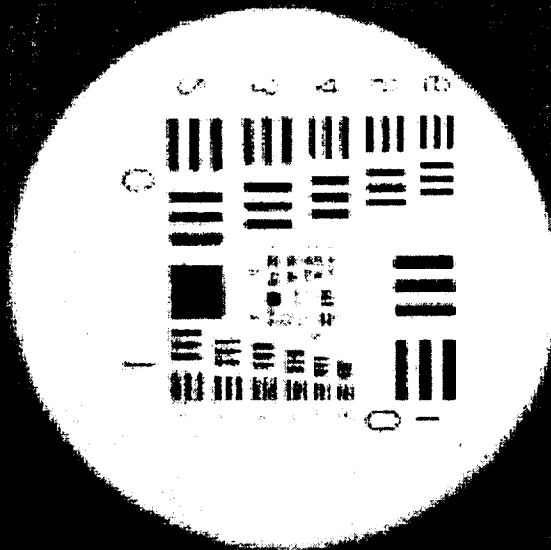
Film#215215

xmin= 0 DN
xmax= 1000 DN
Wide bar vertical
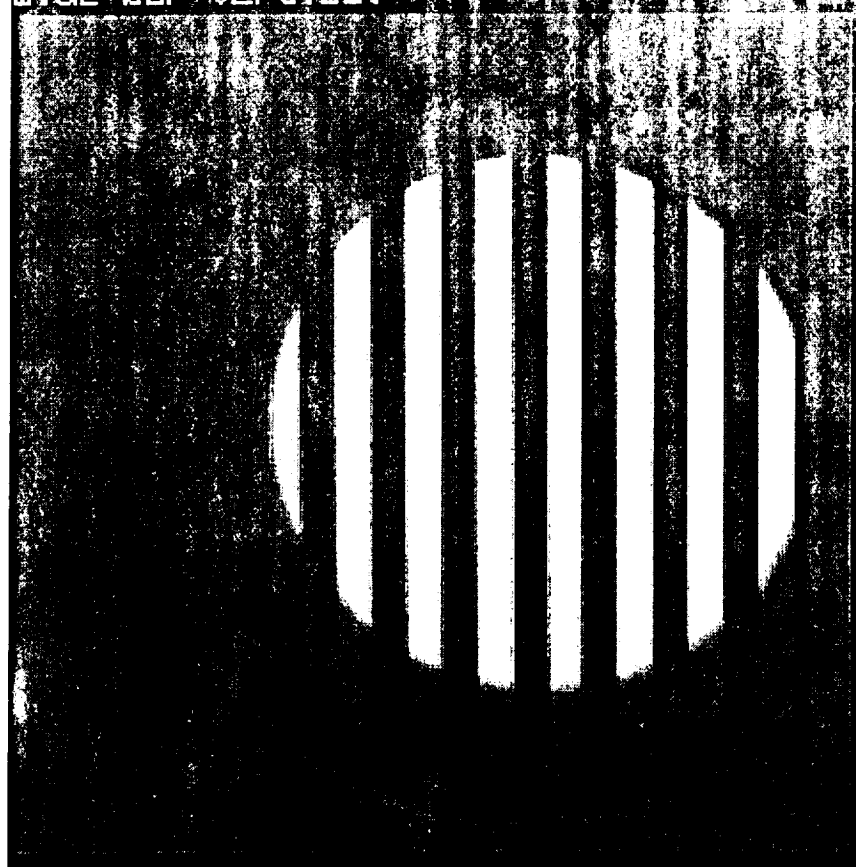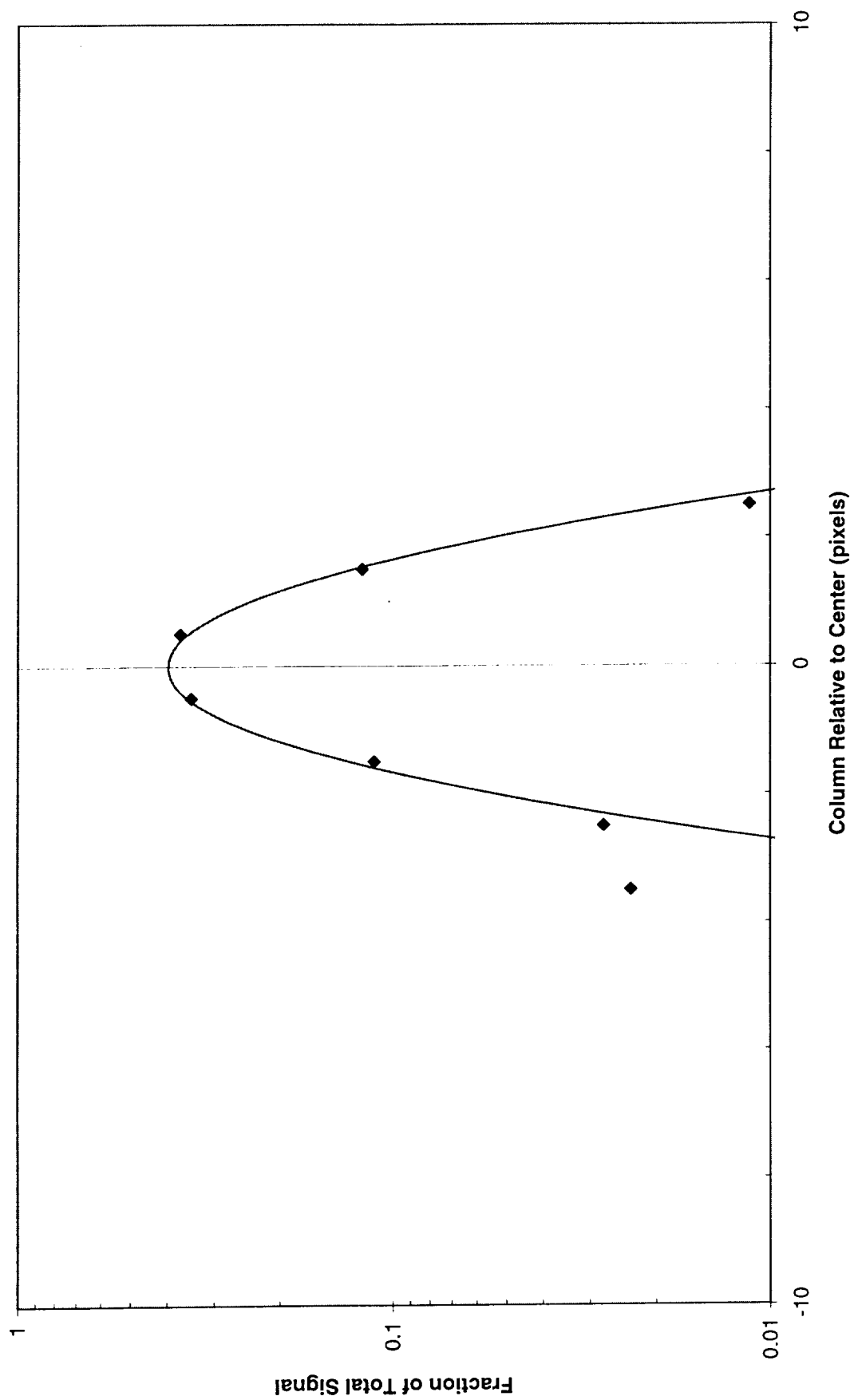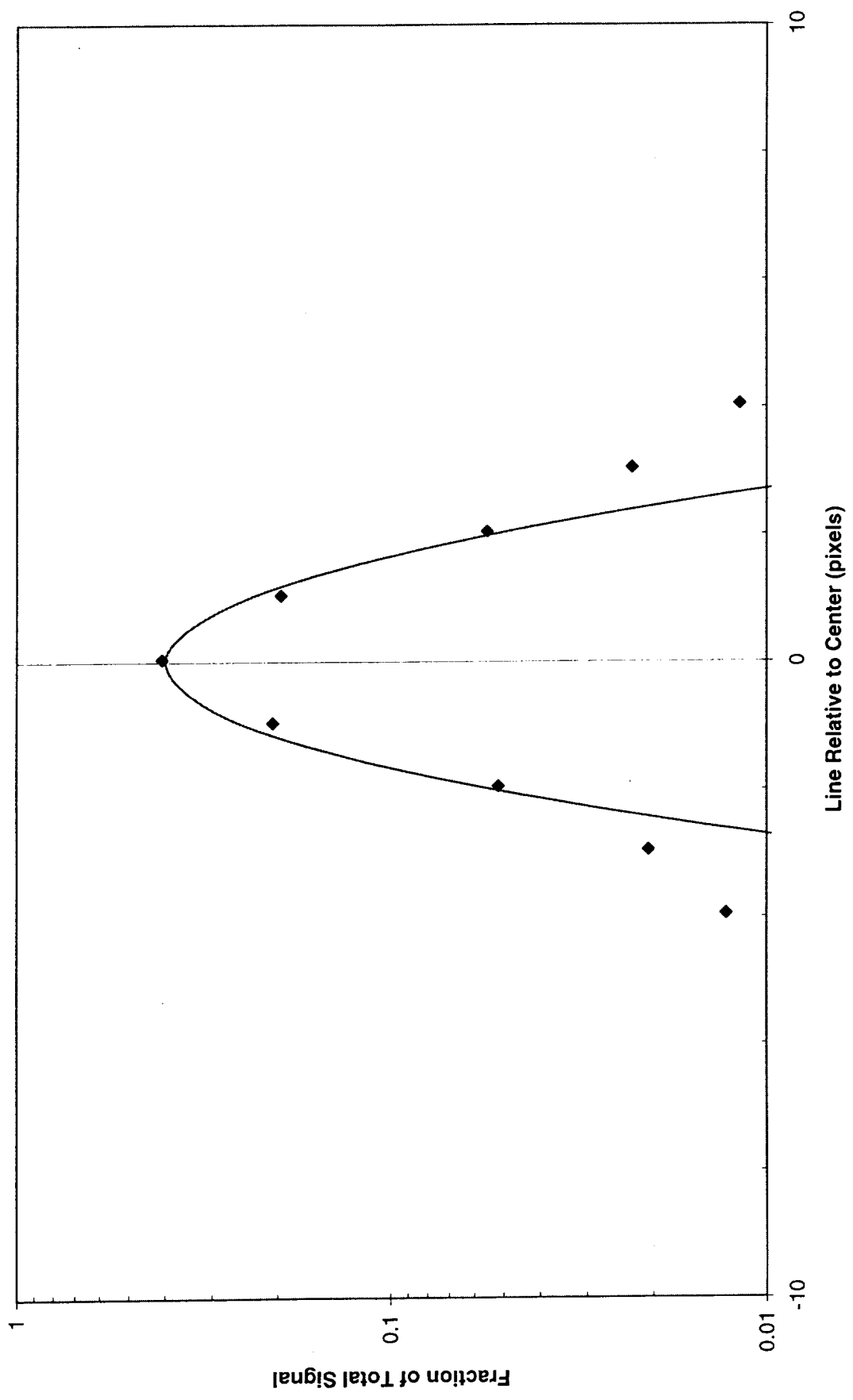
VASSIS Contrast Transfer Function

VASSIS Line Spread Function @ 1 um 15351

VASSIS Line Spread Function @ 1 um 15042

VASSIS Line Spread Function @ 1 um 43054

Column Realtive to Center (pixels)

Fraction of Total Signal